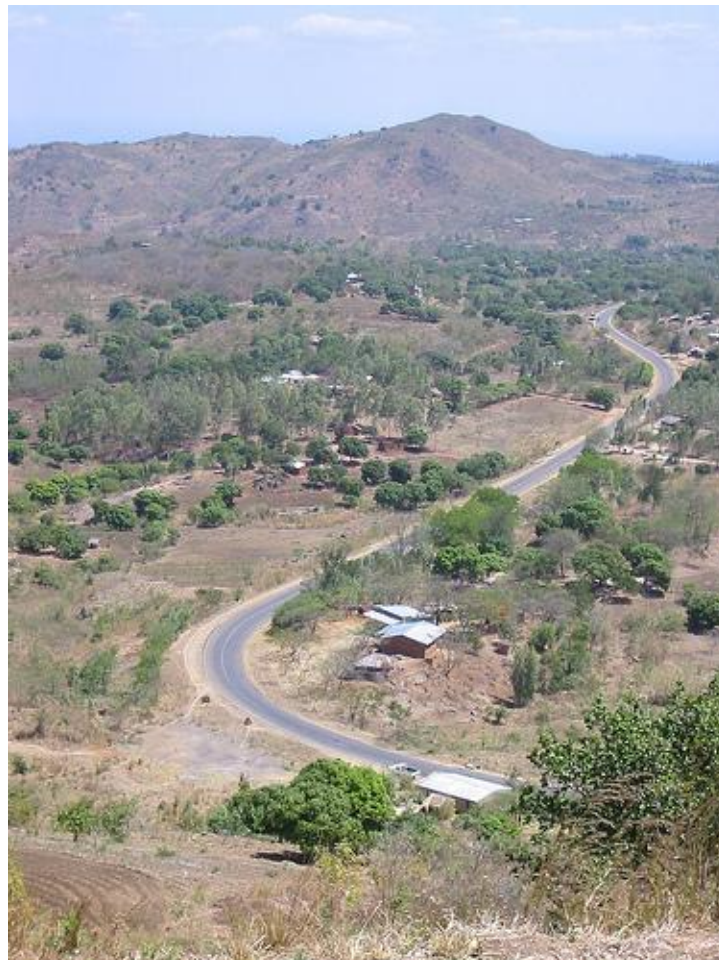


Master Thesis in Geoscience

Groundwater Modelling in the Chikwawa district, lower Shire area of southern Malawi

Media Sehatzadeh



UNIVERSITETET I OSLO

DET MATEMATISK-NATURVITENSKAPELIGE FAKULTET

This page intentionally left blank

Groundwater Modelling in the Chikwawa district, lower Shire area of southern Malawi

Media Sehatzadeh



Master Thesis in geoscience

Discipline: Environmental Geology, Hydrogeology & Geohazards

Department of Geosciences

Faculty of Mathematics and Natural Sciences

UNIVERSITY OF OSLO

June 1st 2011

© Media Sehatzadeh, 2011

Tutors: Per Aagaard, Professor at the Inst. of Geosciences. University of Oslo

Chong-Yu Xu, Professor at the Inst. of Geosciences. University of Oslo

This work is published digitally through DUO – Digitale Utgivelser ved UiO

<http://www.duo.uio.no>

It is also catalogued in BIBSYS (<http://www.bibsys.no/>)

All rights reserved. No part of this publication may be reproduced or transmitted, in any form or by any means, without permission.

Cover photo: View of Shire Valley, "I Love Malawi" Blog,

http://ilovemalawi.blogspot.com/2008_05_01_archive.html (visited 27/05/11)

Table of Contents

ABSTRACT	6
INTRODUCTION.....	7
Background	7
The salinity problem.....	8
Thesis objective.....	9
THE AREA	10
Geology.....	10
East African Rift Systems (EARS)	10
Structure of the Area.....	11
Precambrian: Basement Complex.....	18
Karoo System	18
Igneous Rocks.....	20
Cretaceous System	22
Superficial Deposits	23
Topography.....	24
Hydrology.....	26
Precipitation and temperature	26
Shire River	27
Groundwater.....	28
DATA.....	30
Precipitation.....	30
Temperature	32
Boreholes.....	33
MODEL.....	35
Model's geometry	37

Boundaries	38
Areal Recharge	39
Methods for estimating recharge	40
Thornthwaite method	42
Theisen polygon	45
Model Calibration.....	47
Hydraulic conductivity	48
Transient flow simulation	49
Initial conditions	49
Areal recharge time series	49
Specific yield.....	49
RESULTS	50
Areal recharge.....	50
Calibration results	54
Parameters.....	55
Calculated hydraulic heads	56
Model's sensitivity.....	59
Transient flow simulation	61
Areal recharge time series	61
Groundwater fluctuations	61
The effect of faults	64
Hot spots.....	68
A geological scenario	72
DISCUSSION	76
CONCLUSION	78
ACKNOWLEDGEMENT	78

REFERENCE	79
Appendix A: Precipitation data	82
Appendix B: Temperature record	84
Appendix C: Boreholes data for the model	85

ABSTRACT

This thesis contains modelling study of groundwater flow in the Chikwawa district, lower Shire Area in the southern regions of Malawi, in order to test out the working hypothesis that deeper groundwater circulation and dissolution of salts in subsurface sediments can explain the high groundwater salinity in parts of the Chikwawa district. There have been evidences of high salinity in Karroo system (in Red beds) and in Cretaceous rocks (in Lupata series) according to the available literature on geology, and there are hotspots located close to major faults where groundwater may discharge.

The 3D groundwater flow model of the problematic area in the western part of Shire River is derived by MODFLOW (PMWIN) simulations, where hydraulic conductivity attributed to the different major rock-types and faults were assigned. The semi-distributed areal recharge for the model is calculated using the Thornthwaite water balance approach based on the three meteorological stations in the area.

Despite the shortcomings, the calibrated model succeeds in producing groundwater head distribution in steady state that makes a good fit to the observations. Moreover it produces time series of groundwater table for the area in transient flow simulation. Results also show that the major faults in the area must be highly conduit and have a significant role in the groundwater flow patterns.

The Mwanza fault has not been found directly as the source of the high salinities by the model. However, studying the flow line in cross sections under the possible geological scenario in which the Mwanza fault continues along the Shire River suggests that in the discharge area close to the river there may be upward groundwater flow lines through Mwanza fault. It is quite possible that these flows carry out dissolved salt and are responsible for the salinity in the hot spots.

The model has a very high potential to be improved with field measurements from soil sampling to regular borehole measurements, pumping tests and geophysical studies.

INTRODUCTION

According to the UN statistics, 30% of the global freshwater resources is stored in the form of groundwater (UN-Water 2011). It is of both economic and environmental importance, therefore, to understand and study the properties and controlling factors groundwater flow, as well as to develop methods and techniques for its study and possible modification (TÓTH 2009). In Africa groundwater represents a significantly main water resource and a strategic source of freshwater essential in a region that is frequently affected by drought, and therefore it is important to study the groundwater systems in the African countries in order to maintain this vital source and provide necessary information for finding solutions for problematic areas.

This study is a contribution to the Norwegian Cooperation Program for Development, Research and Education (NUFU) project “Capacity Building in Water Sciences for Improved Assessment Management of Water Resources” under theme 2: Groundwater. NUFU supports cooperation between universities, university colleges and research institutions in Norway and developing countries.

Background

Malawi is located in southeast Africa within the western branch of the East African Rift system (EARS), within latitudes 9°S and 18°S and longitudes 32°E and 36°E. Malawi, with its 12 million inhabitants and an economy mostly based on agriculture, is highly dependent on groundwater resources in both rural and urban areas (Mkandawire 2002). In fact the primary sources of water for human consumption are water wells: hand pumped in rural areas and motorized in urban centers (Mkandawire 2002). That amplifies the consequences of any problem with the quality of the groundwater obtained from boreholes. The role of groundwater is especially crucial in the Chikwawa district (marked on figure 1), which has been described as one of the hottest and driest parts of the country (Staines 2002).

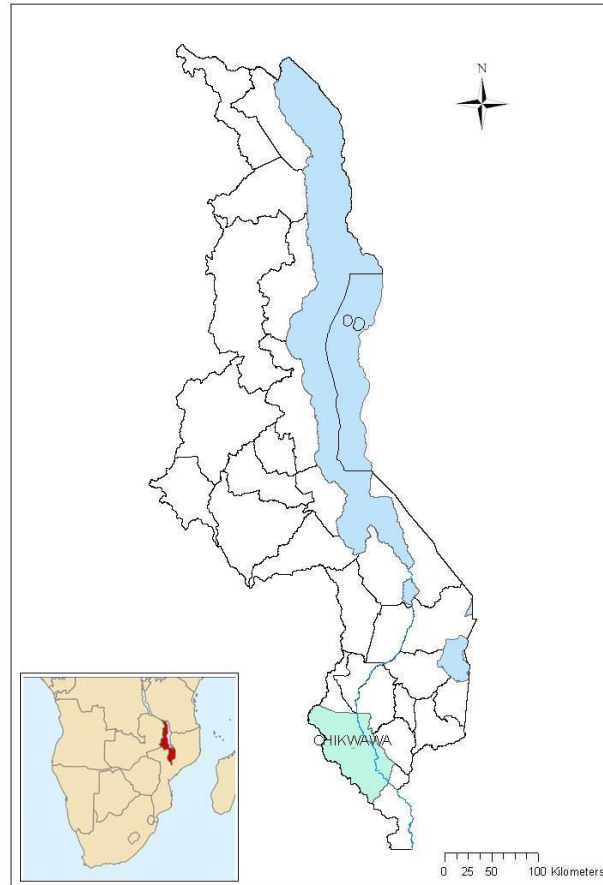


Figure 1. *District of Chikwawa on the map of Malawi*

The salinity problem

The problem with the quality of the groundwater in the district of Chikwawa is that the salinity of groundwater is extremely high and the water is nowhere near drinkable. The electrical conductivity measurements performed in the area clearly exhibits the hot spots, as shown in figure 2.

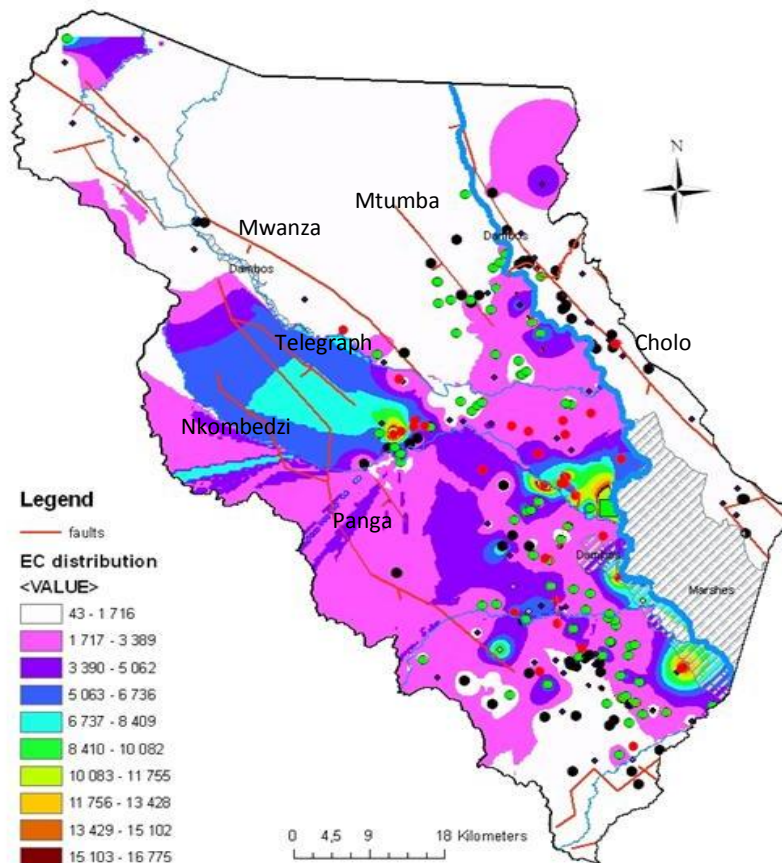


Figure 2. *Electrical conductivity distribution (microS/cm) Major and minor faults are marked by red lines*

Thesis objective

The locations of the hot spots are mostly aligned with the one of the major faults in the area, the Mwanza fault. Therefore, it is crucial to have a good understanding of the groundwater system in the area in order to locate the source of salinity. The objective of this thesis is to use 3D modelling in order to find the groundwater flow pattern in the area based on the available data, and explore the significance of the faults in the flow pattern. The major delimiting factor of this study is the lack of data and in particular, geophysical works on the area. This of course means high potentials in the area for further research, which will improve the model built in this study in the future.

THE AREA

Geology

Unfortunately, sources of information on Malawi's Geology are limited. Moreover, the available sources are quite old; e.g. "the geology of the country west of the Shire River between Chikwawa and Chiromo" by F. Habgood, which happens to be the main geological source for this study, is published in 1963. It being cited in almost all papers about Malawi implies that no later geology resource has been developed for Malawi. Though, this lack of publications opens up opportunity for further geological investigation in the area.

East African Rift Systems (EARS)

Continental rift zone is always accompanied by impressive examples of the early stages of continental breakups by extension (Ring et al. 1992). Some rifts eventually turn into oceans, but most of them abort after some kilometers of extensions (Ring et al. 1992). The East African Rift is an active continental rift zone in eastern Africa (Mougenot et al. 1986) and is one of the most remarkable relief features in the geology of Africa (Ring and Betzler 1995). It is formed within a large-scale zone of weakness in the lithosphere (Ring and Betzler 1995) as a narrow divergent tectonic plate boundary in which the African Plate is in the process of splitting into two new tectonic plates called the Somali Plate and the Nubian Plate (Mougenot et al. 1986). EARS is illustrated in Figure 3.

The rift consists of eastern and western branches (Castaing 1990, Ring et al. 1992, Ring and Betzler 1995) which dissect the entire eastern part of Africa (30° to 40°E and 15° to 25°S) (Ring and Betzler 1995). The eastern branch spreads into diffused network of grabens in northern Tanzania (Ring and Betzler 1995). The western branch is characterized by deep rift lakes and rift valleys, (e.g., Lake Malawi and Shire valley) (Castaing 1990, Ring and Betzler 1995). The Malawi rift, which is a southern extension of the western branch of the Cenozoic East African Rift System, extends 900 km from Rungwe volcanism in Tanzania to the Urme graben in Mozambique (Ring et al. 1992).

The Malawi rift is composed of border fault systems, step faults, half graben, horsts and monoclinical structures (Chapola and Kaphwiyo 1992). Regional uplift in the western branch show the greatest absolute rift subsidence in Africa that is manifested by very deep lakes

(e.g., Lake Tanganyika which is the second deepest lake in the world) (Ring and Betzler 1995). Rift formation has two general states of normal faulting and strike-slip dominated system which follows that (Ring and Betzler 1995). Rotation of extension and shortening axes result either in localized transpression and uplift or transtension in Malawi rift (Ring and Betzler 1995).

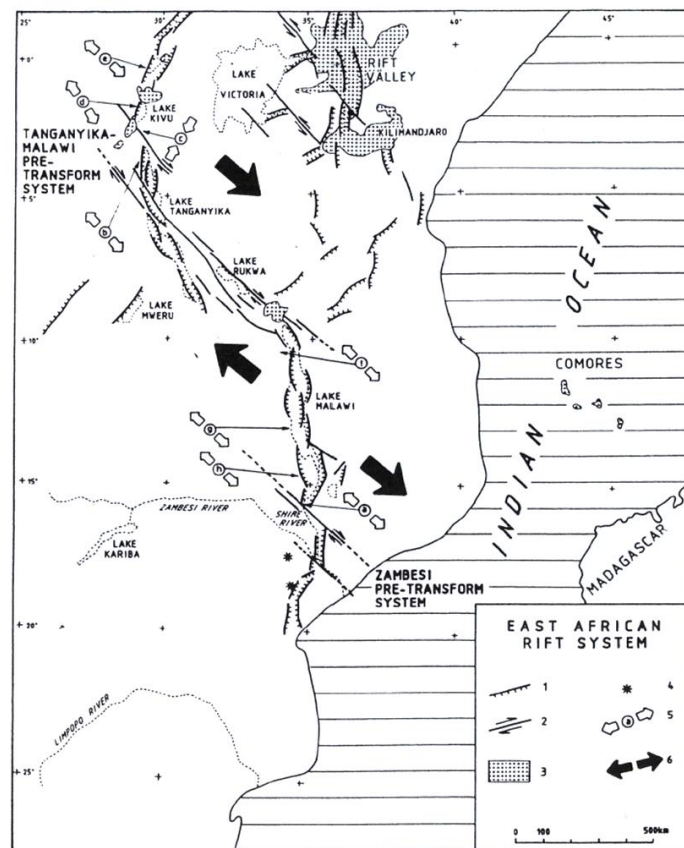


Figure 3. Recent East African Rift System (Castaing 1990)

- 1: Rift boundary normal faults. 2: Pre-transform faults. 3: Cenozoic and recent volcanic.
4: Cenozoic granites. 5: Direction of the extension. 6: General extension.

Structure of the Area

Faults

Since Malawi rift is seismically active mostly in the rift faults, it is responsible for the low magnitude earthquakes in the area (Chapola and Kaphwiyo 1992). The strike-slip regime, which has had a major role after the rotation of the Rift Malawi, has amplified the uplift of basement ridges in the rift, and created alluvial basins because of local transtension (Ring et

al. 1992). Vertical displacements along the East African Rift Zone triggered erosion of Precambrian and Mesozoic rocks (Dill and Ludwig 2008).

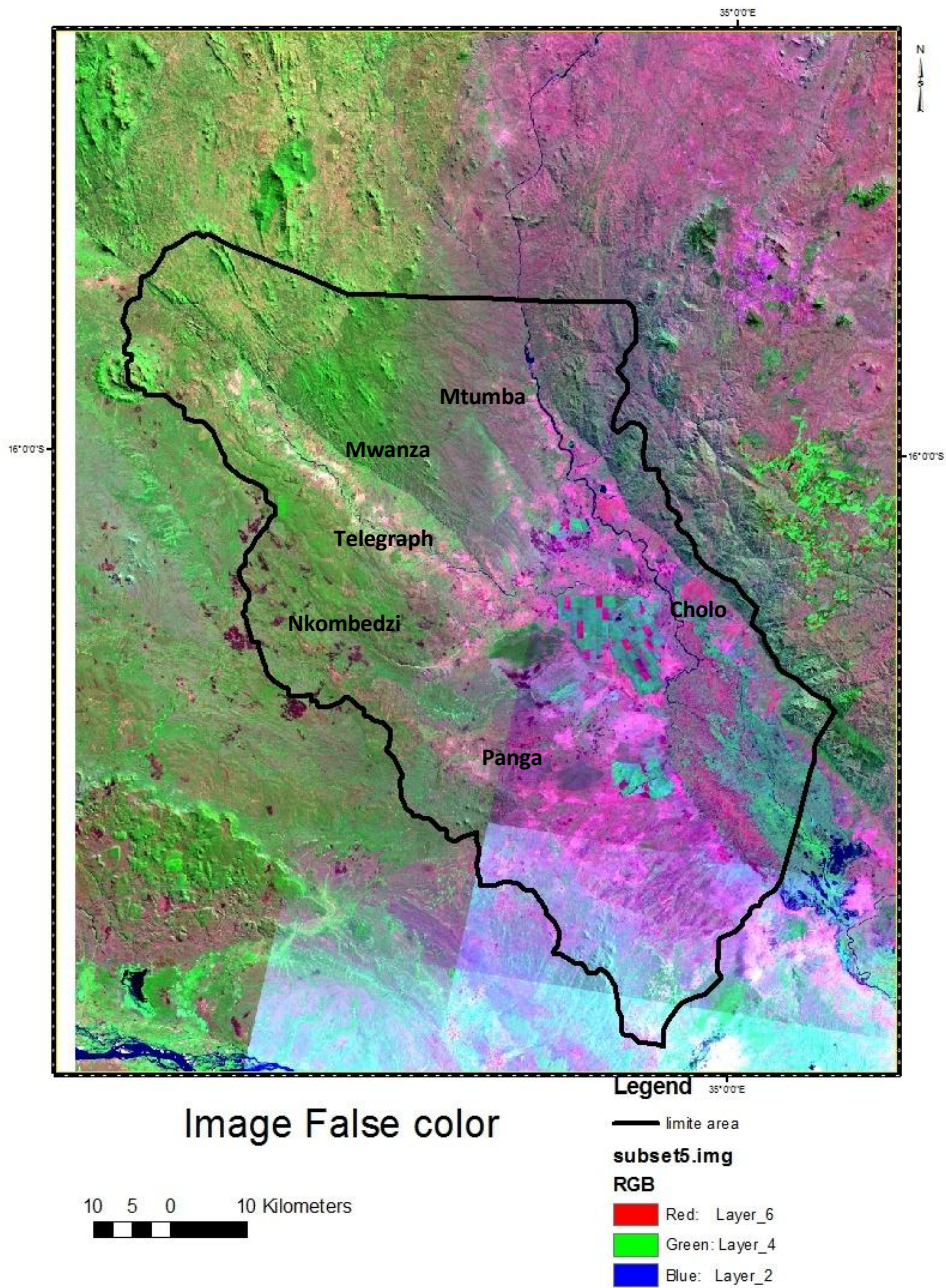


Figure 4. *Faults visible on the satellite image of the region with false colors. The outcropped bedrock in the north, alluvium inside the valley and the marshes in the south are also visible*

The structural evolutions in this zone controlled the emplacement of igneous rocks, which delivered heavy minerals to gather in the placer deposits (Dill and Ludwig 2008). The Karroo rifting period and the magmatism which put an end to it, were controlled by **NW-SE**

extension, which resulted a roughly NE-SW troughs articulated by Tanganika-Malawi and Zambesi pre-transform systems (Castaing 1990). These were sinistral slip systems with a slight normal component which enabled the Mwanza fault to play a significant role in the evolution of the Karroo basins of the Shire Valley (Castaing 1990). The extension was in **NE-SW** in the Cretaceous, but it once more became **NW-SE** in the beginning of Cenozoic and controlled the evolution in the transition of the Recent Rift System (Castaing 1990). Figure 5 from Habgood (1963) illustrates faults in the lower Shire area.

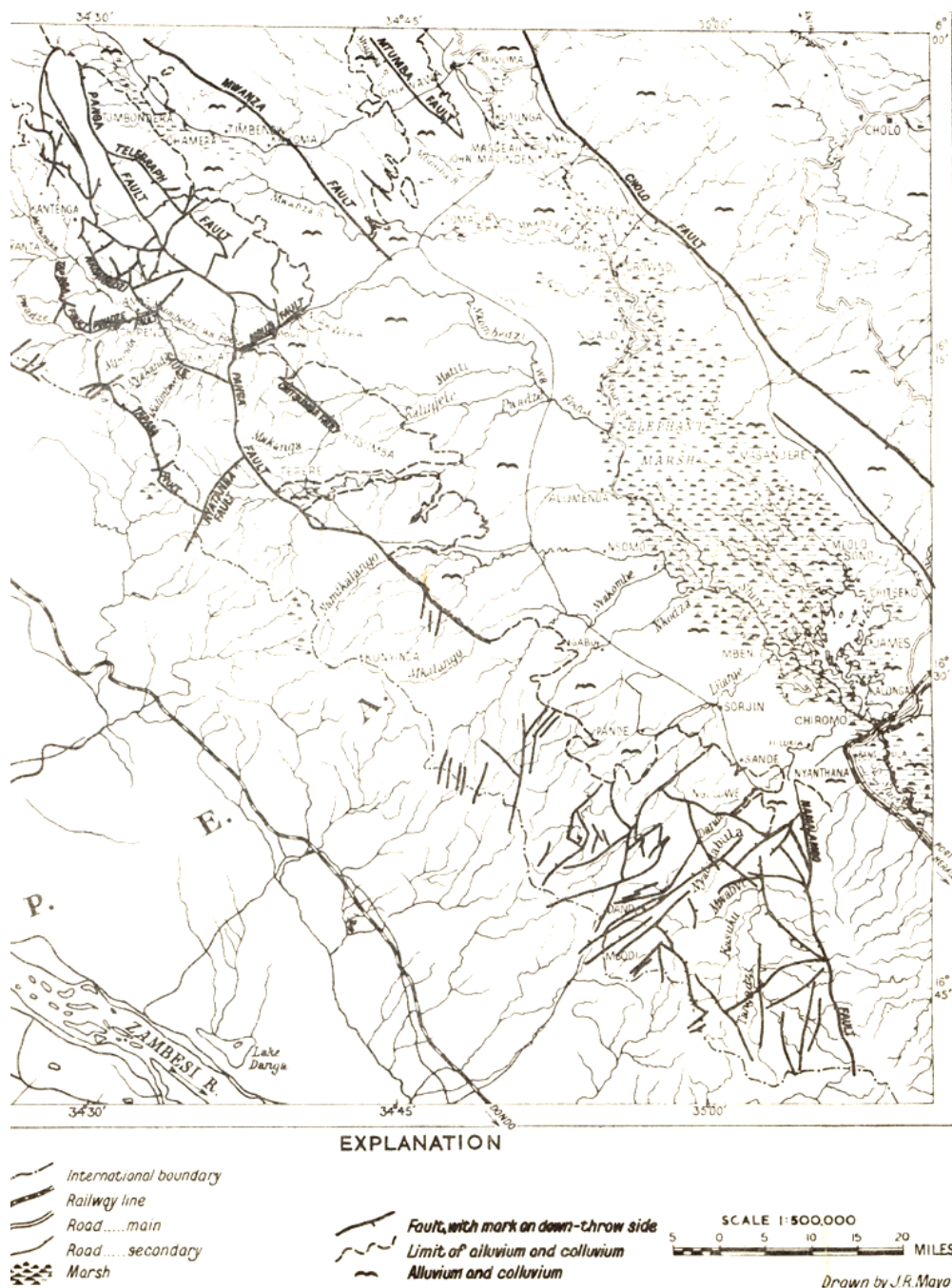


Figure 5. Faults of the area (Habgood 1963)

The Mwanza and Cholo faults function with a strong dextral strike-slip component, and also are considered as pre-transform faults opening Lake Malawi and Urema graben (Castaing 1990). The Mwanza fault is active both as normal and slip fault (like it used to be in Karroo period) and affects the sedimentation in Lengwe and Mwabvi basins (Castaing 1990). The faults in the study area are listed in the table 1.

Table 1. *Information on faults in the Chikwawa district, west of Shire River*

GROUP	NAME	Direction	DESCRIPTION
Karoo's boundary faults	Mwanza	NW-SE	Strike-slip and normal fault (Castaing 1990) the fault is marked by a hard white quartz rock, but the fault scarp disappears beneath the terrace alluvium of the Shire plain (Habgood 1963)
	Panga	NW-SE	A strike fault. It cuts many faults but is not itself cut by any. It is the most important fault in this group. Easy to locate from broken dolerites (Habgood 1963)
Faults cutting Karroo formation	Nkombedzi	NW-SE	A strike fault, it throws Sandstones against Coal Shales. Easy to locate from broken dolerites (Habgood 1963)
	Telegraph	NW-SW	Throws Mwanza Grits and Shales against Lower sandstones. Marked on the ground by low scarp of resistant Lower sandstones (Habgood 1963)
Minor faults	Mtumba	NW-SE	N.A
	N.A	NE-SW	The small fault in the southernmost part of the area

Rocks and Formations

Metamorphic and Crystalline igneous rocks form most of the basement in Africa, and underlie much of Malawi (Chilton and Smith-Carington 1984). The geology around Malawi rift is dominated by Basement Complex gneisses and granulites (Chapola and Kaphwiyo 1992). Overlying the basement are limited Permo-Triassic Karroo sequences and Cretaceous red beds in the north and south, Tertiary lacustrine sediments along the lake shore, Shire River and lake beds (Chapola and Kaphwiyo 1992). There are igneous rocks and dykes and sills among the sedimentary rocks (Habgood 1963, Chapola and Kaphwiyo 1992). Figure 6 illustrates the situation:

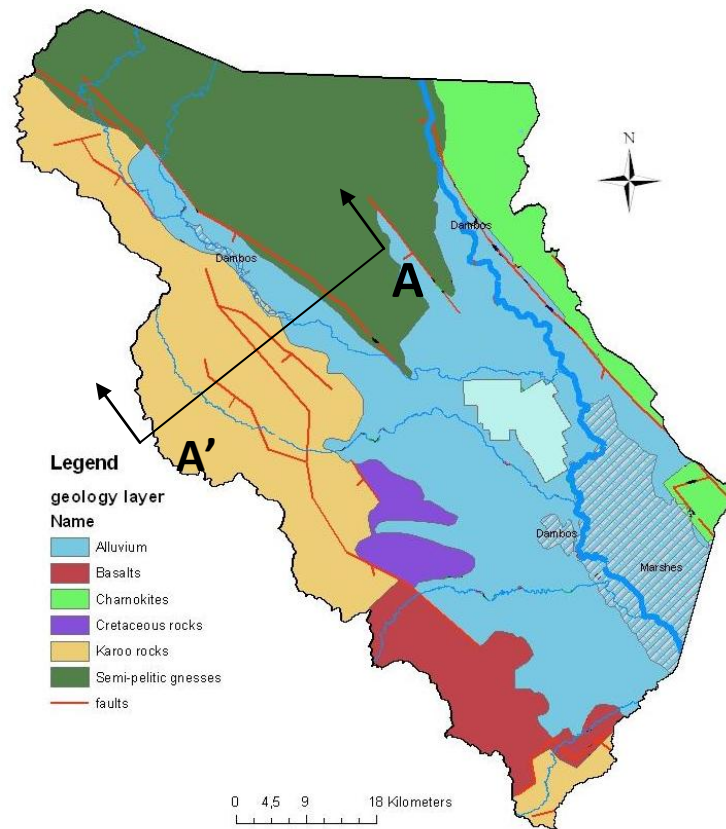


Figure 6. Geological map of Chikwawa district with cross section A-A' specified on it

Castaing (1990) obtained a sketched vertical section of Lengwe basin in Karroo system (section A-A') as below:

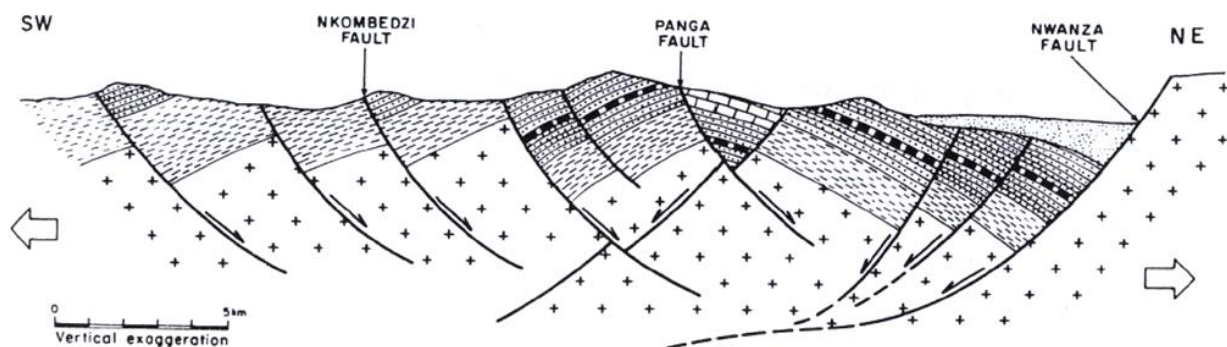


Figure 7. Section A-A' from Figure 6 (Castaing 1990)

- 1: Recent deposits. 2: Mwanza Grits and Shales. 3: Lower Sandstones. 4: Flaggy sandstones. 5: Coal Shales. 6: Pan-African basement.
7: Quartz. 8: Normal faults. 9: extension

Stratigraphy of the Shire Valley is presented by Habgood (1963) as in table 2.

Table 2. *Shire valley's succession (Habgood 1963)*

South Africa	Shire Valley		Europe
Stormberg Series	Basaltic Lavas	3500 ft	Rhaetic to Lias
	unconformity		
	Red Sandstones	500 ft	Upper and Middle Triassic
Upper Sandstones	2000 ft		
			Lower Triassic
Beaufort Series	unconformity		Upper Permian
	Red Beds	1000 ft	
	Mwanza Grits and Shale	3000 ft	
	Lower Sandstone	4000 ft	
Ecca Series	Coal Shales	2000 ft	Lower Permian
	Basal Conglomerate (?)		
Dwyka Series			Upper carboniferous

Habgood (1963) also illustrates the geologic development of the Chikwawa Chiromo area as in table 3.

Table 3. *Timeline of the Chikwawa Chiromo area (Habgood 1963)*

Basement complex Gneisses in Precambrian		Deposition of geosynclinal sediments, folding and faulting of sediments by NE-SW compression. Migration of sediments and intrusion of lit-par-lit pegmatites, earlier faults acting as loci		
Lower Paleozoic		Period of erosion		
Upper Paleozoic	Possible deposition of Nachipere sediments and gentle folding, period of erosion			
	Lower Chikwawa Group	Upper Paleozoic, Upper Ecca	Possible deposition of local basal Conglomerates on uneven down-warped surface. Downwarping of Coal Shales continues irregularly (2000 ft)	
Upper Paleozoic, Lower Beaufort		Rapid downwarping, widespread flooding and scouring of neighboring land surface leads to formation of lower sandstones (4000 ft). Downwarping, flooding and scouring lead to desert conditions and formation of Mwanza Grits and Shales (3000 ft). Desert condition and low relief leads to formation of red beds (1000 ft)		
Mesozoic	Karoo	Middle and upper Beaufort		Slight Earth movement with no deposition
		Upper Chikwawa	lower and middle Stormberg	Rapid subsidence and scouring of neighboring land surface, formation of upper sandstones (2000 ft). Desert condition with low relief leads to formation of red sandstones (500 ft)
		Upper Stormberg		Initiation of major tectonic disturbance, boundary faults and major Karroo faults, leads to extrusion of plateau lavas, intrusion of dykes and sills in the Karroo sediments and dyke swarm in the Basement. Basaltic lavas (3500 ft)
	Late Jurassic		Tectonic disturbance continues. Brecciating dolerite in Karroo faults and allowing influx of hydrothermal fault rocks material	
	Early Cretaceous		Partial flooding of area. Scouring neighboring land surface, Lupata series are the result	
Cenozoic		Formation of drifts and river deposits. Erosion and possible earth movements. Results are alluvium and colluviums		

Precambrian: Basement Complex

Due to Epeirogenic events, Precambrian rocks (also known as Pan-African basement (Castaing 1990)) are brought up against Karroo system in Mwanza Fault and exposed in its northern side, and then, due to prolonged weathering under tropical conditions, peneplain and inselberg hills are developed in them (Chilton and Smith-Carington 1984). These rocks are highly metamorphic and resistant to erosion, mostly gneiss which after going under intense folding and granitization, have become a tectonically stable shield for millions of years (Chilton and Smith-Carington 1984). The basement rocks form some of the highest land in the region. They are principally hornblende and hornblende-biotite-gneisses (which is the most common), and probably isoclinally folded and step faulted, with strong joints developed in them (Habgood 1963). There is evidence of potash metamorphism over a wide area and also bands of quartzofeldspathic granulite running parallel to Mwanza fault which are frequently schistose in part due to earth stresses (Habgood 1963). Some of the thicker bands have a granulite core with schistose margins, while thinner ones are schistose throughout (Habgood 1963). Marbles close to Mwanza river, about one mile north-east from Mwanza fault, are in a 15 (ft) thick band and have a vertical dip (Habgood 1963). They consist of small interlocking grains of pink calcite showing flow structures around lumps of massive garnet and dipole (Habgood 1963).

Karoo System

Sedimentary Rocks

The foundation is part of the lower Shire-Zambesi sedimentary basin which includes Lengwe and Mwabvi basins (Castaing 1990). The base of Karroo is not exposed in the area; the Coal Shales, a formation of carbonaceous and coaly shales with inter-bedded sandstones, is the lowest part of the sequence outcropping (Habgood 1963). Normal faults have influenced the thickness of the beds, and preferential trends of these beds reveal two sub-orthogonal directions of extension during the filling of the basins: a major NW-SE trend and a less important NE-SW (Castaing 1990). The Karroo sedimentation is controlled by extensional tectonic regime (Castaing 1990).

The Coal Shales

This is the lowest formation of Karroo that is exposed in the area (Habgood 1963). Basal conglomerate with rounded pebbles and boulder of local gneiss as large as 2 feet is very common (Habgood 1963). The coal shale probably underlies the whole Karroo area (Habgood 1963). The formation consists of grey and black mudstones and carbonaceous shales, and thin coal bands with interbedded grits and sandstones (Habgood 1963). The formation is the most intruded by dykes and sills which are explained later in the igneous rocks (Habgood 1963).

The Lower Sandstones

It is mostly made of cross-bedded, feature-forming, pebbly grits, feldspathic grits and arkoses (Habgood 1963). The formation is cut by different faults, of which the larger fractures shatter the rock on each side of the plane of movement and lead to weathering in these fractions (Habgood 1963). The grits are composed of quartz and feldspar (Habgood 1963). Arkoses are normally grey-buff and coarse grained and contain 60% feldspar at the most (Habgood 1963). It seems then that these deposits represent alluvial fans and deltas laid down quickly due to rapid weathering and erosion of basement rocks (Habgood 1963). No fossils have been found in the lower Sandstones but since they follow the Coal Shales conformably, the formation has been assigned to the Upper Ecca or Lower beaufort (Habgood 1963). Unlike the Coal Shales, the formation is not much intruded by large dolerites, but by thin dykes that fill pre-existing faults (Habgood 1963).

Mwanza Grits and Shales

The upper limit of the lower Sandstones is taken as the top of the feature-forming massive grits, which are conformably succeeded by softer weathering grits and well-bedded sandstones which pass up into mudstones and shales (Habgood 1963). The grits are arkostic, current-bedded and calcareous and the formation is covered by infertile, thin sandy soil and therefore well exposed (Habgood 1963).

The Red Beds

The Red Beds are soft, easily eroded, poorly exposed and the boundary of their outcrop is complicated by faulting (Habgood 1963). The formation is made up of mudstones, marls and siltstones (Habgood 1963). The mudstones are red or chocolate in color and contain iron

oxide and little mica (Habgood 1963). The mudstones gradually turn into marls with increased calcite content and irregularly bedded, grey limestones (Habgood 1963). Many of these beds indicate deposition in a subaerial environment when relief of the area was low and some might have been laid down in shallow pools of high salinity, though some found fossils like Ostracods point to presence of a fresh water environment (Habgood 1963). The formation is also intruded by dolerite sills which are veined by crystalline calcite (Habgood 1963).

The Upper Sandstones

Plenty of fossils have been found in this formation and they indicate a Stormberg age of the beds (Habgood 1963). The medium-grained buff and white sandstones and quartzites pass by alternation with pink and white, richly calcareous sandstones into an upper succession of poorly stratified desert-type deposits (Habgood 1963). The deposition of Stormberg sediments was terminated by faulting followed by the eruption of basaltic lavas (Habgood 1963, Castaing 1990).

Igneous Rocks

The Basaltic Lavas

Fault activities along the East African Rift during the Lower Jurassic triggered eruption of basaltic lava of Stormberg Group, and these volcanic activities increased during Upper Jurassic to Lower Cretaceous (Habgood 1963, Dill and Ludwig 2008). The earliest lavas contain some glass in their matrix where they meet sedimentary Rocks (Habgood 1963). Weathered surfaces are rare (Habgood 1963). Thin bands of sandstones occasionally occur between the earlier flows. These are invariably fine-grained with sub-angular rounded grains of quartz (<2mm) in a brown iron-stained cement (Habgood 1963). A few thin bands of white, cream to mave and pink ash are also found in them, which must represent periods of eruption from some minor volcanic centers (Habgood 1963). The lavas mainly consist of holocrystalline augite-labradorite-basalts, the feldspar occurring in laths with intergranular pyroxene, which has a lot of magnetite (Habgood 1963). Glassy and porphyritic types are also present, often vesicular near the surface (Habgood 1963). Basalt from the center of the flow is dense, compact and holocrystalline, the feldspar laths from 0.4 to 0.5 mm long with

porphyritic and vesicular types occurring near the surface of the flow and glassy material forming chilled contacts (Habgood 1963).

The Intrusive Rocks

The dyke swarm north-east of Mwanza Fault

At the end of the Karroo sedimentation, during the Stormberg volcanic episode, the network of dolerite dykes followed the NE-SW fracture system more easily due to the affirmation of the NW-SE extensions of the Malawi rift. (Castaing 1990) There is a swarm of dolerite dykes striking north-east from the Mwanza fault and occurring up to six or seven miles (Habgood 1963). These dykes cut Basement Complex rocks and product easily seen on the ground and defected on the aerial photographs (Habgood 1963). But individual dykes are rarely more than 40 feet wide (Habgood 1963). The dykes are vertical and show little displacement where they are cut by the fault (Habgood 1963). The result of this displacement is jointing in dolerites which makes it blocky and solid (Habgood 1963). The swarm is almost certainly from Stormberg age (Habgood 1963). The dolerites are fine-grained but in larger dykes they are coarser (Habgood 1963). They are ophitic and typically holocrystalline except in the chilled phases (Habgood 1963). Magnetite is abundant as cubes and octahedral crystals (Habgood 1963).

Dykes and sills intruded into the sediments

Dykes are intruded along most of major faults; but as mentioned before, they are most common in Coal Shales and Lower Sandstones outcrop, especially south of Nkombedzi River (Habgood 1963). They are generally thin, and occupy a small portion of the fault zone (Habgood 1963). When faulting causes enough width of gouge, it is filled with large irregular bodies of altered dolerite (Habgood 1963). Dykes occupying Panga fault are the longest in the area (Habgood 1963). They tend to increase in width southwards and may have been one of the feeding channels for the plateau lavas (Habgood 1963). Dykes have been crushed (due to renewal of movement along the containing faults) and jointed, have been exposed to more weathering than what occurred in sediments, so they occupy depressions which are covered by alluvium (Habgood 1963). The dolerite of the dykes is usually blue-black, dense and compact, weathering to form a thin red crust; except in Coal Shales, in which dyke-rocks are very frequently bleached to a yellow-brown color and thinly veined with crystalline calcite (Habgood 1963). The dyke rocks are normal labrodorite-pyroxene-dolerites that have

experienced alteration (Habgood 1963). Different intrusive bodies show all stages of soda metasomatism from fresh dolerite to albitized-diorite and the alteration can be pneumatolysis, occurring where intruded rock is more or less impermeable and has prevented the escape of the groundwater and caused its solution in the magma (Habgood 1963). Where dolerite dykes cut the Coal Shales, the feldspar is frequently albitized and fresh while the ferro-magnesian minerals have been more or less replaced by iron oxides or calcite (Habgood 1963).

Numerous **sills** occur in the sediments and are especially frequent in the Coal Shales (Habgood 1963). Their thickness varies from a couple of centimeters to a 100 meter (Habgood 1963). They are frequently displaced by faults, showing movement was resumed after their intrusion (Habgood 1963). The bodies intruded into Mwanza Shales and Grits, the Red Beds and the Upper Sandstones tend to be much less regular in form due to relatively poorly developed bedding in these formations (Habgood 1963). The sills are similar to the dykes but in the thicker bodies, coarser material is occasionally developed and amygdules are sometimes formed (Habgood 1963). Alteration of dolerites is similar to dykes; formation of albitized-diorite is also common especially in bodies intrusive into carbonaceous shales (Habgood 1963). In Coal Shales formation the majority of sills are intruded into beds of carbonaceous shales and almost all acquired the yellow-brown color and the petrological characters of diorite dykes (Habgood 1963).

Cretaceous System

The Middle Jurassic to Cretaceous was a transition period between the Karroo rifting and the formation of recent East African Rift System (Castaing 1990).

The Lupata Series

They overlie the Karroo formation unconformably and consist of a succession of pebbly conglomerates, coarse sandstones, sandy shales and marls, all fairly calcareous and characterized by a pink to brick-red color (Habgood 1963). The formations are extremely ill-sorted and contain pebbles of basalt and basaltic glass with angular fragments of quartz, quartzite, feldspar of local origin (autochthon) and large rounded fragments of hornblende- and biotite-gneiss (Habgood 1963). The cement is normally crystalline calcite with some iron staining but this is frequently replaced by quartz in optical continuity (Habgood 1963). The

general massive and soft nature of the sediments makes it very difficult to see the structure, thickness and cuttings by faults (Habgood 1963).

The outcrop of sandstones gives rise to dry infertile country and vegetation characteristic of saline groundwater (Habgood 1963).

The Calcareous Siliceous Fault Rocks

There are hydrothermal fault rock associated with the Karroo boundary faults and with all major and many of minor fractures cutting the area (Habgood 1963). It is commonly associated with faults cutting the Karroo and it occurs as coarsely crystalline calcite, as white and colorless quartz reef or as banded siliceous glass (Habgood 1963).

Superficial Deposits

A large part of the Shire valley is covered by unconsolidated quaternary alluvium which are highly variable, interdigitating sequences of clays, silts, sands and occasional gravels (Maida 1985, Mkandawire 2002), all of which have alluvial origin (Habgood 1963). Much of the infilling of the valley is pedisegment deposit, a result of downhill movement, debris, rain wash and stream action (Habgood 1963). The variation in the soil types in the area is undoubtedly significant; Maida (1985) has obtained the ranges of 8-25% silt and 15-65% clay for in the middle of Chikwawa district (in Ngabu).

Alluvial sand and silt from northwest of Shire valley contain green hornblende (Habgood 1963). The mineral assemblage of sand shows that their origin is the hornblende-rich Precambrian gneiss from north of Mwanza fault (Habgood 1963). In the south of the terrace alluvium, a reddish-brown gritty loam replaces the silt and sand to the north, and is bordered on west by Lupata Sandstones (Habgood 1963). The loam's assemblage and the presence of calcareous nodules suggest that the drift derives from Lupata Sandstone formation, which itself is derived from the local Precambrian rocks (Habgood 1963). The sands contain magnetite, hematite, and pyroxenes among heavy minerals and labradorite (Habgood 1963). Quartz, in subgranular to fairly well rounded grains dominates the light minerals (Habgood 1963).

Topography

Malawi has a wide range of relief, which strongly influence climate, hydrology, occurrence of groundwater and population distribution (Mkandawire 2002). The Shire valley consists of a flat floodplain within tens of kilometers of the river (Habgood 1963), but the rift valley escarpment areas fall steeply from the plateau areas and slopes are often very dissected (Mkandawire 2002).

Topography of the region is illustrated in Figure 8.

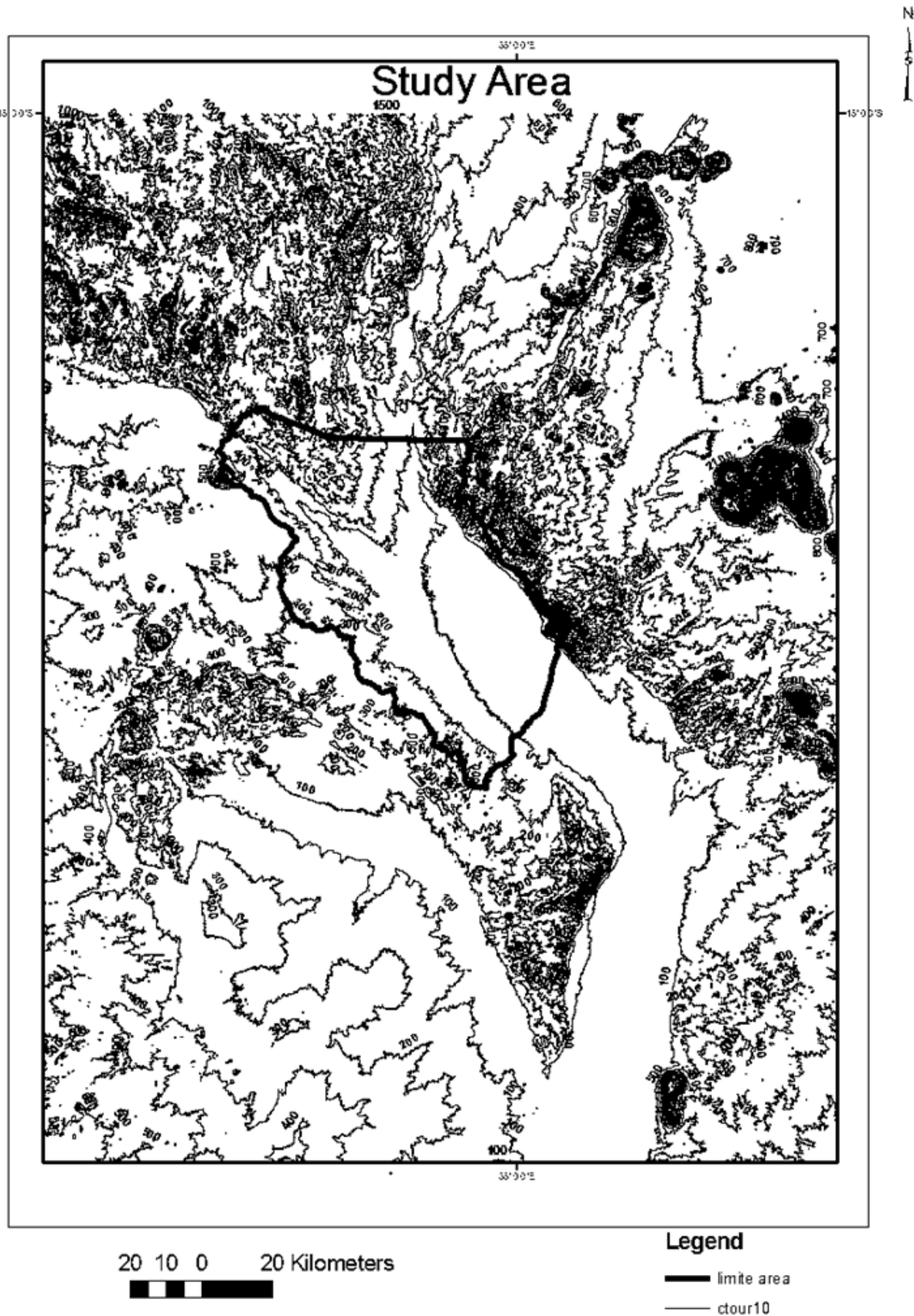


Figure 8. District of Chikwawa on the topographic map of the region with contour lines for elevation in m.a.s.l. with the interval of 100m

Hydrology

Precipitation and temperature

In Malawi 95% of the annual precipitation occurs in the rainy season from November till April, while the rest of the year is dry season (Malawi-Meteorological-Services 2006). The annual average precipitation in Malawi varies from 725 to 2500mm, and maximum annual precipitation occurs along Lake Malawi and in a few distinct areas in the south-east (Malawi-Meteorological-Services 2006). Figure 9 shows the distribution of the average annual precipitation in the country:

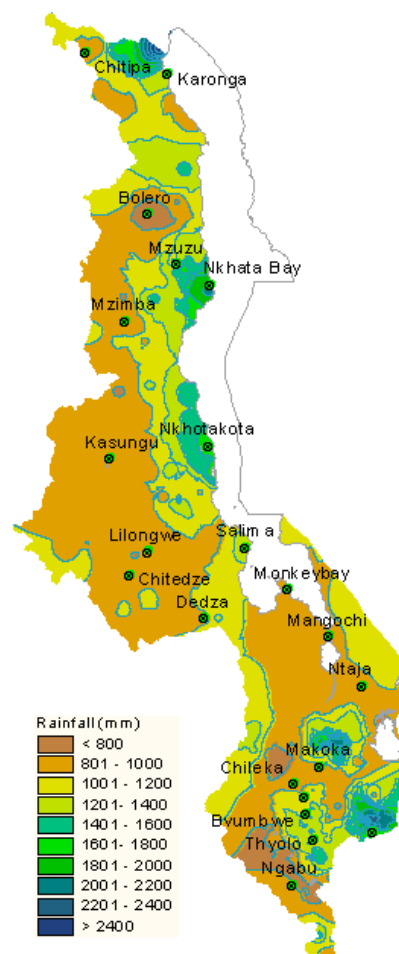


Figure 9. *Distribution of average annual precipitation in Malawi in mm (Malawi-Meteorological-Services 2006)*

The cool and dry winter lasts from May to August, with mean temperatures ranging from 17 to 27°C (Malawi-Meteorological-Services 2006). September and October are the hottest and

driest months of the year with mean temperature of 25 to 37°C (Malawi-Meteorological-Services 2006).

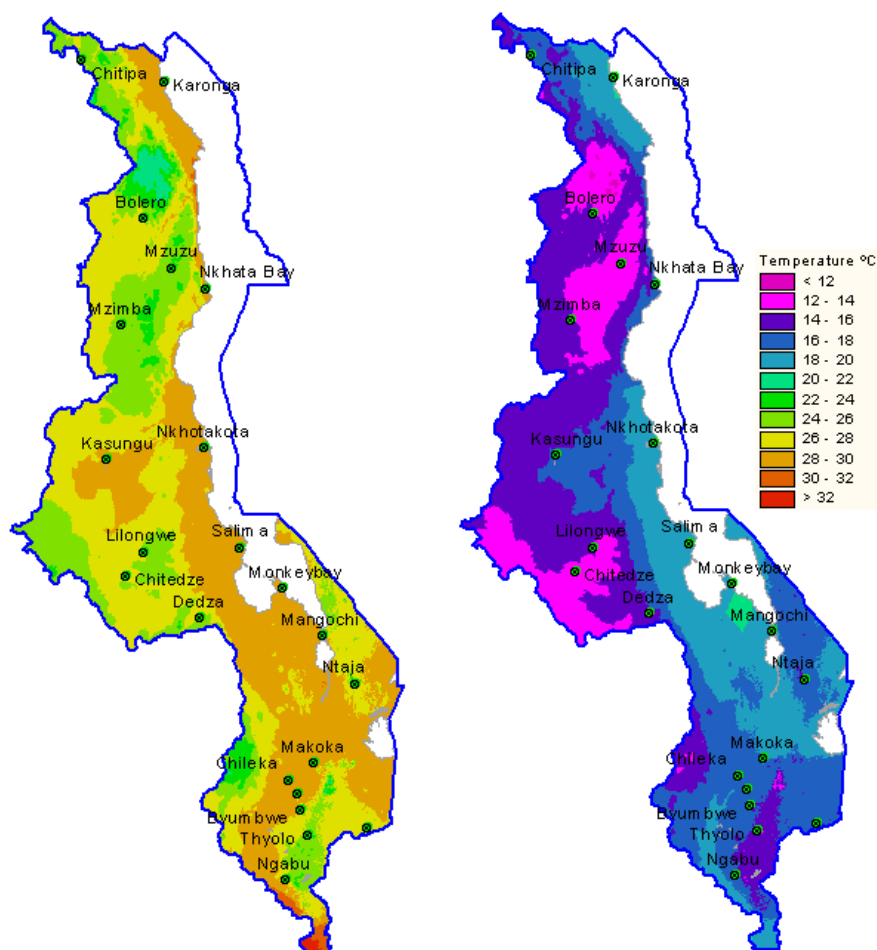


Figure 10. *Distribution of minimum and maximum annual temperature in Malawi (°C)*
(Malawi-Meteorological-Services 2006)

Chikwawa district receives the mean annual rainfall of 1150–1240 mm per year while monthly mean temperatures range from 27°C to 30°C (Staines 2002).

Shire River

Shire River is 402 km long and issues from the southern shore of Lake Malawi, of which it is the only outlet. Where Shire then enters its valley, between Matope and Chikwawa, it drops 384 m through 80 km of gorges and cataracts, falling successively over Kholombidzo (formerly Murchison) Falls, Nkula Falls, and Tedzani Falls, through the Mpatamanga Gorge,

and over Hamilton Falls and Kapichira (formerly Livingstone) Falls. Dams at Nkula Falls and Tedzani Falls, northwest of Blantyre, harness the river's waters for hydroelectric power (Encyclopædia-Britannica 2011). Below Chikwawa the river enters a wide marshy extension of the Mozambique coastal plain, the only area of Malawi below an elevation of 150 m. The lower Shire River valley's borders are distinct only to the northeast (the Cholo Escarpment) and the southwest (the Nsanje Hills). The chief tributary, the Ruo River, joins the main stream in the lower valley, forming a narrow levee on which the village of Chiromo is located. The replenished waters then pass through Elephant Marsh (414 square km) and Ndindi Marsh on a tortuous lower course to the confluence with the Zambezi River 48 km below Cena (Sena), Mozambique (Encyclopædia-Britannica 2011).

The Shire River's flow was formerly totally dependent upon the level of Lake Malawi and the varying volume of the Ruo River; but a dam has been built at Liwonde in order to regulate the flow from Lake Malawi through the hydroelectric stations and to provide flood control in the lower reaches (Encyclopædia-Britannica 2011).

There is not much data on the hydrology of the river other than the understanding that within Chikwawa district, the river has the altitude 50 m.a.s.l. Generally, depending on the time of the year and the location, the mean monthly discharge in the river can vary from 300 to more than 600 (m^3/s) (Glad 2010) and During the rainy season the lower part of the valley floor experiences annual flooding, mainly from the Shire River (Monjerezi et al. 2011). Moreover, a little upstream from the lower Shire valley, the measurements result in a baseflow index (BFI) of 0.42 (Palamuleni 2010). This means that the baseflow (groundwater discharge into the river) is responsible for 42% of the total river discharge.

Groundwater

The low rainfall, porous nature of the soil and the flatness of the terrain cause surface water supplies to be completely inadequate (Habgood 1963). Groundwater resources in Malawi occur mainly in three aquifers namely basement complex, fractured and fault zones, and alluvial formations (Mkandawire 2002). The piezometric level generally follows the topography, and it has been suggested that the groundwater is under unconfined to confined conditions (Mkandawire 2002).

The groundwater table's seasonal fluctuations are generally estimated as 1-5 m in Malawi (Chilton and Smith-Carington 1984). Monitoring the groundwater level with autographic recorders at several sites, Chilton & Smith Carington (1984) obtained seasonal fluctuations of 1-3.5 m for weathered basement aquifers. As for the alluvial basins, the groundwater level fluctuates by about 1-3 m on a seasonal basis (Mandeville and Batchelor 1990).

Hot springs are found along the Mwanza Fault, representing the most recent stages of the Cretaceous hydrothermal activity (Cooper and Bloomfield 1961)

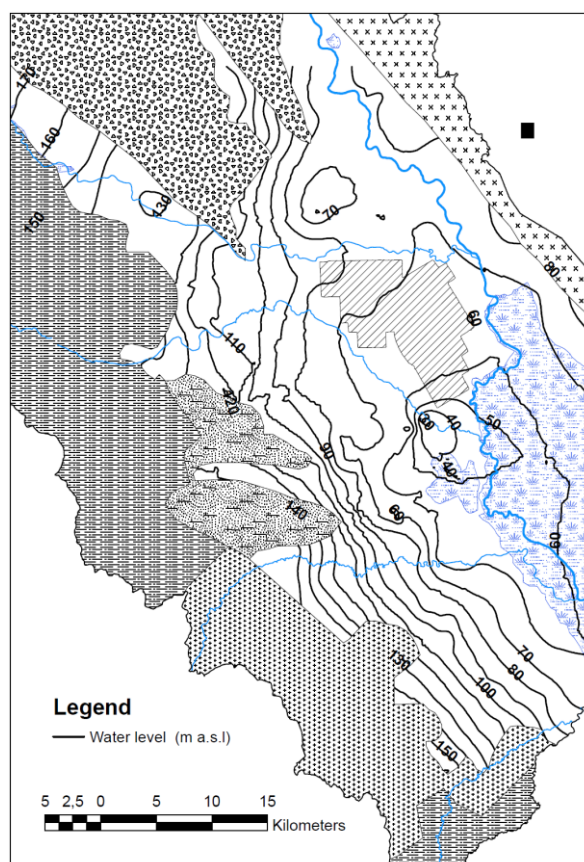


Figure 11. *Groundwater level (m.a.s.l) in the alluvium, interpolated based on observations from boreholes (Monjerezi et al. 2011)*

In general, the water level contours display a regime of groundwater flow towards the Shire River. It seems that at one point the groundwater table decreases even below the river's level (50 m.a.s.l). It could be possible that the river is partially influent in that area; or more probably this low point is caused by incorrect observed head of 16.76 from one single located there (borehole 188 in Appendix C) which is discussed again later in the results part.

DATA

Precipitation

The precipitation data available is on daily basis from 10/10/1978 to 31/12/2008 and obtained from 23 meteorological stations in Malawi, but there are a lot of gaps in the data ranging from some days to several years. For the complete precipitation record please see Appendix A.

Of 23 stations available, 5 are within or close enough to the area, as shown in the figure below:

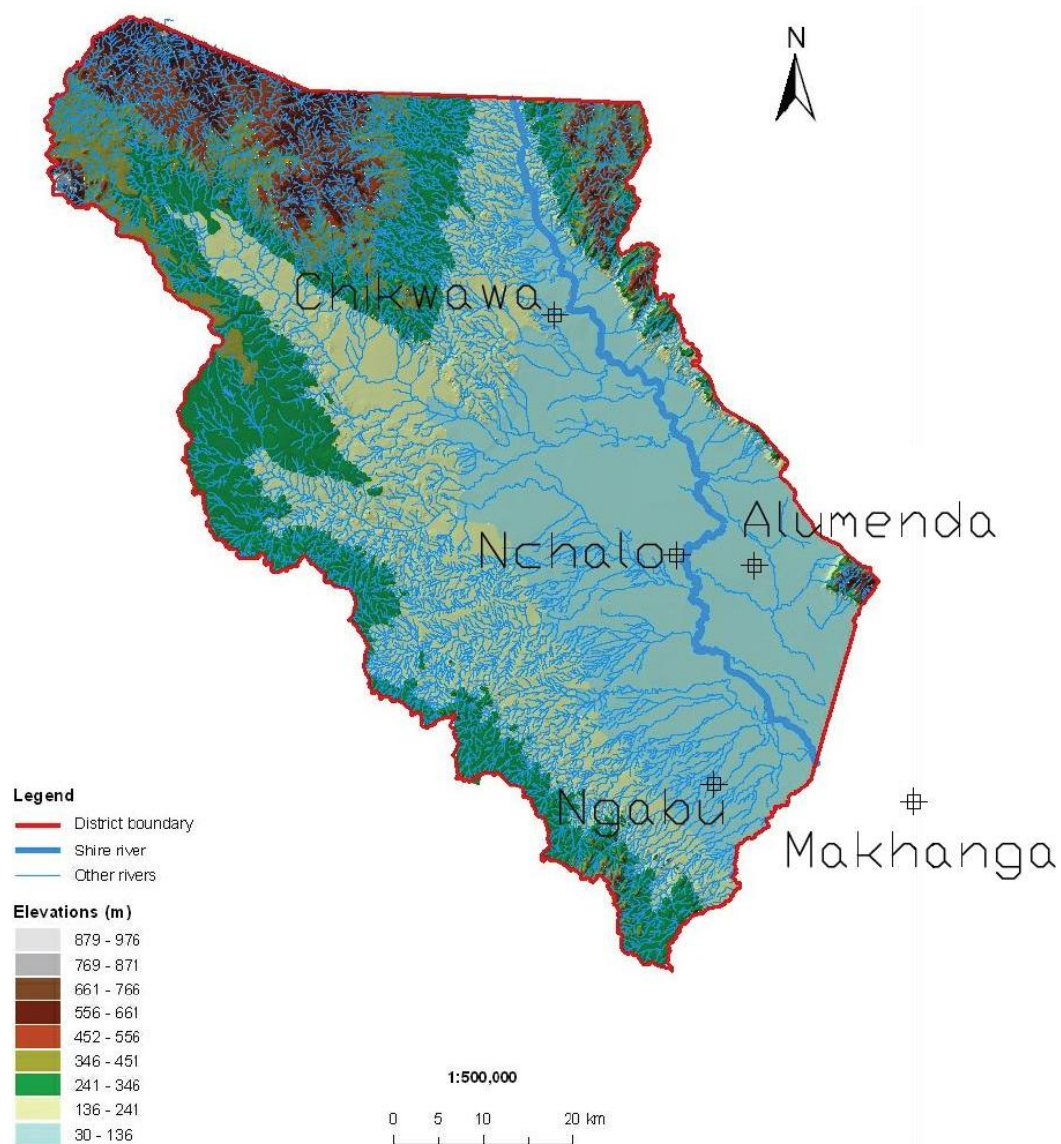


Figure 12. Meteorological stations within or near the Chikwawa district. Elevations illustrated by colors

The elevation and UTM coordinations of the stations are listed in table 4.

Table 4. UTM coordination and altitude of the meteorological stations

Station	Easting	Northing	Altitude (m.a.s.l)
Chikwawa	690442.7	8226929	107
Nchalo	705178.3	8200235	52
Alumenda	712650.5	8199056	58
Ngabu	708140.7	8174749	102
Makhanga	729473	8172319	76

The precipitation record for the 5 meteorological stations is available for a 2 years period from May 2000 to April 2002:

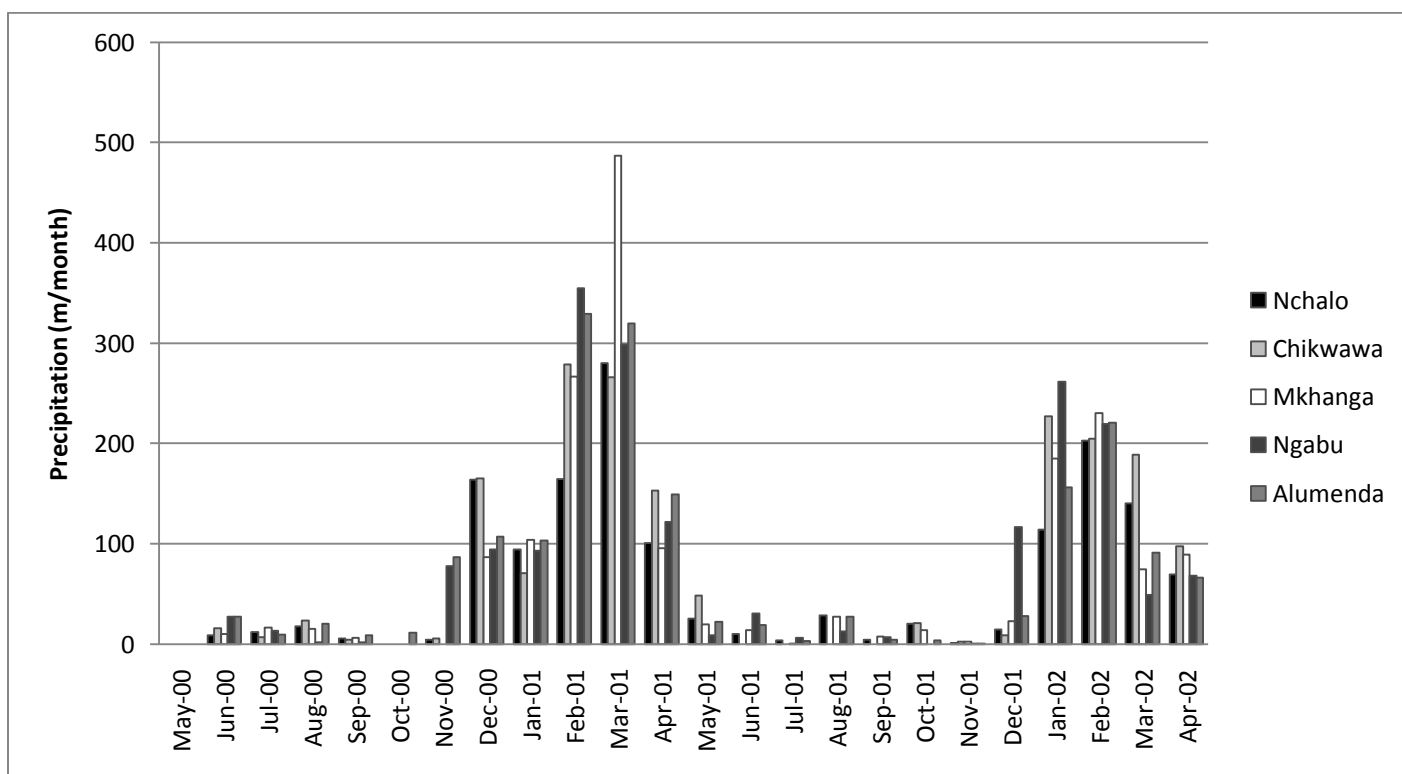


Figure 13. Precipitation data in the period of May 2000 to April 2002

Which shows the two periods of dry and rainy season for every year.

Temperature

The temperature record is only available for the stations Nchalo, Makhanga and Alumenda, and only available in the form of maximum and minimum monthly temperatures (from January 1971 to December 2005). Therefore, it is assumed that the mean monthly temperature is equal to the average of maximum and minimum monthly temperatures. Moreover, the temperatures for Chikwawa and Ngabu are extrapolated from temperature in Nchalo, using the linear rate of -0.6°C per 100 meters increase in the altitude. For the temperature record please see to Appendix B.

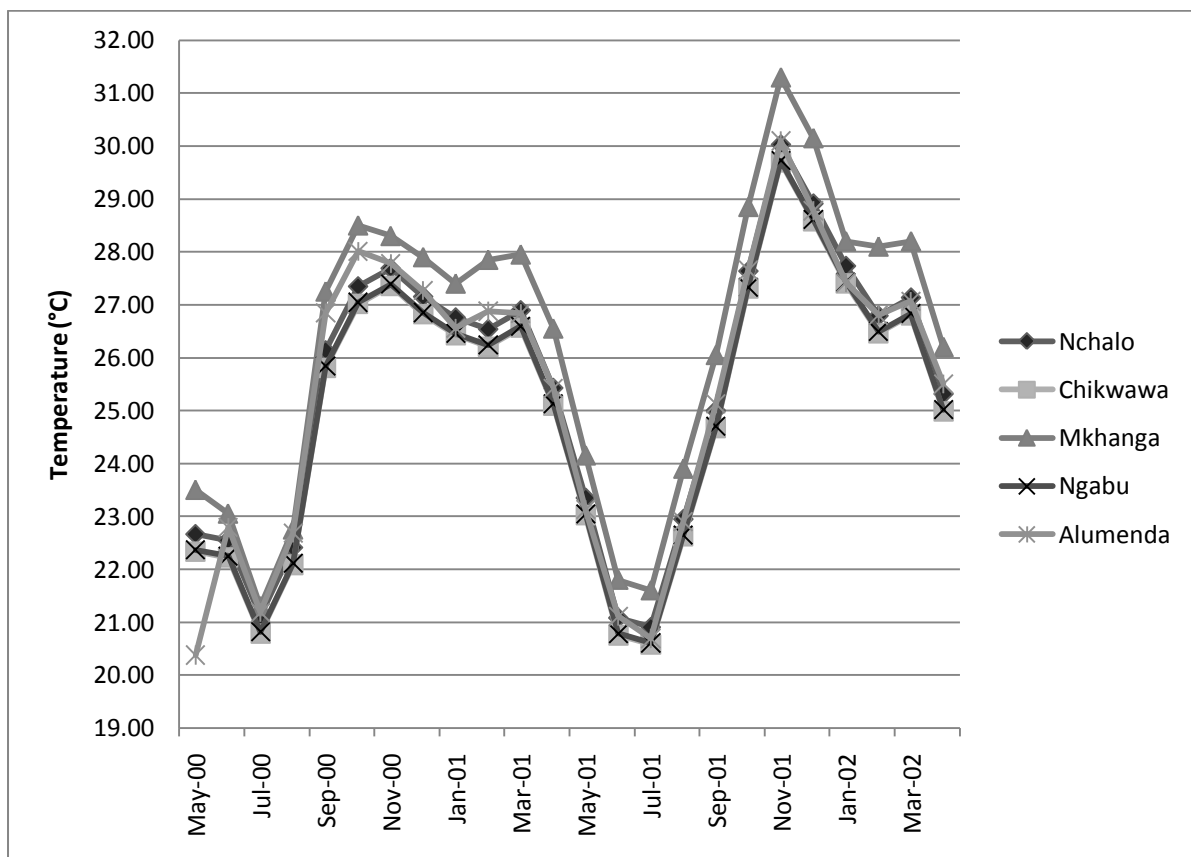


Figure 14. Average monthly temperature data for the stations in the period of May 2000 to April 2002 (data stations Chikwawa and Ngabu are extrapolated based on Nchalo's record)

Note that due to proximity of the elevations in Chikwawa and Ngabu, they appear almost identical on the chart.

The rainy season in 2001-2002 is perceived hotter and drier than 2000-2001.

Boreholes

The groundwater level observations are obtained from the 305 boreholes in the district of Chikwawa. The data is not of the best quality since the observations are made in different times of the year, and in different years (apparently from 1973 to 2008 though the data are not dated). It is understood that at least some, if not all of these boreholes are used by local people for drinking, washing and (in case of high salinity) extracting salt.

An interpolation based on the data from boreholes gives a first impression of the groundwater table, and later on is used for definition of model boundaries.

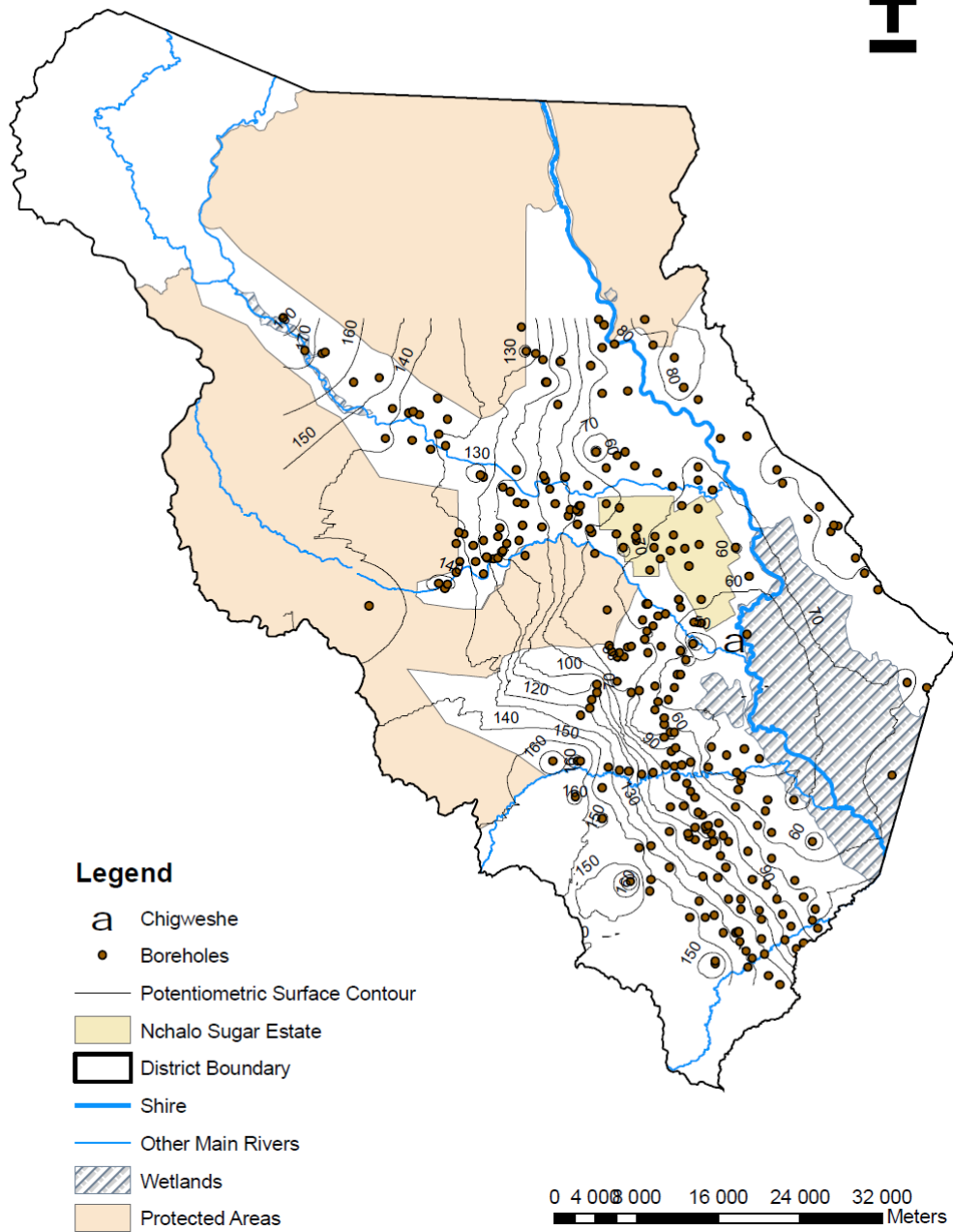


Figure 15. Boreholes in the Chikwawa district with groundwater level interpolation based on observations from them. Contour lines for groundwater head are in m.a.s.l.

As will be explained later, 263 of the 305 boreholes are located within the modelled area. For more information on boreholes please see Appendix C.

MODEL

The process of groundwater modelling is basically solving a partial differential equation explaining the water flow through a porous medium (soil, fractured rock, etc.) as below:

$$\frac{\partial}{\partial x} \left(K_{xx} \frac{dh}{dx} \right) + \frac{\partial}{\partial y} \left(K_{yy} \frac{dh}{dy} \right) + \frac{\partial}{\partial z} \left(K_{zz} \frac{dh}{dz} \right) - W = S_s \frac{\partial h}{\partial t} \quad (1)$$

Where K_{xx} , K_{yy} and K_{zz} are values of hydraulic conductivity along respectively the x, y and z axes [LT^{-1}];

h is the potentiometric head [L];

W is the volumetric flux per unit volume and represents sources and/or sinks of water [T^{-1}];

S_s is the specific storage of the porous medium [L^{-1}];

And t is the time [T].

Equation (1) can be simplified in case of homogeneous (constant K) or isotropic ($K_{xx}=K_{yy}=K_{zz}$) medium. The term $S_s \frac{\partial h}{\partial t}$ also matters only in the transient flow simulations; i.e. when the groundwater pattern is variable in time (e.g. seasonal fluctuation). This term is however regarded zero in steady state simulations which are time independent.

There is no general analytical solution for the equation (1). But it is always possible to use a digital groundwater flow model in order to numerically solve it. The numerical solution is by its nature never impossible, just too time consuming to be done manually. This makes computer programs the best tool for numerical solutions. The two different methods in numerical solution are "finite element" and "finite difference" methods. In finite element method the area is divided into triangles, Heads are defined at any point within an element by an interpolation function, material properties are defined element by element, continuity is fulfilled at every side of the element and velocities are determined from derivatives of the head distribution and element properties. While in finite difference method the area is meshed into square shape cells, material properties are defined for each cell, hydraulic heads and continuity are considered for every cell's center and velocities are determined from fluxes between adjacent cells.



Figure 16. *Model's shape in Finite element (right) and Finite difference (left)*

The commercial modelling software used in this thesis is Processing MODFLOW 5.3.1 (PMWIN), which uses finite difference method, so it represents the aquifer system by a sequence of layers each meshed into rows and columns. The software assumes that all properties are constant within each cell and hydraulic heads are calculated at the center point of each cell. With N number of cells in a model, there are N simultaneous equations to be solved.

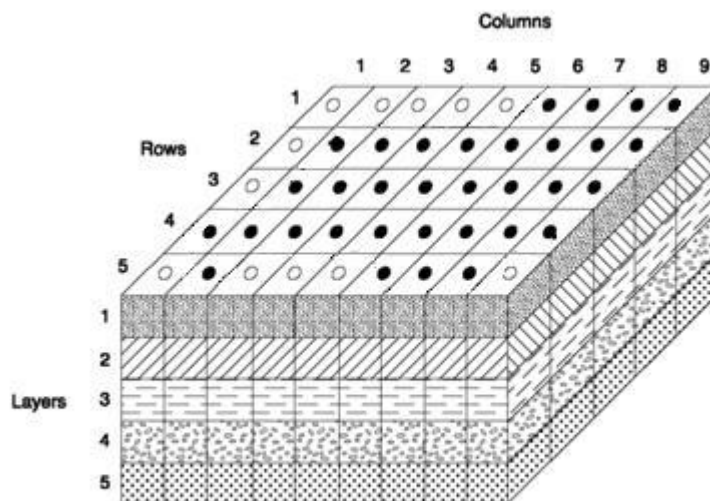


Figure 17. *MODFLOW's representation of the aquifer (black and white nodes respectively represent active and inactive cells and the interface between them is the model's boundary) (Chiang and Kinzelbach 2001)*

The assumption that the properties within each cell remain constant in the finite difference method, simplifies the terms such as $\frac{\partial h}{\partial x}$ and $\frac{\partial h}{\partial t}$ and makes it possible for the software to calculate h for each cell based on the value of h from the previous one (previous cell and/or previous time step). In order to have a starting point, the software needs initial and boundary conditions. There are three types of boundary conditions: Dirichlet type in which the head is known (special case: constant head), Newman type in which the head gradient is

known (special case: no flow boundary or zero hydraulic gradient) and Cauchy type which is combination of the previous two.

The initial conditions are the head distribution in the time zero, which is needed for the transient flow model.

Model's geometry

The problematic area in the western side of the Shire River is defined into the model as a one layer unconfined aquifer as big as 2941 Km² with mesh size of 1 km by 1 km.

Elevation of the top of the aquifer is defined based on the topographical maps using the mean value between each two contour lines (e.g. 150 for the interval between 100 and 200). However, an unconfined aquifer is not sensitive to the values for elevation of the top of the layer.

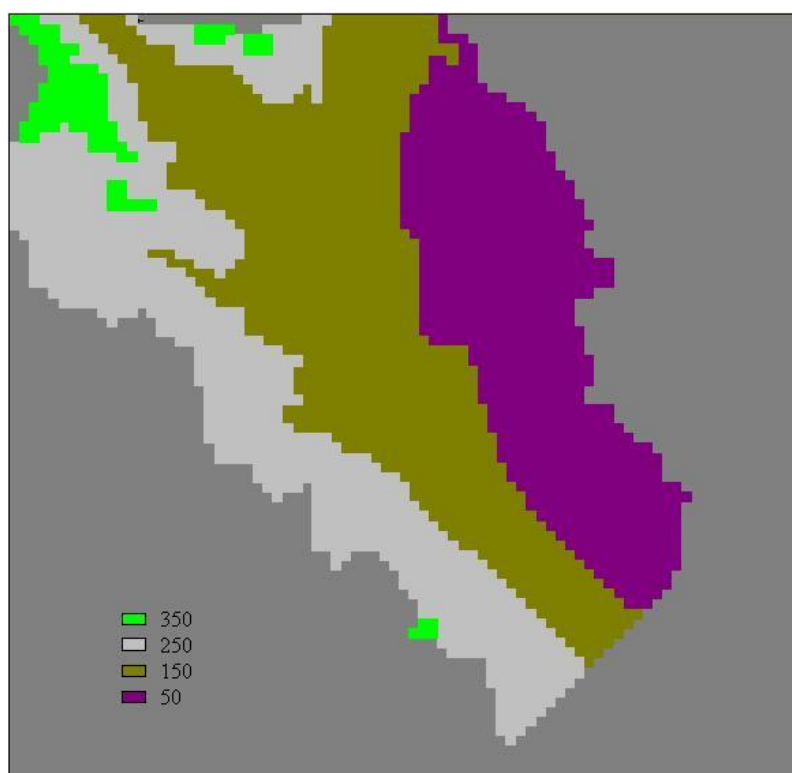


Figure 18. *Elevation of top of the aquifer defined for the model (m.a.s.l) based on the topographical maps*

In the absence of geophysical data, the elevation of the bottom of the aquifer is unknown; therefore the safest assumption for the bottom of aquifer is the simplest, which is a constant value for all cells. The value for the elevation of bottom is defined -150 m.a.s.l after

some trial and error with respect to the best fit with fixed values for other parameters. The total depth of the aquifer varies from 200 to 400 meters, which is reasonable compared to the size of the area.

Boundaries

In the east, the Shire River is a Dirichlet type boundary with a constant head. As for the model boundary in the west, groundwater divide between the two basins of Shire and Zambezi rivers is a no flow boundary (Newman) for the model.

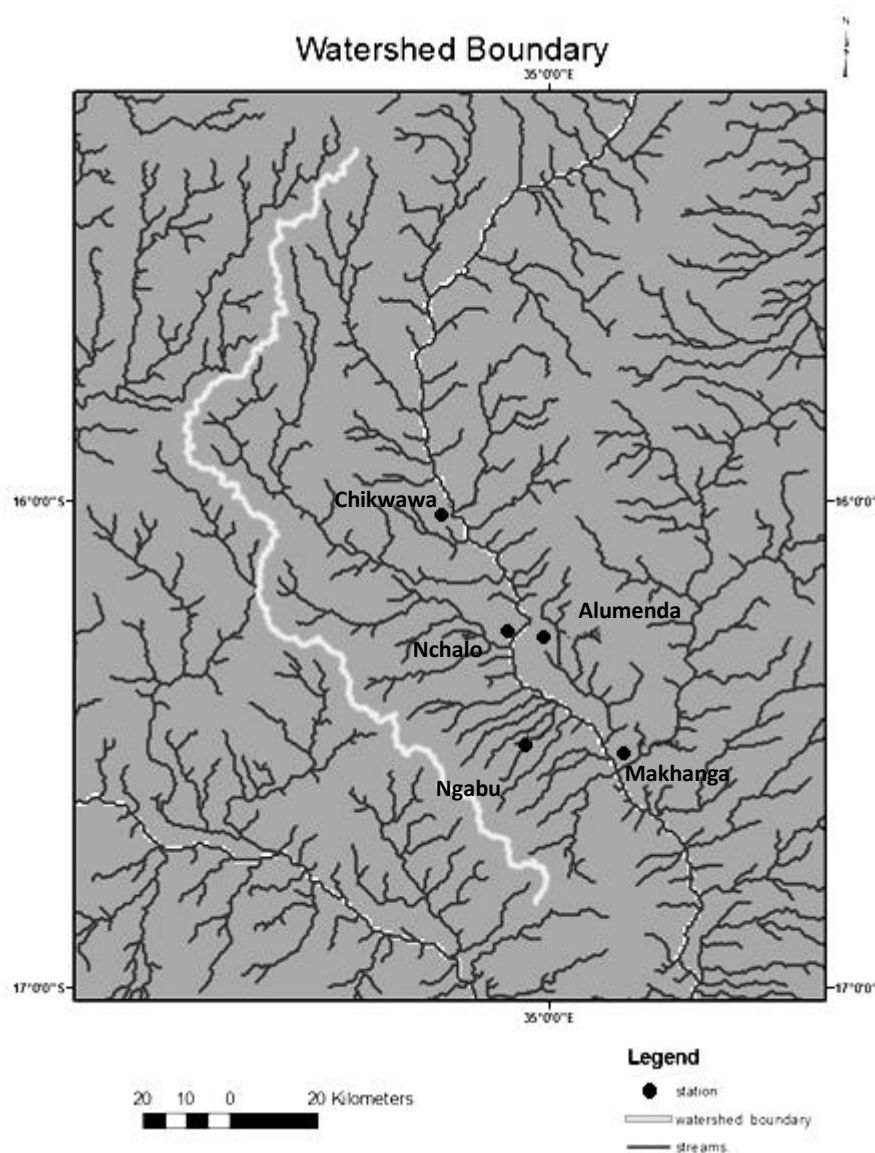


Figure 19. Watershed boundary between Shire River (on the East) and Zambezi River (on the West) used as no flow boundary in the model. Meteorological stations are also shown on the map

In the north and south, a no flow boundary is estimated using the interpolated head contour lines that were obtained from observations from boreholes (Figure 20).

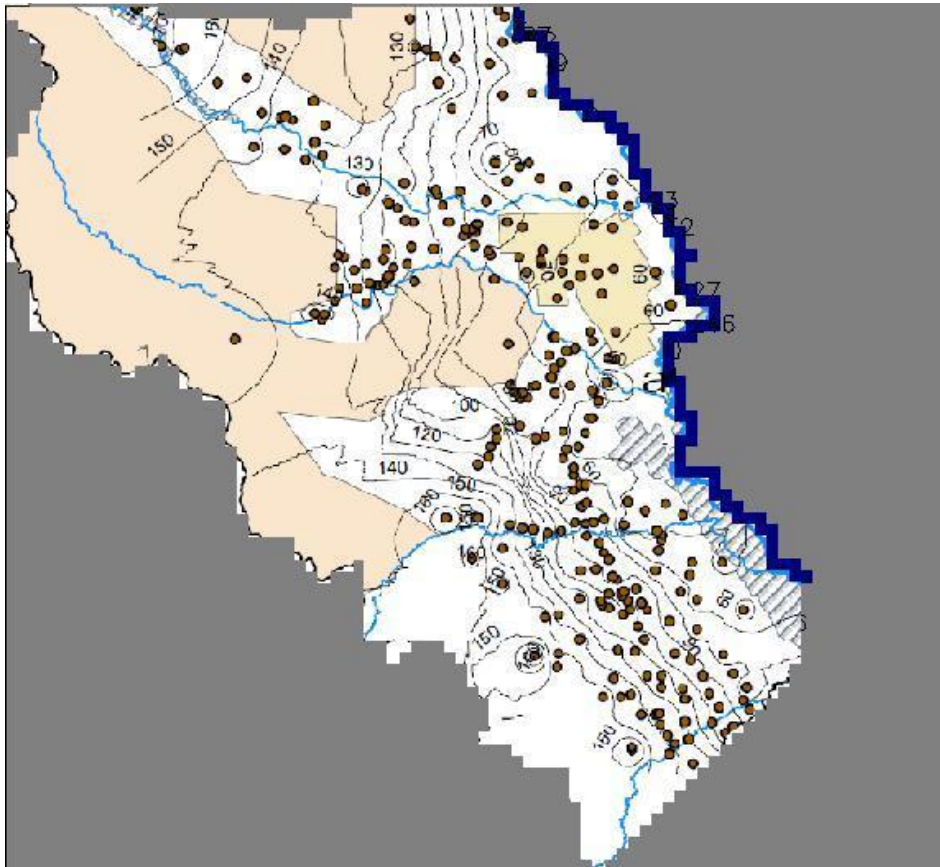


Figure 20. *Interpolated hydraulic head contour lines used in order to define no flow boundaries in North and South for the model*

With these boundaries, the area is complete. Out of the 305 boreholes with available data, 263 of them are within the defined area. Appendix C includes the list of active and inactive boreholes for the model along with their coordination and observed hydraulic head.

Areal Recharge

Recharge is defined as the downward flow of water reaching the water table, adding to groundwater storage (Healy 2010). Generally, the selection of methods for estimating recharge depends on goal of the study, the budget, and the available data.

Methods for estimating recharge

Healy (2010) has collected the methods based on the basis of types of required or available data, and presents the following groups in his book “Estimating Groundwater Recharge”:

Water budget methods

These methods are based on the water balance of one or more control volumes (in soil, atmosphere, etc.) for study (Healy 2010). Any control volume whose water-budget equation contains recharge as a component can be used to estimate recharge. A water budget equation for a unit soil is very common to use (Healy 2010).

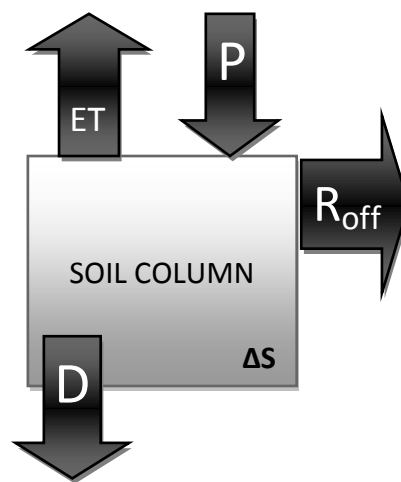


Figure 21. Schematic diagram showing water budget for a one-dimensional soil column. D is drainage out the bottom of the column, which is equal to groundwater recharge, P is precipitation, ET is evapotranspiration, R_{off} is runoff and ΔS is change in the storage (Healy 2010)

The methods are different from each other by their approach for calculating/measuring the terms in the water balance. In order to simplify, ΔS can be neglected by choosing the time period as one year, or a period in full years. P and R_{off} can be measured. As for evapotranspiration, there are several ways to calculate or measure it. Potential evapotranspiration can be calculated from pan evaporation measured in meteorological stations. Other methods can be grouped into five categories: water budget, mass-transfer, combination, radiation, and temperature-based (Xu and Singh 2002). The choice between methods can be made based on the available data, for example Penman-Monteith equation requires data from radiation, soil-heat flux, humidity, aerial boundary layer and total canopy resistance; while Thornthwaite (1948) is based on temperature data.

Due to the universal nature of water balance, many (if not most) methods for estimating recharge are based on some form of water budget equation (Healy 2010). They can be applied over the wide range of space and time scales and the lack of assumptions on the mechanisms that drive the individual components in a water-budget equation provides these methods with additional flexibility (Healy 2010).

The accuracy of the estimated recharge is dependent on the accuracy with which the other components in the water budget can be determined (Healy 2010). This is particularly important when the magnitude of recharge is small relative to that of the other variables (Healy 2010).

Modelling methods (Healy 2010)

Simulation models are widely used in all types of hydrologic studies, and many of these models can be used to estimate recharge. The predictive capability of models can be used to evaluate how changes in climate, water use, land use, and other factors may affect recharge rate. Inverse modelling can be used to quantify the uncertainty in model predicted recharge rates if the model accurately represents the hydrological system. Because of the difficulties of setting up a complex watershed or groundwater-flow model, one should conduct an evaluation a priori to determine whether the benefits obtained from a model justify the costs that will be incurred.

Methods based on surface-water data (Healy 2010)

Streamflow data are commonly used to estimate recharge rates in humid and sub-humid regions, partially due to the abundance of streamflow data and the availability of computer programs for analyzing them. The methods estimate exchange rates between groundwater and surface-water, which can be from stream to groundwater (losing stream), or vice versa (gaining stream). These methods are similar in the way that they all require data on streamflow, stream stage or surface-water chemistry.

Physical methods (saturated and unsaturated zones) (Healy 2010)

Estimates of recharge can be obtained from measurement of downward water flux or change in water storage within the unsaturated zone, or measurement of groundwater level over time and space. These methods all require field work. Recharge estimation methods that are based on measurements of groundwater levels are especially widely used because

of the ease with which they can be applied and the abundance of available data in local, state and federal databases.

Chemical tracer methods (Healy 2010)

Tracers have a wide variety of uses in hydrologic studies: providing quantitative or qualitative estimates of recharge, identifying sources of recharge, providing information on velocities and travel times of water movement. The most commonly used natural environmental tracer is chloride. Other tracers in this category include chlorine-36 and tritium. Chemical tracer methods of course require field work.

Heat tracer methods (Healy 2010)

As with chemical and isotopic tracers, spatial or temporal trends in surface and subsurface temperatures can be used to infer rates of water movement. Temperature can be measured accurately, economically and with high frequencies, which makes heat an attractive tracer. Analytical and numerical models are also useful to simulate heat flow, and be calibrated based on measurements.

Thornthwaite method

Calculation of potential evapotranspiration

In the late 1940s and through 1950s C. W. Thornthwaite and colleagues at the Laboratory for Climatology of Drexel University developed a systematic approach to identify relations among precipitation, potential evapotranspiration and actual evapotranspiration in a study of watershed water budgets (Healy 2010). This approach laid the foundation for the development of watershed models in the following decades (Healy 2010). Since the Thornthwaite method requires only air temperature and precipitation data (soil moisture measurements can be used too if available), it is used in this study.

In the Thornthwaite method mean monthly temperature is correlated with evapotranspiration as determined from a water balance for valleys where sufficient moisture water was available to maintain active transpiration (Xu and Chen 2005).

The method includes the following steps, explained by Xu & Chen (2005):

Step 1: the annual value of the heat index I is calculated by summing monthly indices over a 12 month period. The monthly indices are calculated as below:

$$i = \left(\frac{T_a}{5}\right)^{1.51} \quad (2a)$$

$$I = \sum_{j=1}^{12} i_j \quad (2b)$$

In which i_j is the monthly heat index for the month j and should always be equal to or greater than zero. T_a (°C) is the mean monthly temperature and j is the number of months (1 to 12).

Step 2: unadjusted monthly values of potential evapotranspiration ET'_p (mm) is calculated based on a standard month 30 days, with 12 h of sunlight per day:

$$ET'_p = C \left(\frac{10T_a}{I}\right)^a \quad (3)$$

In which C is a constant and is equal to 16, and $a = 67.5 \times 10^{-8}I^3 - 77.1 \times 10^{-6}I^2 + 0.0179I + 0.492$

Step 3: ET'_p is adjusted depending on the number of days N in a month and the duration of average monthly or daily daylight d (h):

$$ET_p = ET'_p \frac{d}{12} \frac{N}{30} \quad (4)$$

Values for d in each month are linearly interpolated for the latitude 16°S based on values presented for latitudes 15°S and 20°S from FAO (1977). The resulting values of d are listed in table 5.

Table 5. *Values for duration of average monthly daylight, d (hours) linearly interpolated for latitude 16°S based on FAO (1977)*

month	D (hours)
January	12.64
February	12.22
March	11.78
April	11.36
May	11.14
June	11.24
July	11.58
August	12.00
September	12.52
October	12.86
November	13.06
December	12.96

Budgeting soil-moisture storage to yield surplus

Xu & Chen (2005) recommend using daily data for dry locations like the area of this study where the mean potential evapotranspiration may exceed or be higher than the mean precipitation. But in the absence of daily temperature record (and therefore daily potential evapotranspiration), soil water budget calculations are made using monthly rainfall totals.

For each time step (month) one of the three cases below is true (Xu and Chen 2005):

- $ET_p(t) > P(t)$, then soil water will be depleted to compensate the supply. At the same time, $ET_a(t) < ET_p(t)$ and surplus will be zero. The amount of $ET_a(t)$ is proportional to $W(t)/W^*$. In which W^* is the soil capacity or porosity \times depth of unsaturated zone. In order to avoid loops, it is safe to use $W(t-1)$ instead of $W(t)$.
- $ET_p(t) = P(t)$, then $ET_a(t) = ET_p(t)$ and surplus is zero.
- $ET_p(t) < P(t)$, then $ET_a(t) = ET_p(t)$. $W(t)$ is first estimated with surplus zero and when $W(t) > W^*$, surplus = $W(t) - W^*$; otherwise surplus will be zero.

Since the soil moisture in first time step $W(1)$ is unknown, Xu & Chen (2005) suggest a balancing routine to force the net change in the soil moisture from beginning to end in a N step period to zero. In order to do so, the initial soil moisture is set to W^* and the budget calculations are made up to the time step $N+1$ based on simple water balance equation below:

$$W(t) = W(t - 1) + P(t) - ET_a(t) \quad (5)$$

Then $W(1)$, the initial soil moisture at time 1, is set to the soil moisture at time $N+1$ and the budget is recomputed until the difference $W(1)-W(N+1)$ is small enough (less than 0.01 mm in this case)

The average W^* is assumed to be 200 mm, and the sensitivity of areal recharge to its value is later verified in the calculations. The surplus obtained is yet to be distributed between groundwater recharge and surface flow. Since in the Shire catchment (in area north from Chikwawa) 7.5% of precipitation turns into surface flow (Palamuleni 2010), it is assumed that the areal recharge to the groundwater is equal to surplus minus $0.075P$. The value $0.075P$ goes to the surface flow including the tributaries.

Theisen polygon

Theisen polygon method is originally an approach for areal estimation of precipitation based on data from meteorological stations by dividing the region among them and then calculating the average precipitation of the area by giving each station a weight proportional to its corresponding subregion. The subregions are obtained by drawing perpendicular bisectors of straight lines linking each pair of adjacent stations. In this study, it is used for making a semi-distributed recharge over the area.

Five stations Chikwawa, Nchalo and Ngabu are inside the modelled area, yet in Theisen polygon method stations Alumanda and Makhanga are also considered since they are very close to the Shire River. The resulting lines are shown in figure 22.

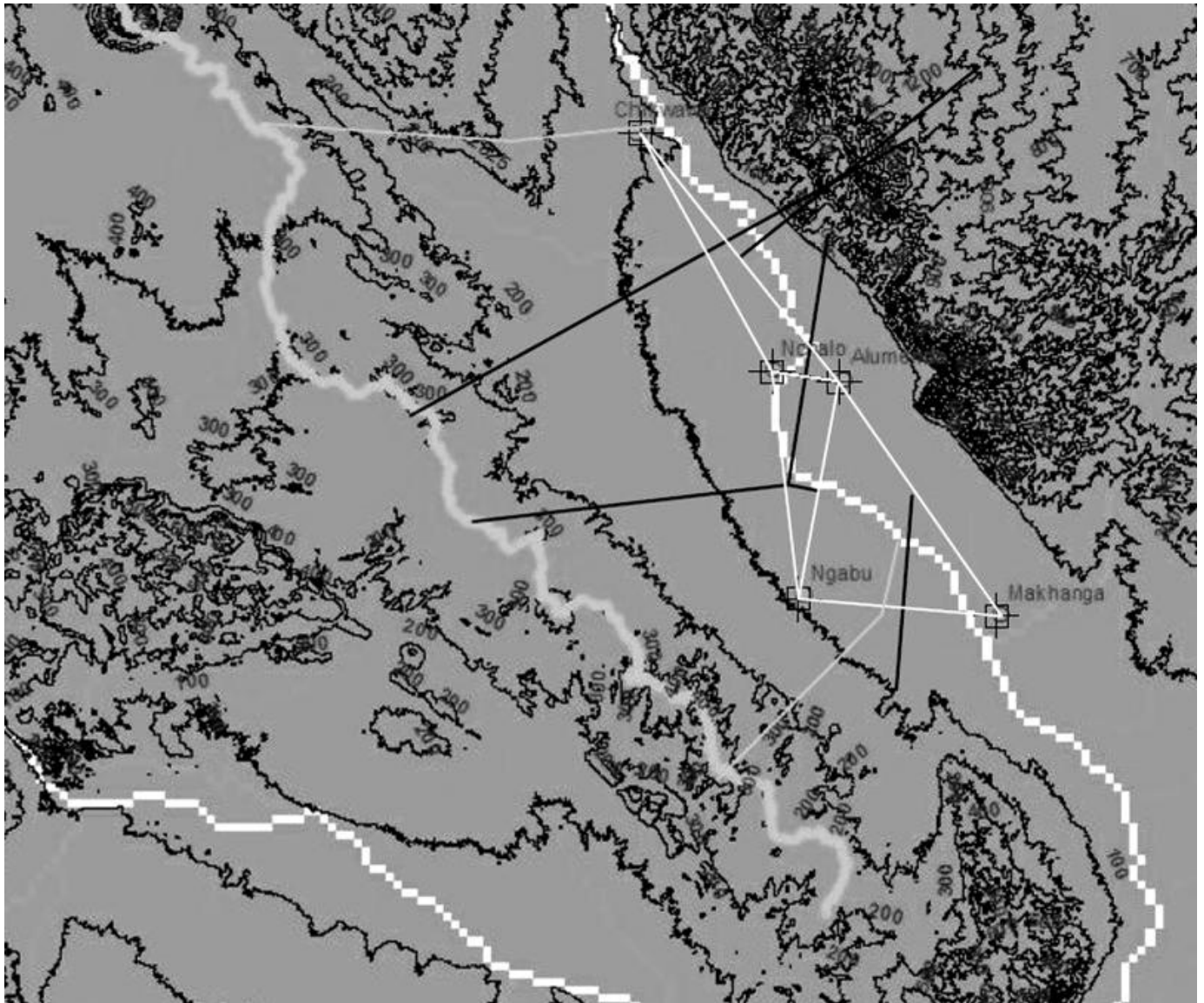


Figure 22. *Thiessen polygon method for the 5 stations within or near the area. The black lines are perpendicular bisectors of lines linking the stations (the white lines), which divide the area between Chikwawa, Nchalo and Ngabu and leave Makhanga and Alumenda out.*

Due to the geometry, the area corresponding to the stations Makhanga and Alumenda are obtained as zero. Therefore, the areal recharge distribution for the model is as illustrated in figure 23.

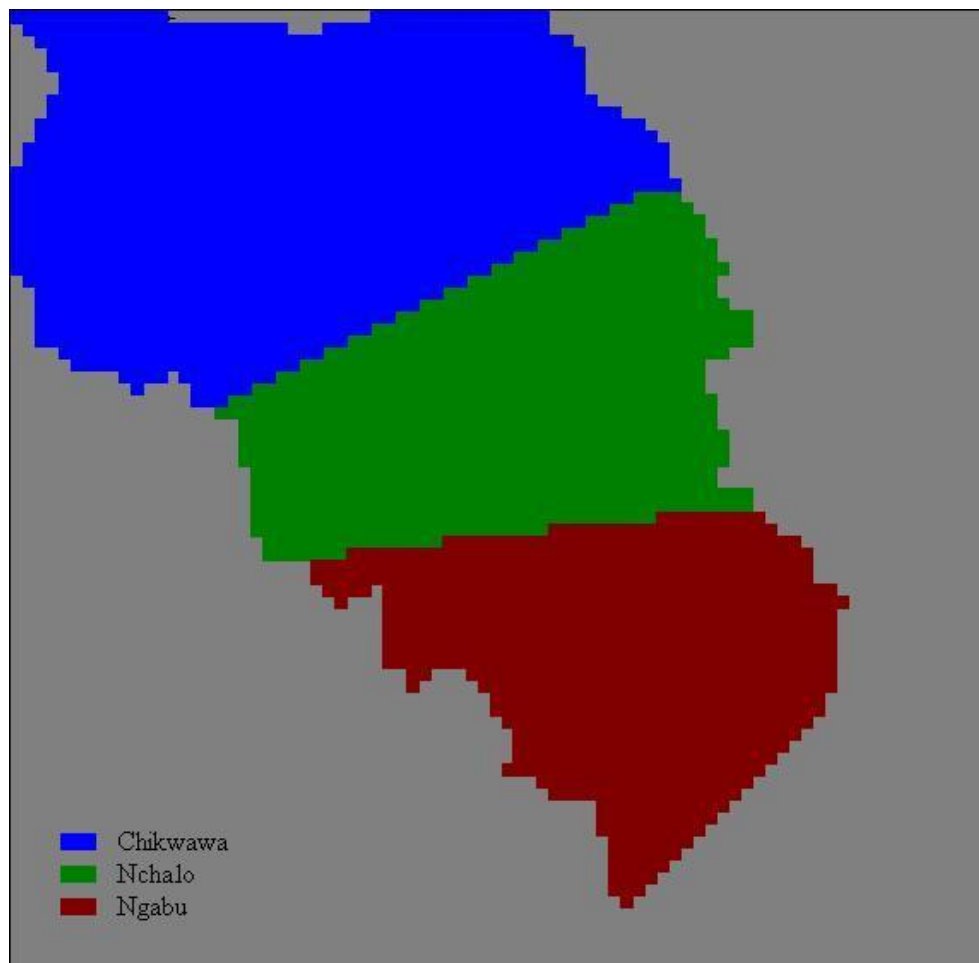


Figure 23. *Areal recharge distribution for the model. The obtained value for each station is applied to its corresponding area.*

The recharge for each zone is equal to the amount obtained for the corresponding meteorological station uniformly distributed in that zone.

Model Calibration

In groundwater modelling, the values for transmissivity T and storativity S are not often known and therefore are either obtained by field measurements such as pumping test or determined by Calibration or inverse modelling. In PMWIN, the parameters are hydraulic conductivity K and specific yield S_y . The former is calibrated based on hydraulic heads, while the latter is calibrated based on fluctuations. Unfortunately, with no time series observation from boreholes in this study, the calibration can be done only in steady state flow simulation for K parameters.

Parameters can be determined by manual calibration which is use a trial-and-error process of parameter adjustment or automatic optimization which is done by the software and uses mathematical search algorithms that seek to minimize differences between selected features of modelled and observed outputs by systematic trial alterations in the values of the model parameters.

Hydraulic conductivity

The values of hydraulic conductivities are obtained by calibration based on the observations from the boreholes. Based on the geology of the area, the assigned cell hydraulic conductivity is defined into 10 groups (Figure 24). It is assumed that the geology seen on the surface continues uniformly all the way down to the bottom of aquifer. Within its borders, each zone is assumed to be homogeneous and isotropic.

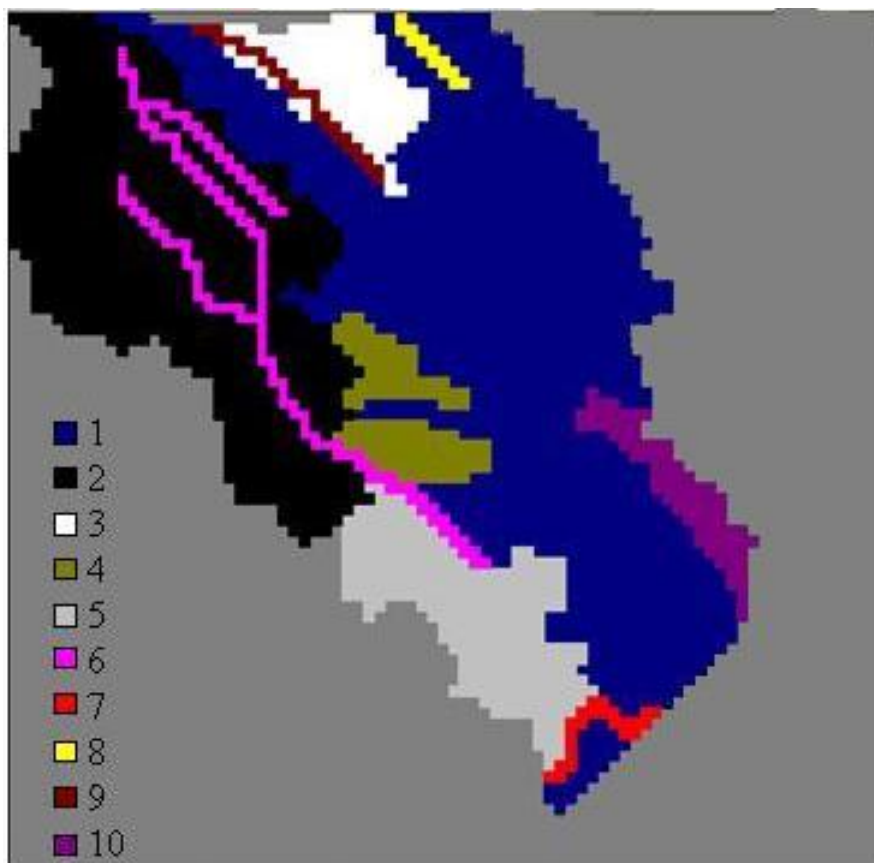


Figure 24. *Hydraulic conductivities based on geology of the area including the faults*
 1: Alluvial sediments, 2: Karroo sedimentary rocks, 3: Precambrian bedrock, 4: Cretaceous rocks, 5: Basaltic lavas, 6: Major Karroo faults (Panga, Telegraph and Nkombedzi), 7: the minor fault in south (name not available), 8: Mtumba fault (minor fault), 9: Mwanza faults (Karoo boundary fault), 10: Marsh area

Transient flow simulation

Initial conditions

For the initial hydraulic head for the model, the calculated head for each cell in the steady state simulation is applied to that cell.

Areal recharge time series

The areal recharge time series are calculated with the same approach used for average annual recharge for calibration in steady state flow. It is assumed that the surface flow in each time step (month) is 7.5% of the precipitation of that month. Therefore, the recharge for every month is equal to surplus from Thornthwaite method minus 7.5% of the precipitation in that month.

Like average annual recharge, monthly values of recharge are semi-distributed in the area using Thiessen polygon method.

Specific yield

The values of specific yield are needed only for the transient flow. In the absence of field measurements or data for calibration, the values are estimated as in Table 6.

Table 6. *Values for specific yield used for transient flow simulation*

Material	Specific yield
Average unconsolidated alluvial deposits (clay - coarse gravel)*	0.24
Karoo and Cretaceous rocks (Med. Sedimentary rocks)*	0.27
Precambrian rocks*	0.26
Basalt*	0.07
Major faults	0.3
Minor faults	0.1
Marsh (Coarse gravel)*	0.21

** (D.A. Morris 1967)*

RESULTS

Areal recharge

Potential evapotranspiration calculated with Thornthwaite method for the three stations Chikwawa, Nchalo and Ngabu is presented in Figure 25.

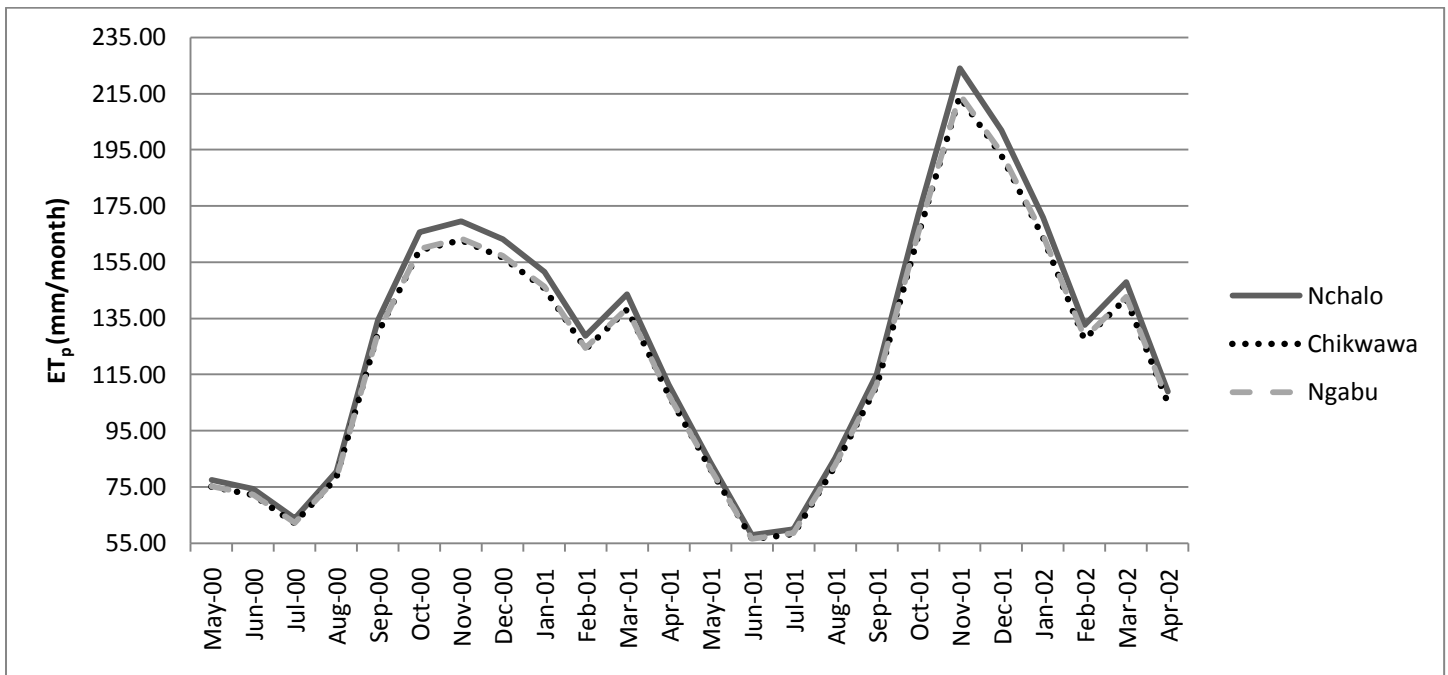


Figure 25. Monthly potential evapotranspiration for the three meteorological stations: Chikwawa, Nchalo and Ngabu, using the Thornthwaite method

Since the temperatures of Chikwawa and Ngabu are both extrapolated from Nchalo and the elevations of these two stations are not that different (Chikwawa 107 m.a.s.l and Ngabu 102 m.a.s.l), the values of potential evapotranspiration calculated for Ngabu and Chikwawa look almost identical on the graph. Following the algorithm from Xu & Chen (2005), actual evapotranspiration and surplus are calculated for each station.

The figures 26 to 28 present the monthly results.

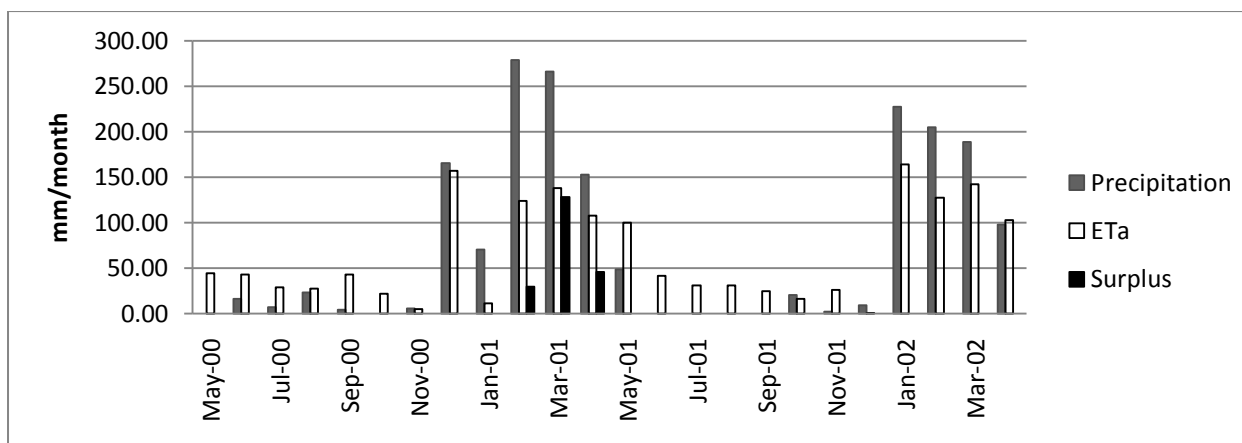


Figure 26. Monthly Precipitation, actual Evapotranspiration and surplus in Chikwawa

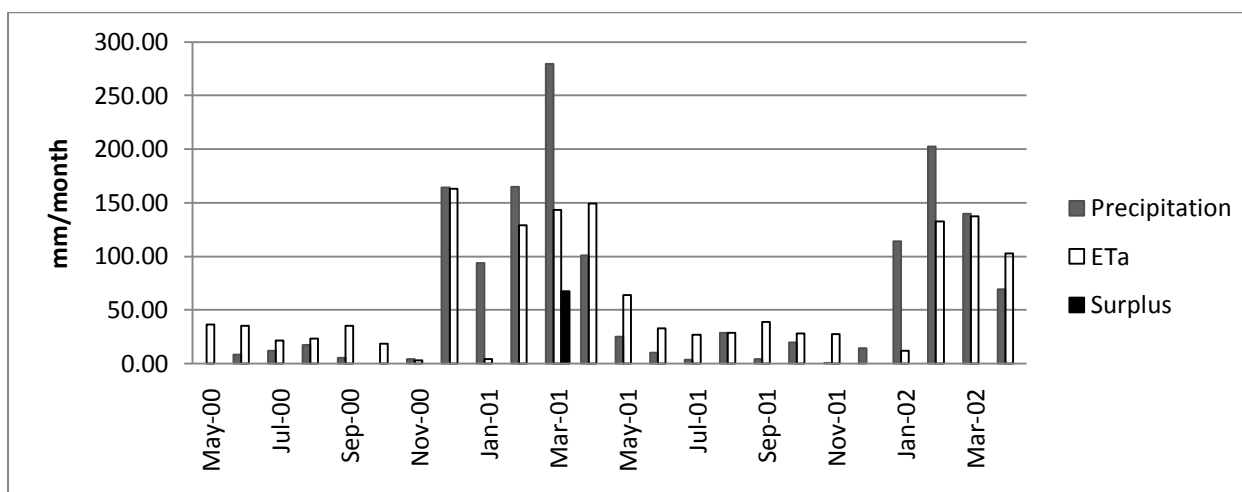


Figure 27. Monthly Precipitation, actual Evapotranspiration and surplus in Nchalo

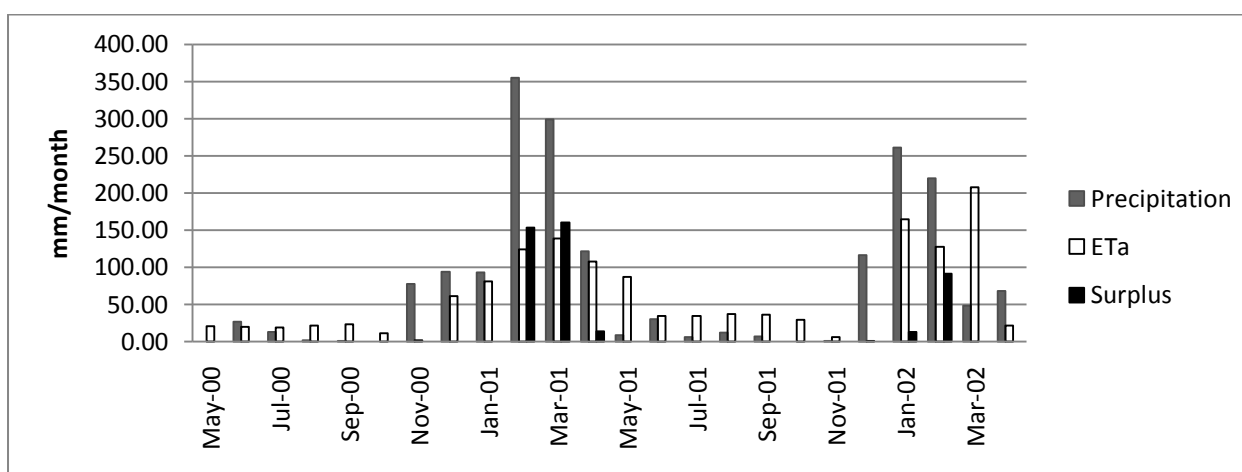


Figure 28. Monthly Precipitation, actual Evapotranspiration and surplus in Ngabu

The two dry and rainy seasons are clearly visible in the results. With high temperature and little precipitation in the dry season, the soil dries out and the soil moisture drops to almost zero. In the beginning of the rainy season all the precipitation is absorbed by the dry soil and only after the soil is saturated (200 mm, which barely happens for Nchalo) there will be surplus.

The surplus and soil moisture in Nchalo are the lowest due to low precipitation and slightly higher temperature (and therefore, higher potential Evapotranspiration). Ngabu receives the highest precipitation (with the potential evapotranspiration similar to Chikwawa) and therefore has the highest surplus and soil moisture.

The difference in the two rainy seasons is obvious on all the graphs: precipitation, surplus and soil moisture are all higher in the first year period.

The soil moisture is calculated from equation 5 and the results are illustrated in figure 29.

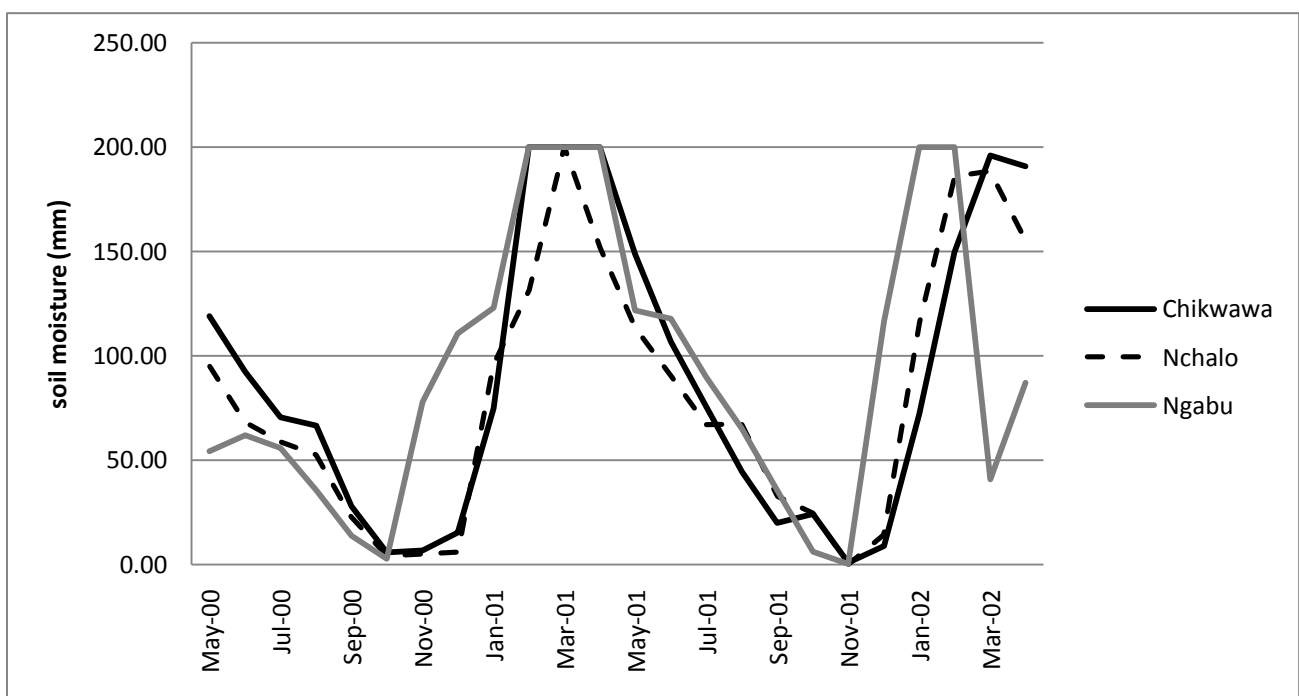


Figure 29. *Calculated soil moisture in 2 years in the three stations*

In the steady state flow simulation, the calibration is based on one value for each borehole, it is necessary to calculate the average annual areal recharge for the model, which is the annual surplus minus 7.5% of the annual precipitation. The resulting values for annual

recharge are presented in table 7. The areal recharge is the highest in Ngabu, while it is found zero in Nchalo.

Table 7. *Average annual areal recharge calculated for each station*

Name	Annual precipitation (mm/year)	Surface flow (7.5%P) (mm/year)	Annual surplus (mm/year)	Calculated recharge (mm/year)
Chikwawa	894.2	67.07	101.49	34.42
Nchalo	741.6	33.73*	33.73	0.00
Ngabu	930.9	69.82	215.97	146.16

* The whole calculated surplus in Nchalo makes 4.55% of the precipitation

Estimated recharge in the alluvial aquifers in Malawi is 1-7% of rainfall (Mkandawire 2002). For this reason, and also in order to avoid dry cells in the model, the recharge in Nchalo is determined as 1% of the precipitation (7.4 mm/year) for the model. However, the areal recharge in Ngabu exceeds the range estimated by Mkandawire (2002) (16% of the precipitation).

Table 8. *Ratios and indices for the stations in the 2 years period*

name	Recharge/P	ET _a /P (Annual mean)	Aridity index%
Chikwawa	0.04	0.87	84.40
Nchalo	0.01	0.94	72.63
Ngabu	0.16	0.76	73.16

The aridity index in the table 8 is a numerical indicator of the degree of dryness of the climate defined as the ratio of water deficiency d , which is calculated as the sum of the monthly differences between precipitation and potential evapotranspiration for those months when the normal precipitation is less than the normal evapotranspiration; to n stands for the sum of monthly values of potential evapotranspiration for the deficient months (Thornwaite 1948, Huschke 1952)

The sensitivity of areal recharge to the field capacity is presented in the figure below:

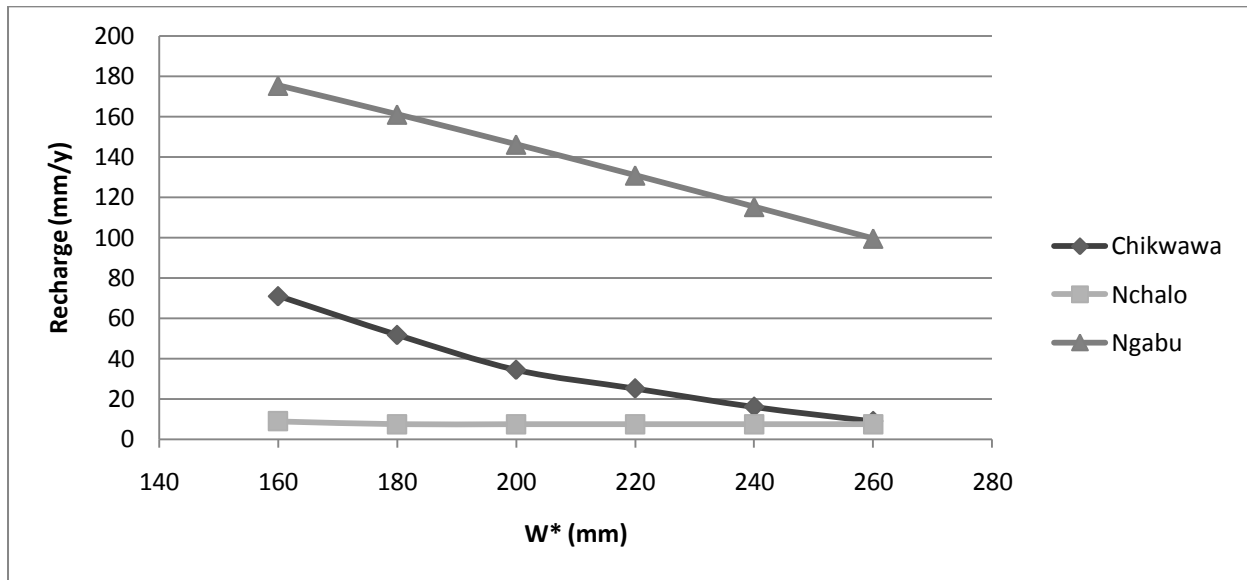


Figure 30. Sensitivity of the calculated annual recharge for each station vs. assumed soil's capacity (W^* for using equation 5)

The situation in Nchalo is pretty dry, which results in zero calculated recharge for most values of W^* and therefore 7.4% fixed recharge. This makes Nchalo completely insensitive to changes in W^* . But for Ngabu and Chikwawa changes are significant. Therefore, the value estimated for W^* has its effects on the modelling results.

Calibration results

In the steady state flow simulation, the hydraulic conductivities are parameters to be calibrated in inverse model PEST provided with interface in MODFLOW based on the average areal recharge and the average groundwater level in the boreholes. Of course in the current available data there is only one reading from each borehole, which leaves no choice other than to use them as average.

PEST searches a parameter set for which the sum of squared deviations between model-calculated and measurement values of heads at the observation boreholes is reduced to minimum.

Parameters

Hydraulic conductivities of different rock types and fault zones (defined on the basis of the geology) and faults are defined as parameters (Figure 24) for the model to calibrate. There are few experimental data in the area. However, permeability measurements in Tanzania on similar cretaceous sandstones have resulted in values of 169.8 and 389.2 md (Nestebly 1989) which converts into the average hydraulic conductivity of $3.03\text{E-}6$ m/s. This value is then used in predefining parameter 4.

The results from calibration by PEST are summarized in the table 9.

Table 9. *Hydraulic conductivities resulted from calibration in m/s with their 95% confidence interval calculated by PEST*

Parameter number	explanation	mean	95% down	95% up
1	K Alluvial sediments	7.62E-05	6.87E-05	8.37E-05
2	K Karroo sedimentary rocks	1.71E-05	-1.94E-06	3.62E-05
3	K Precambrian bedrock	5.01E-08	1.03E-08	8.99E-08
4	K Cretaceous rocks	3.03E-06	N.A	N.A
5	K Basaltic lavas	7.06E-06	4.06E-06	1.01E-05
6	K Major Karroo faults (Panga, Telegraph and Nkombedzi)	1.31E-03	-9.13E-04	3.54E-03
7	K minor fault in the south	3.58E-07	1.90E-07	5.26E-07
8	K Mtumba fault (minor fault)	2.00E-08	8.75E-09	3.13E-08
9	K Mwanza faults (Karoo boundary fault)	2.98E-04	-7.68E-04	1.36E-03
10	K Marsh area	3.89E-03	2.27E-04	7.55E-03

The model's sensitivity to parameters is verified later, but the fact that parameter 2, 6 and 9 include zero in their confidence intervals show that they are insignificant to the model. Figure 31 illustrates the hydraulic conductivities in meter per day for comparison.

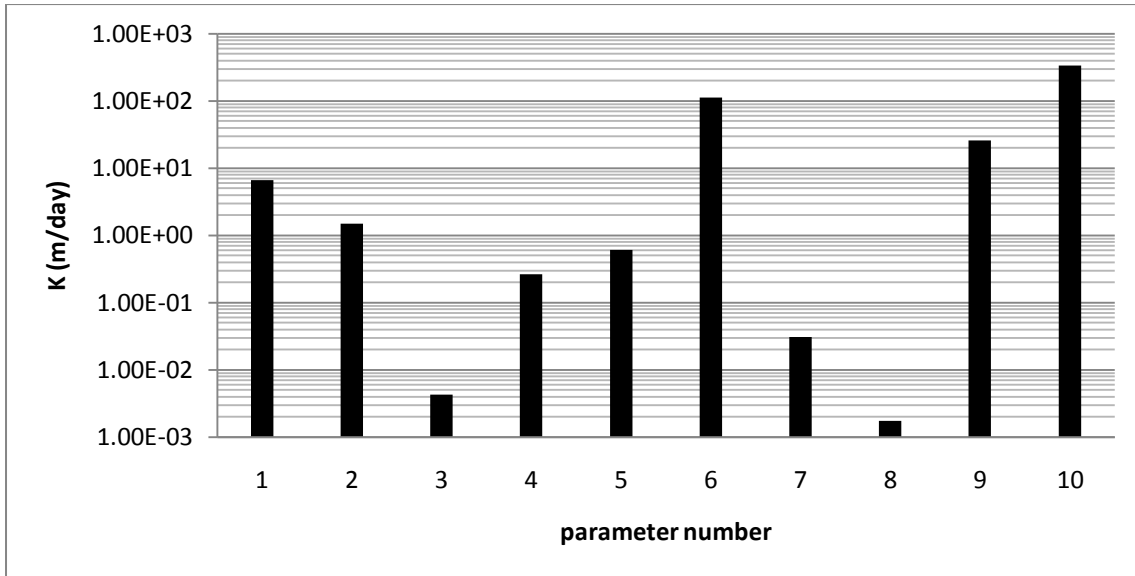


Figure 31. *Values for hydraulic conductivity from calibration*

Calculated hydraulic heads

Distribution of calculated hydraulic heads is presented in Figure 32. Note that the interval between contour lines is not constant. For hydraulic heads from 60 to 200 m.a.s.l the interval is 20 m, while for heads higher than 200 m.a.s.l it is 100 m.

In the area where the Precambrian bedrock outcrops, between Mwanza fault and Mtumba, the groundwater head rises rapidly and far above the surface. Since there is no direct observation in that area, there is a possibility that the results are unrealistic. But on the other hand, the existence of a spring in the same location suggests that the high hydraulic head might be the result of a groundwater going under confined conditions.

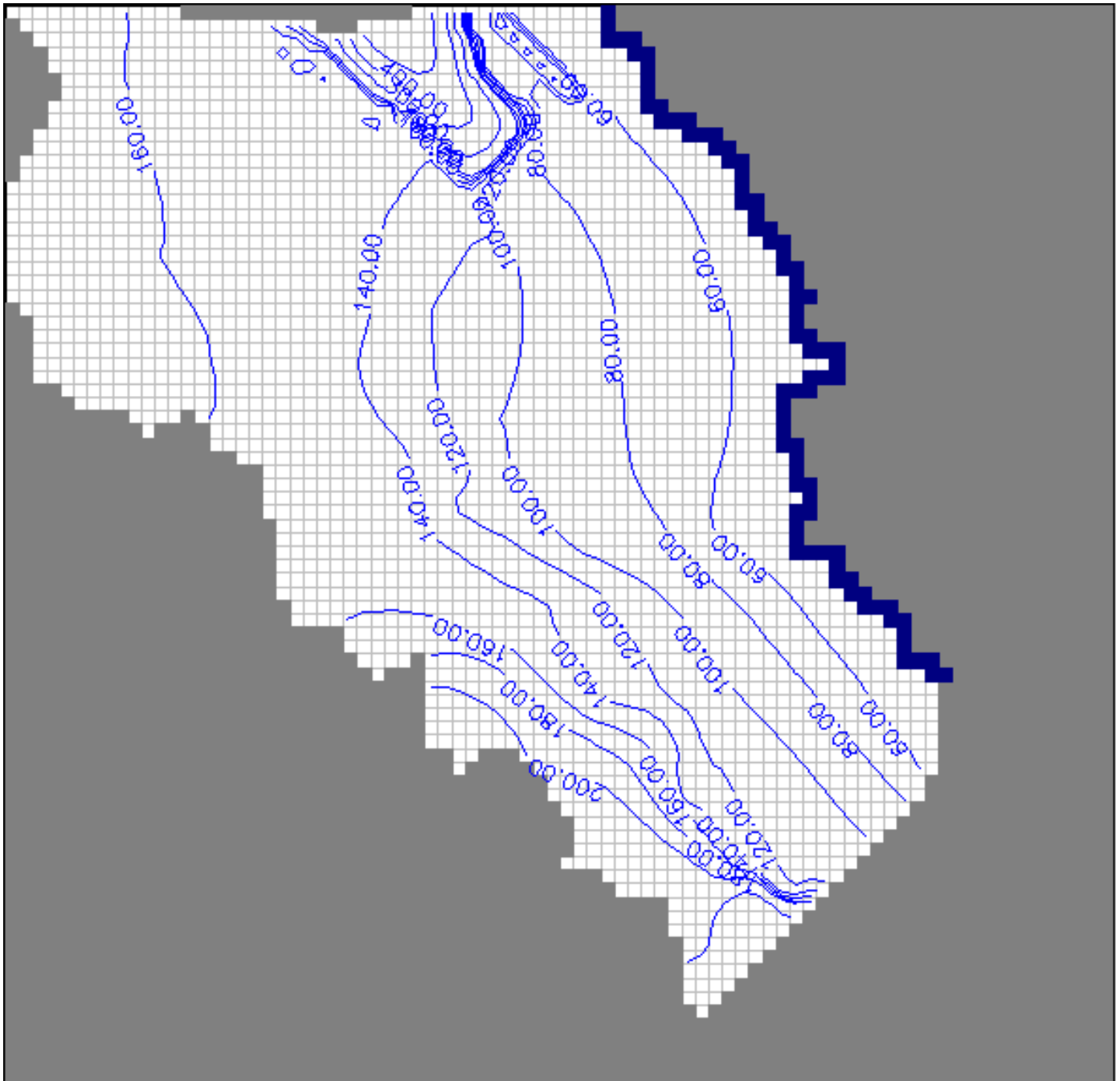


Figure 32. *Calculated hydraulic head contour lines (m.a.s.l.)the interval between contour lines is 20 m for heads from 60 to 200 m.a.s.l. and 100m for heads higher than 200m.a.s.l*

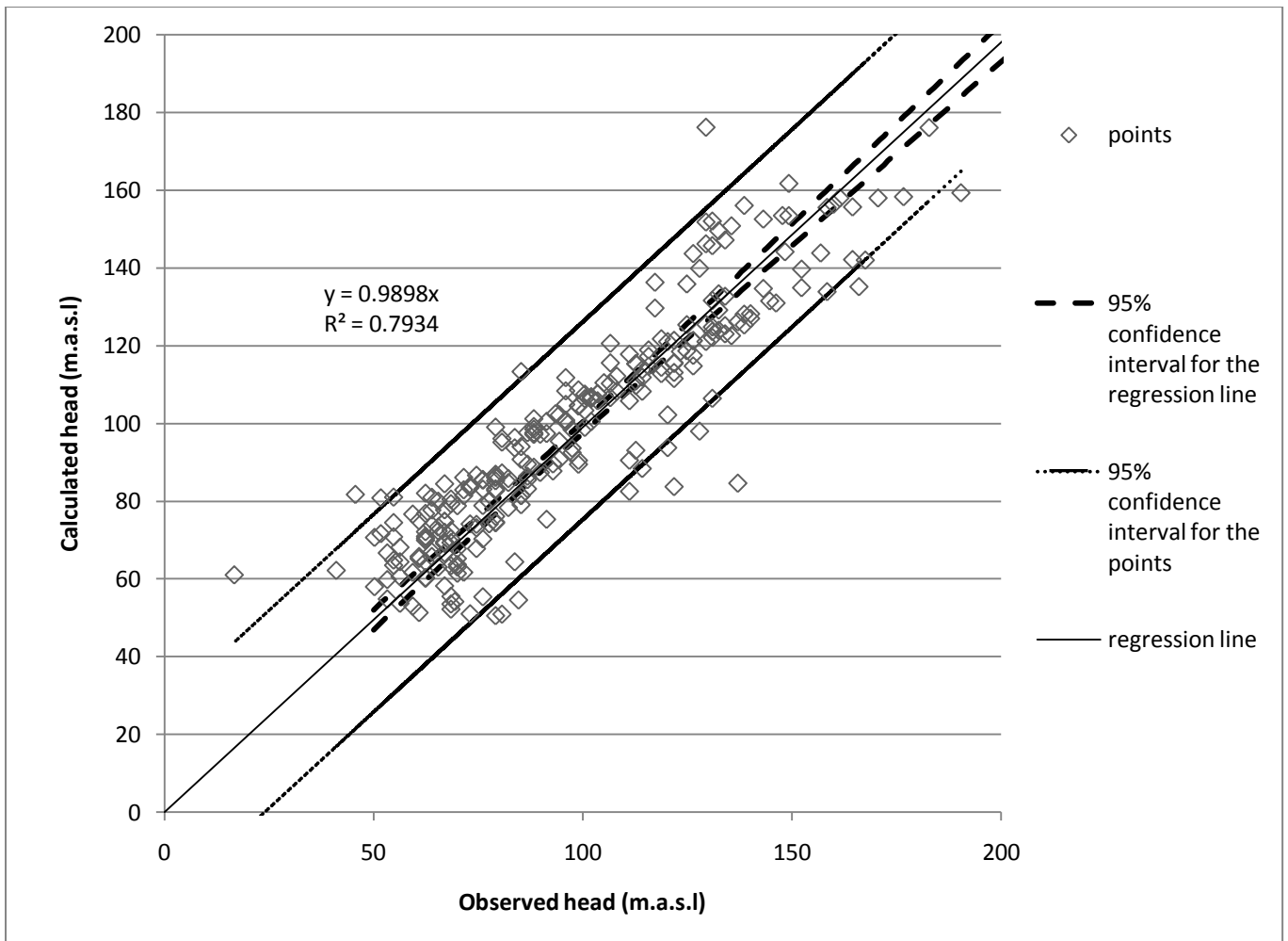


Figure 33. Calculated vs. observed head for boreholes. The regression line for the points with its formula and R^2 are shown on the graph. 95% confidence interval for the regression line and for the points are also shown

A comparison of calculated and observed hydraulic heads in boreholes in Figure 33 exhibits a good relation between the model's results and observations.

Out of 263 boreholes within the modeled area, 162 have a calculated head within $\pm 10\text{m}$ of the observed ones.

The percentage error between calculated and observed head for boreholes is verified in Figure 34. Ignoring the fluctuations is responsible for some of the error, which increases in percentage for boreholes with smaller head. Borehole number 188 should be neglected, for its observed head 16.76 m.a.s.l. must be wrong. The borehole is surrounded by others with observed heads around 50 m.a.s.l.

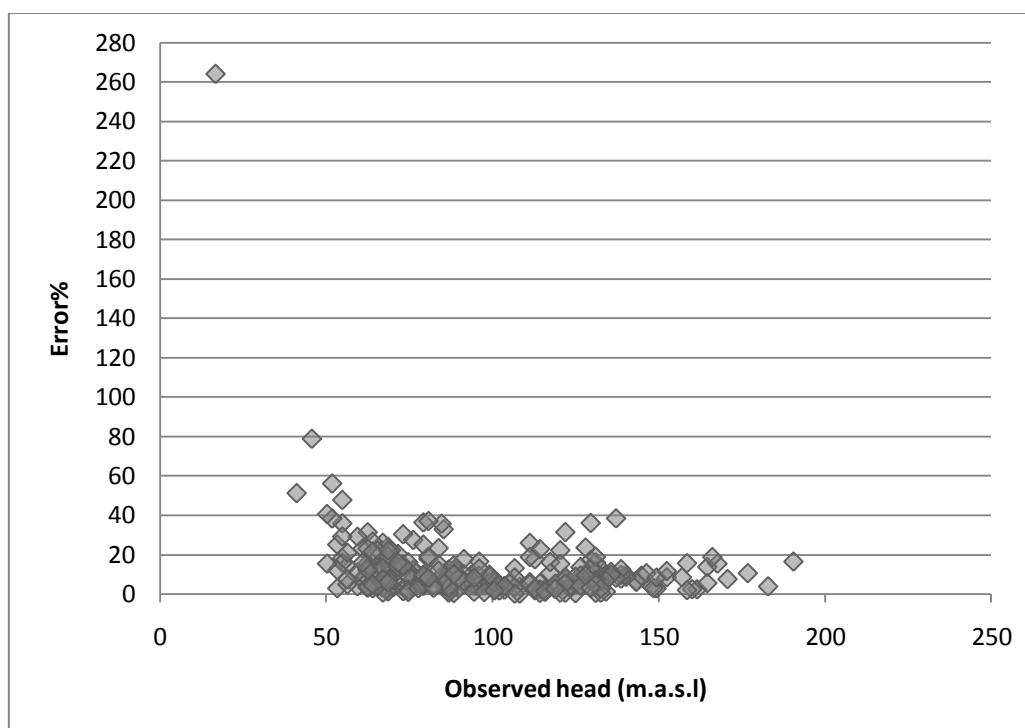


Figure 34. *Percent error between calculated head and observation for each observed head. $Error\% = (calculated\ head - observed\ head) / observed\ head \times 100$*

Model's sensitivity

In order to do a sensitivity analysis, the values of hydraulic conductivities are altered manually in each step. Then based on calculated heads from steady state flow model, the residual sum of squares (RSS) is calculated each time:

$$RSS = \sum_{i=1}^n (observed\ head - calculated\ head)^2 \quad (6)$$

In which i is the borehole number.

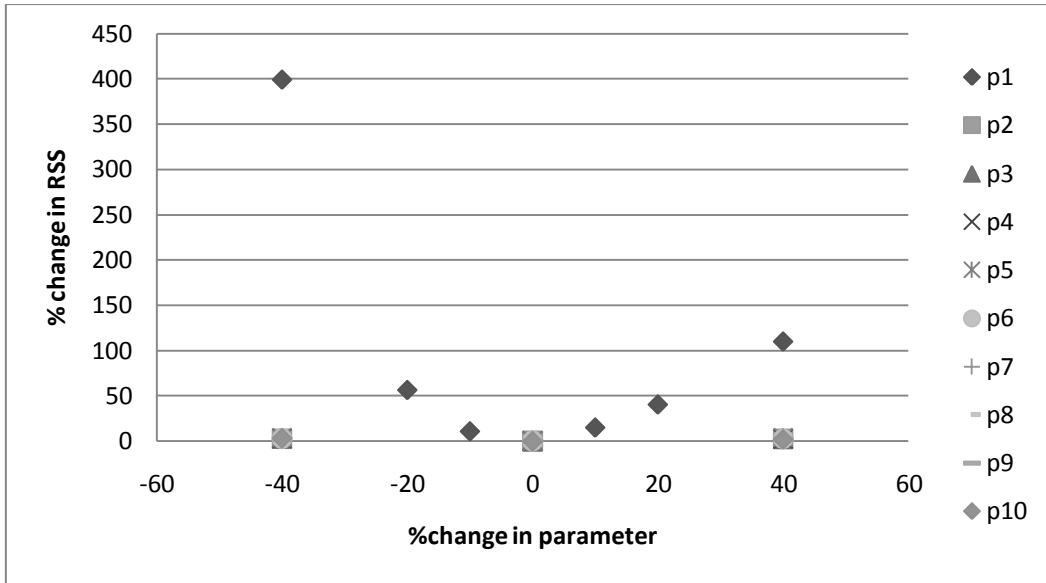


Figure 35. Model's sensitivity to the change in parameters' value. RSS is calculated from equation 6.

The graphs show that model's sensitivity to the parameters is not symmetric, and other than p1 (hydraulic conductivity in the alluvial) the model is fairly insensitive the rest of the parameters; So much that the changes in RSS do not appear in the same graph. Thus the sensitivity of the other parameters (2-10) is shown in Figure 36.

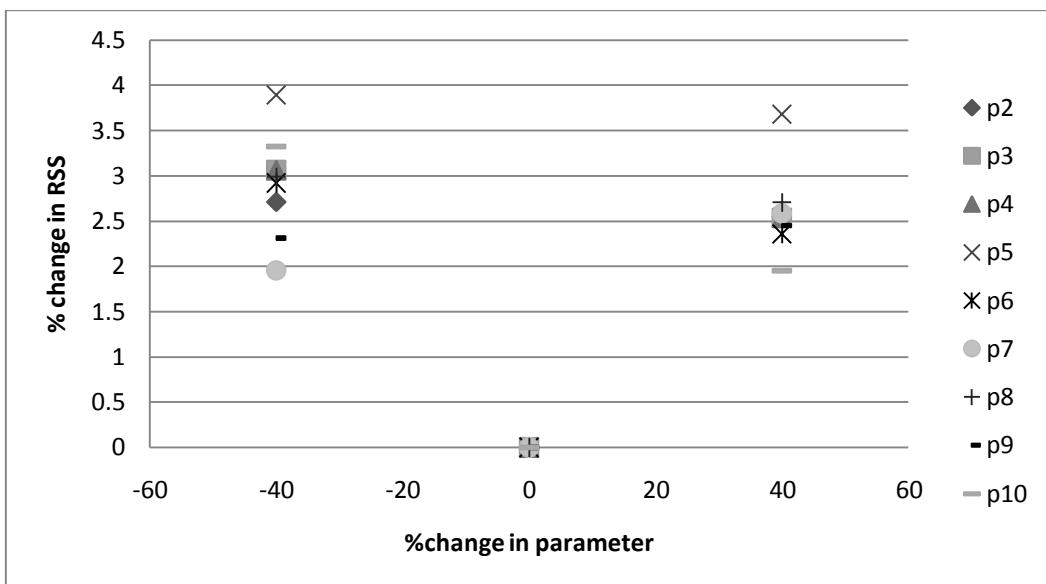


Figure 36. Model's sensitivity re-plotted for the parameters 2-10

Sensitivity analysis results also show that the RSS increases with the change in the parameters' value, which confirms that the model has reached the optimum value for each

parameter (including parameter 4 whose value is defined for the model). However, this also depends on the geometry of the model.

Transient flow simulation

Areal recharge time series

Using the precipitation data and calculated surplus & actual evapotranspirations for the stations (Figures 26 to 28), areal recharge is now calculated on monthly basis with the same approach as average annual recharge. i.e. the recharge for every month is equal to surplus minus 7.5% of the precipitation in that month.

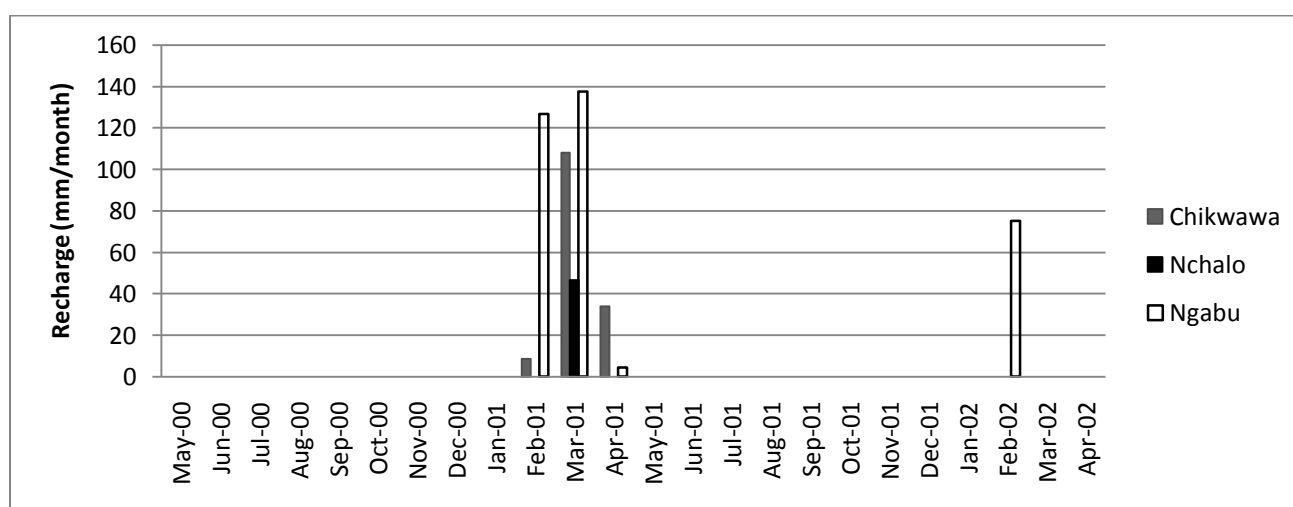


Figure 37. Monthly areal recharge time series used in transient flow simulation

Groundwater fluctuations

The maximum fluctuation in 2 years for boreholes (Figure 38) ranges from min 0.17m to 3.45m, which is within the both ranges of fluctuation estimated by Chilton & Smith-Carington (1984) and Mandeville & Batchelor (1990). The magnitude of maximum fluctuation seems mostly related to the variation in the value of recharge since the biggest fluctuations happen in the southern part of the area where the recharge varies from 0 to 137.57 mm/month.

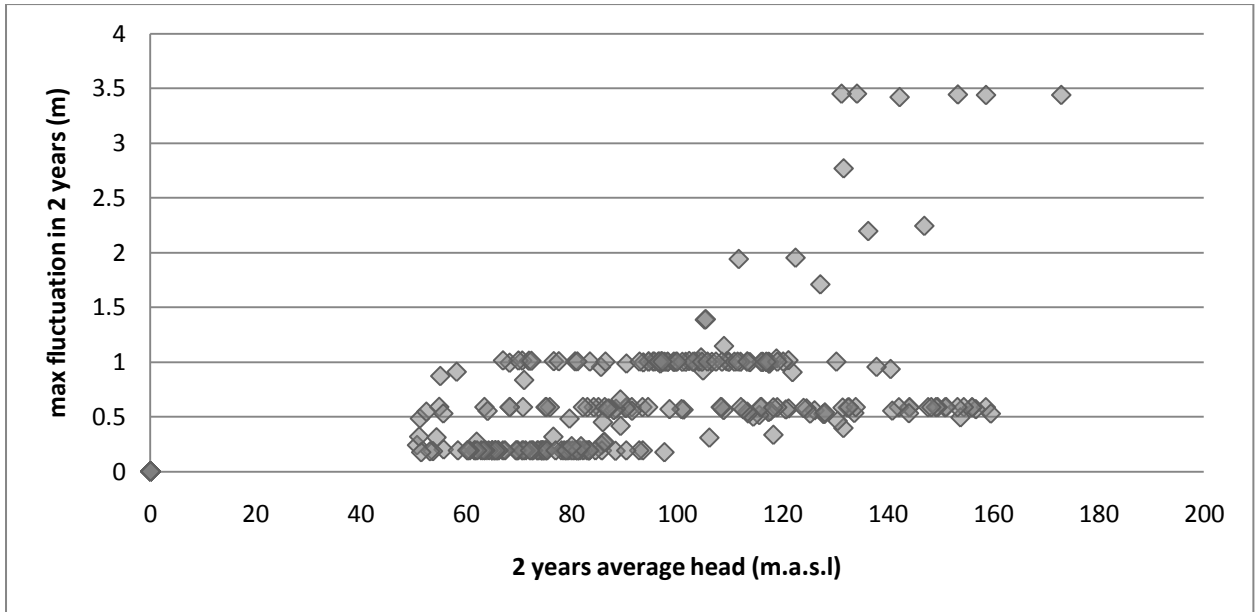


Figure 38. *Maximum fluctuation in 2 years for the boreholes vs. 2 years average calculated head*

Boreholes 113 and 154 in Figure 39 display higher fluctuations compared to boreholes 1 and 17 due to the variations in their areal recharge value. Moreover, since Nchalo and Chikwawa receive zero recharge in summer 2002 (the hotter and drier rainy season), the groundwater table in boreholes 1 and 17 declines gradually. But in boreholes 113 and 154 there is some areal recharge received in Feb 2002 in Ngabu. The effect of this recharge appears on the groundwater level which rises about 1 meter in these boreholes.

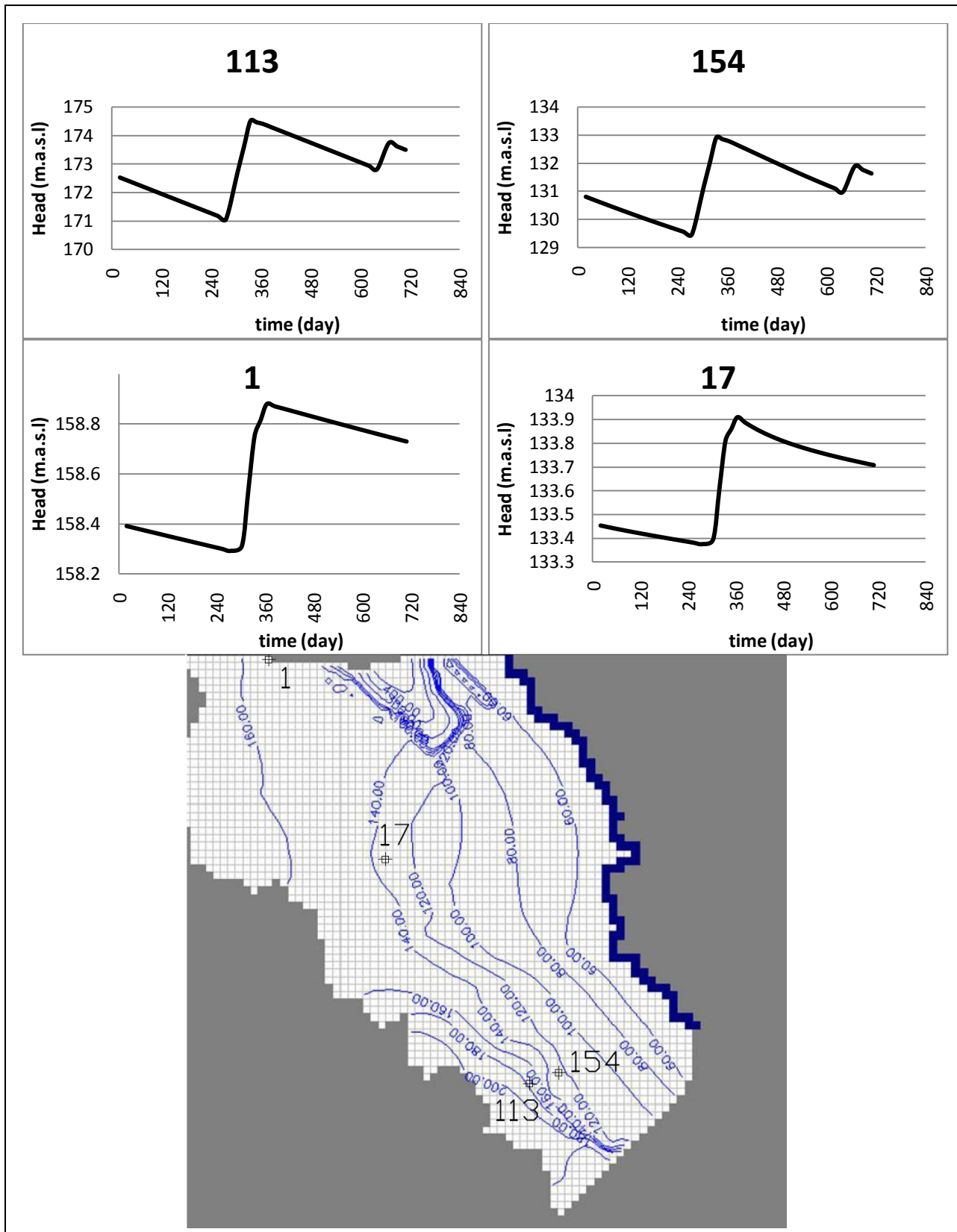


Figure 39. Groundwater fluctuation in 4 sample boreholes (number 1, 17, 154 & 113) from May 2000 to April 2002 with their locations on the map. Contour lines present the calculated hydraulic head from the steady state flow simulation

The effect of faults

Due to fairly high hydraulic conductivities, the major faults act like channels in the system. In order to see the effect more clearly, three different cross sections are decided as perpendicular as possible to the calculated hydraulic head contour lines as illustrated in figure 40.

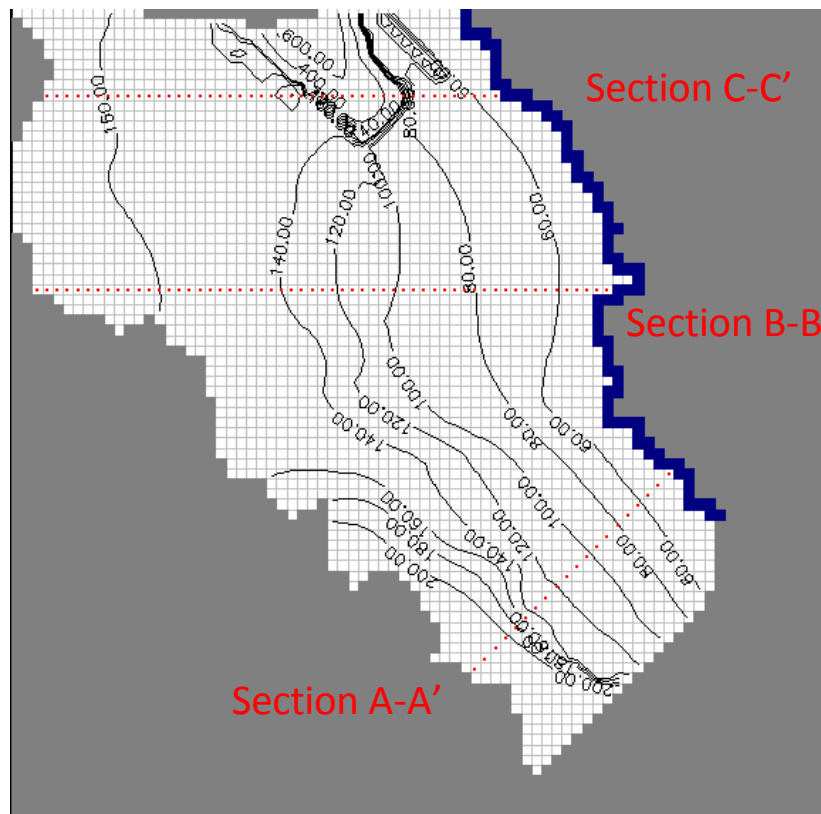


Figure 40. Sections in which the groundwater flow pattern is the closest to 2D

In the absence of geophysical subsurface data, it is assumed that the geology seen on the surface (Figure 41) continues uniformly all the way down to the bottom of aquifer which is the assumption in building the model. The elevation of the ground surface is known among each section. Therefore, the hydraulic heads and flow lines obtained from the model among each section can be verified.

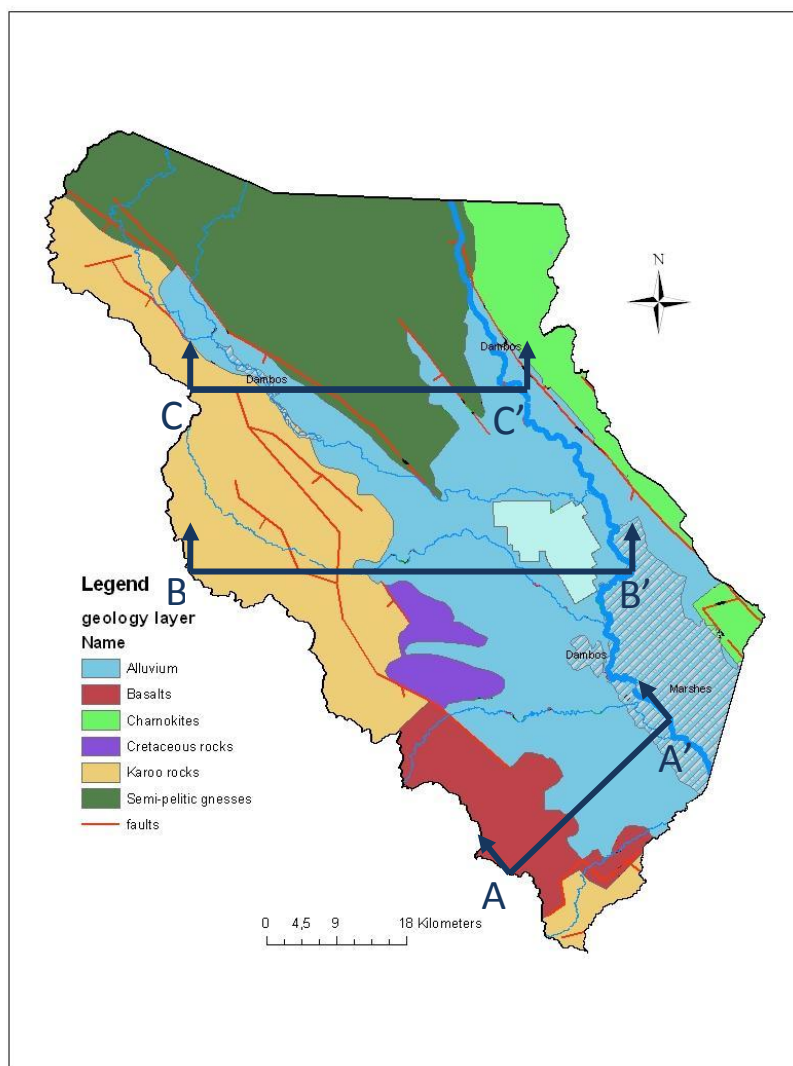


Figure 41. Sections from figure 40 on the geological map

The groundwater table drawn in Figure 42 is extracted from the steady state simulation results, and the flow lines are drawn using particle tracking.

In section A-A', the groundwater flow is almost completely 2D. The hydraulic gradient in alluvial is lower, due to higher hydraulic conductivity.

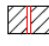
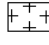



In section B-B', Nkombedzi & Panga faults cut through the section. Since they have high hydraulic conductivities, the groundwater flows into Nkombedzi and off the section, while part of groundwater in Panga flows toward the river.

In section C-C' between Mwanza fault and Mtumba, the groundwater head rises far above the surface. As mentioned before, there is a possibility that the results are unrealistic, or it could mean that groundwater is under confined and artesian conditions. Like section B-B', the Mwanza fault which has high hydraulic conductivity and cuts the groundwater flow and leads it out the section. Although the fault Mtumba has low conductivity, it is not impermeable enough to be considered a barrier fault since its hydraulic conductivity is in the same range as that of Precambrian bedrock. This can also be concluded from the flow lines. A barrier fault would act like a no flow boundary and make the groundwater flow completely upward avoiding it, which does not happen here where flow lines go through the fault.

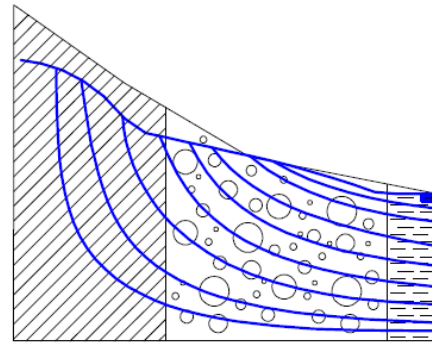
In a simple 1 layer model, the software assumes that the river cells continue all the way down to the bottom of the aquifer and therefore the flow lines are horizontal where they meet the river. But the reality is more complex than that: the gravitational flow lines begin to rise up as they get in the area close to the river, and they finally end up feeding the river. TÓTH (2009) calls this area "the discharge area". Moreover with multi layers, the flow lines would have a tendency to rise where there is a conduit fault or a layer with high hydraulic conductivity K (Marsh for example) on the top of layers with lower K .

vertical exaggeration: 50

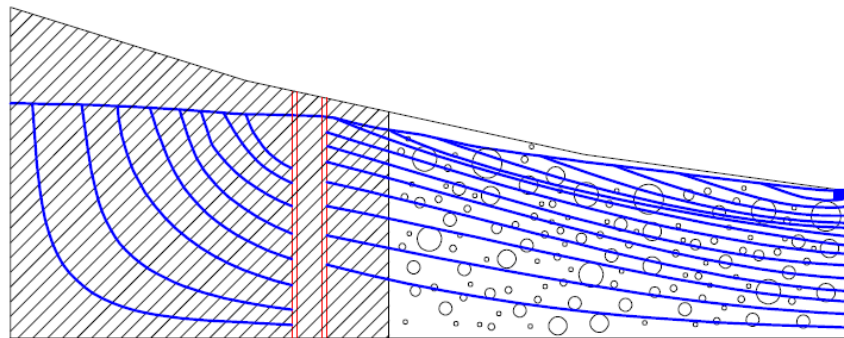
LEGEND

	Fault
	Precambrian bedrock
	Alluvial sediments
	Marsh
	Karoo

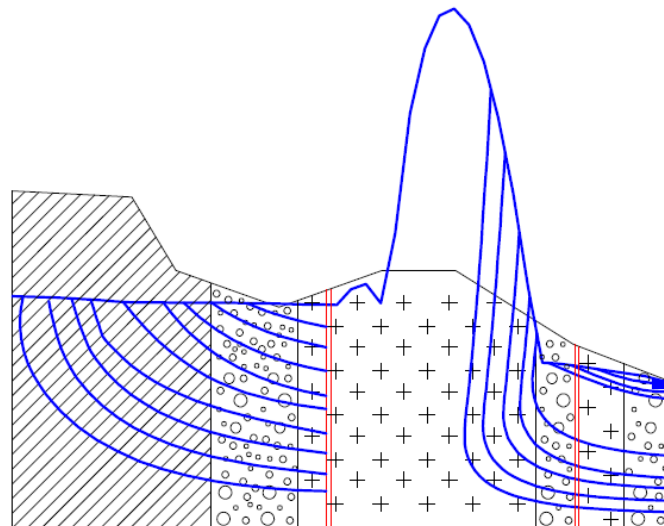
0 5 10Km



section A-A'



section B-B'



section C-C'

Figure 42. Sections with their groundwater level and flow lines calculated by the model

Hot spots

Judging based on the EC distribution, there are 4 main hot spots in the area marked in the figure below in which the salinity of the groundwater rapidly rises. The models makes it possible to check the sources for these points by particle backtracking.

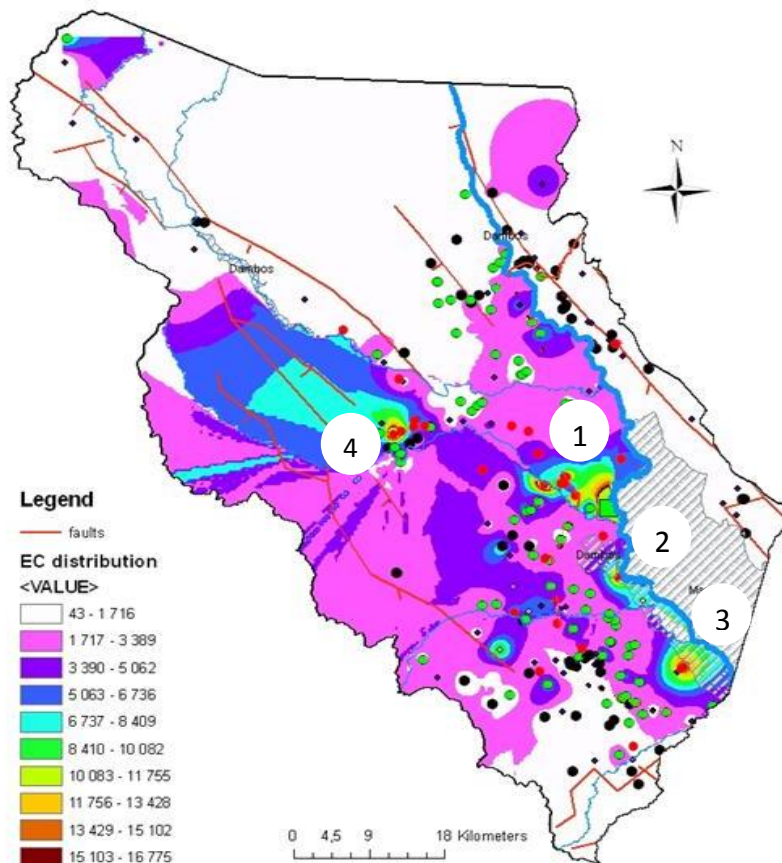


Figure 43. The 4 main hot spots marked on the map of electric conductivity distribution

The figures 44 to 47 show the flow lines in the plan view and two cross sections to the hot spot. Note that in order to make the figure demonstrative, the number of particles in them is kept limited. Nevertheless they are good representatives of their corresponding hot spot.

The current model concludes that the water in spots 1 & 4 comes from the faults within Karroo system (spot 1 from Nkombedzi and spot 4 from Telegraph) while the source of water in hot spots 2 & 3 seems to be in basaltic rocks.

Due to the simplicity of the model and the fact that it is in one layer, the particle backtracking results must be discussed. Once again since the model is in 1 layer, the flow lines are horizontal where they meet the river while they should have been rising in the discharge area. Moreover, the groundwater flowing toward points 2 and 3 may come from Karroo sedimentary rock that may exist beneath basaltic lavas.

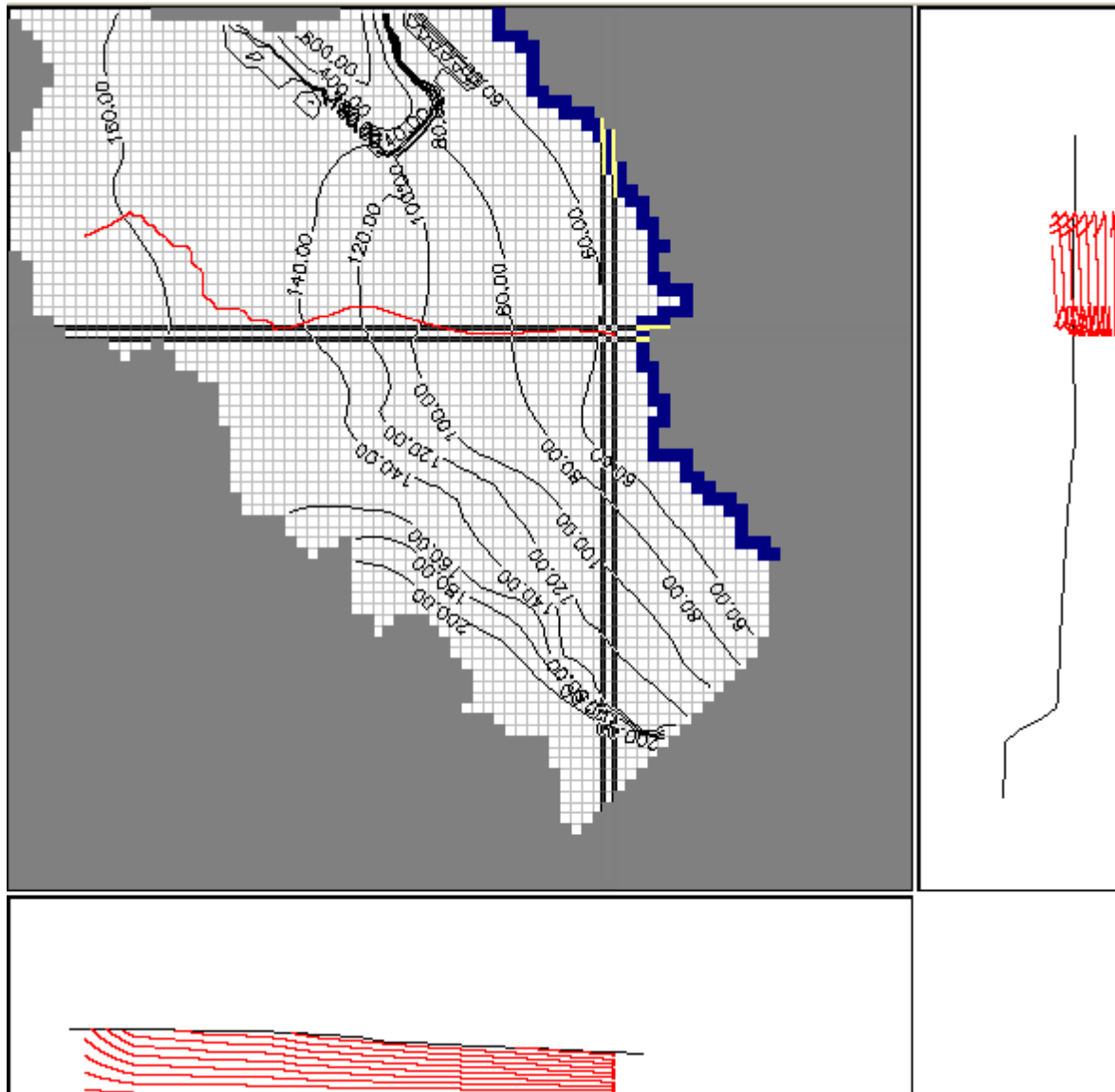


Figure 44. Particle backtracking from hot spot number 1. The path is illustrated in plan view and two projections.

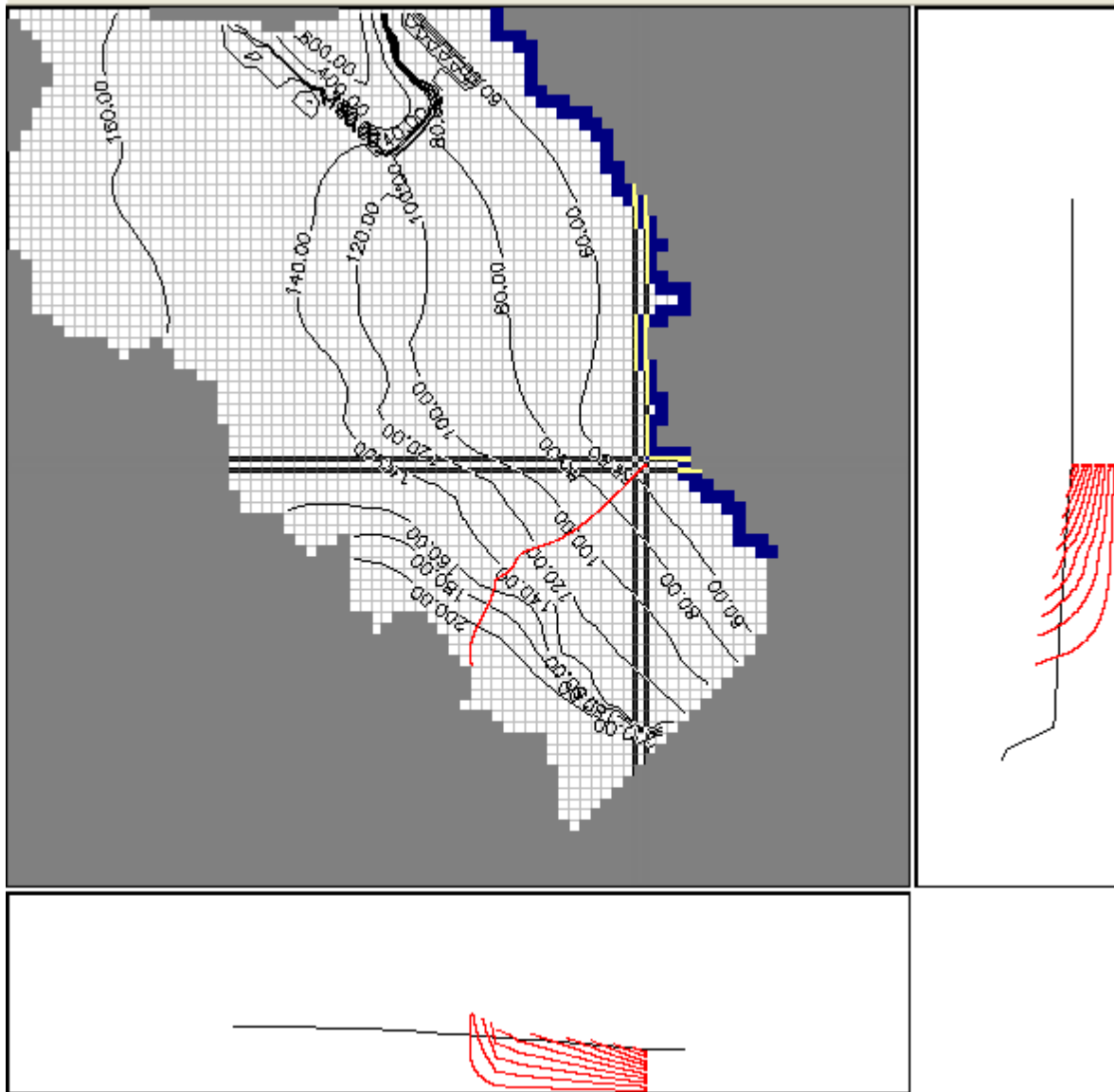


Figure 45. Particle backtracking from hot spot 2. The path is illustrated in plan view and two projections.

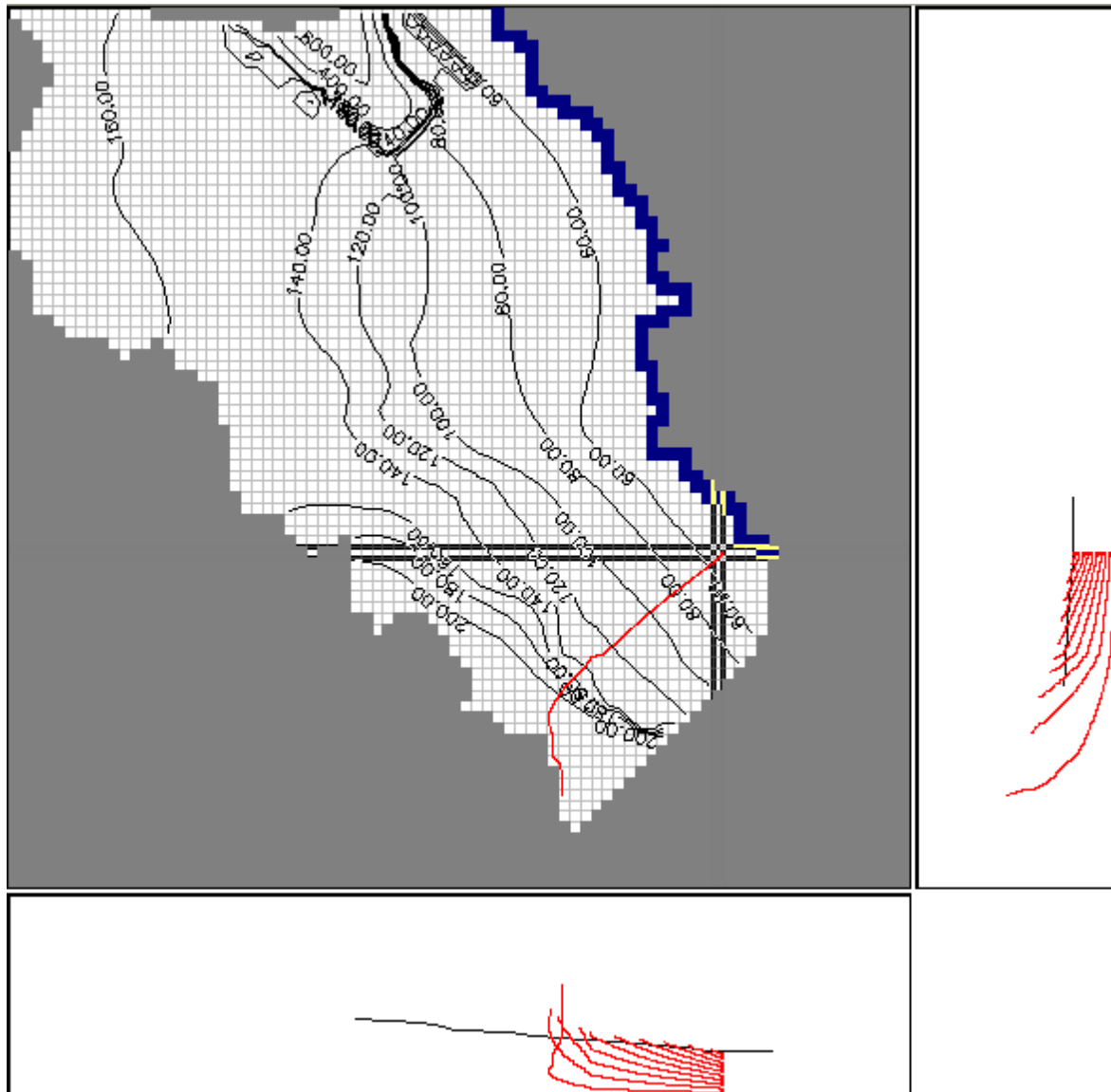


Figure 46. Particle backtracking from hot spot 3. The path is illustrated in plan view and two projections.

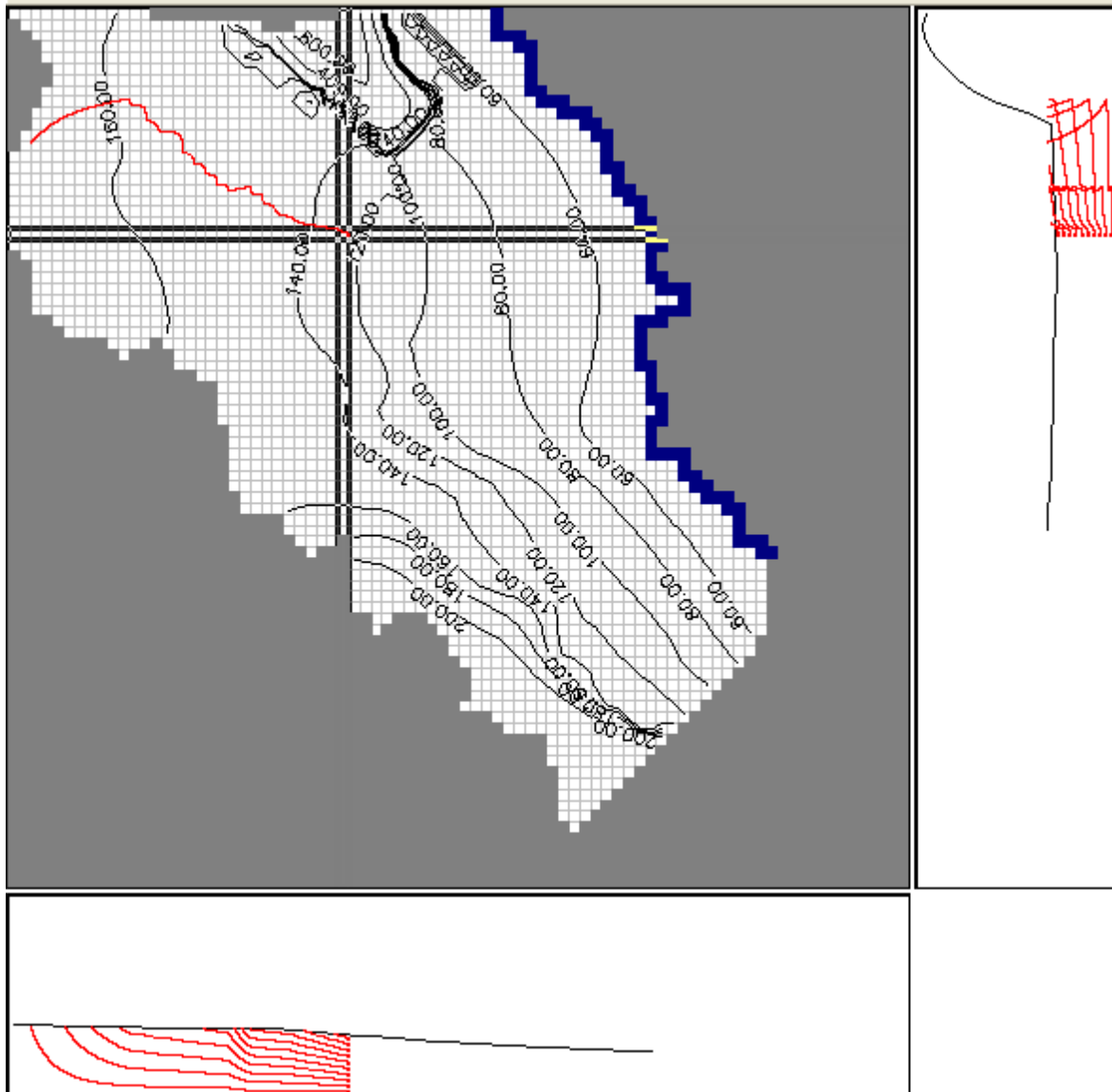


Figure 47. Particle backtracking from hot spot 4. The path is illustrated in plan view and two projections.

Please note that in the Figures 44-47, the black lines in each cross sections display the hydraulic head in that section, but the red lines are projected particle paths and are not necessarily in the same section.

A geological scenario

As said before, our knowledge of the aquifer is limited to what is seen on the surface, which has been the basis for building the model. However, it is very possible that the Mwanza fault continues under the alluvium. The author is not in the position to confirm or disprove this,

but can study the groundwater system under this situation as a scenario. Figure 48 shows the distribution of hydraulic conductivities under this scenario. Since the model is in one layer, the fault is modelled within, rather than under, the alluvium.

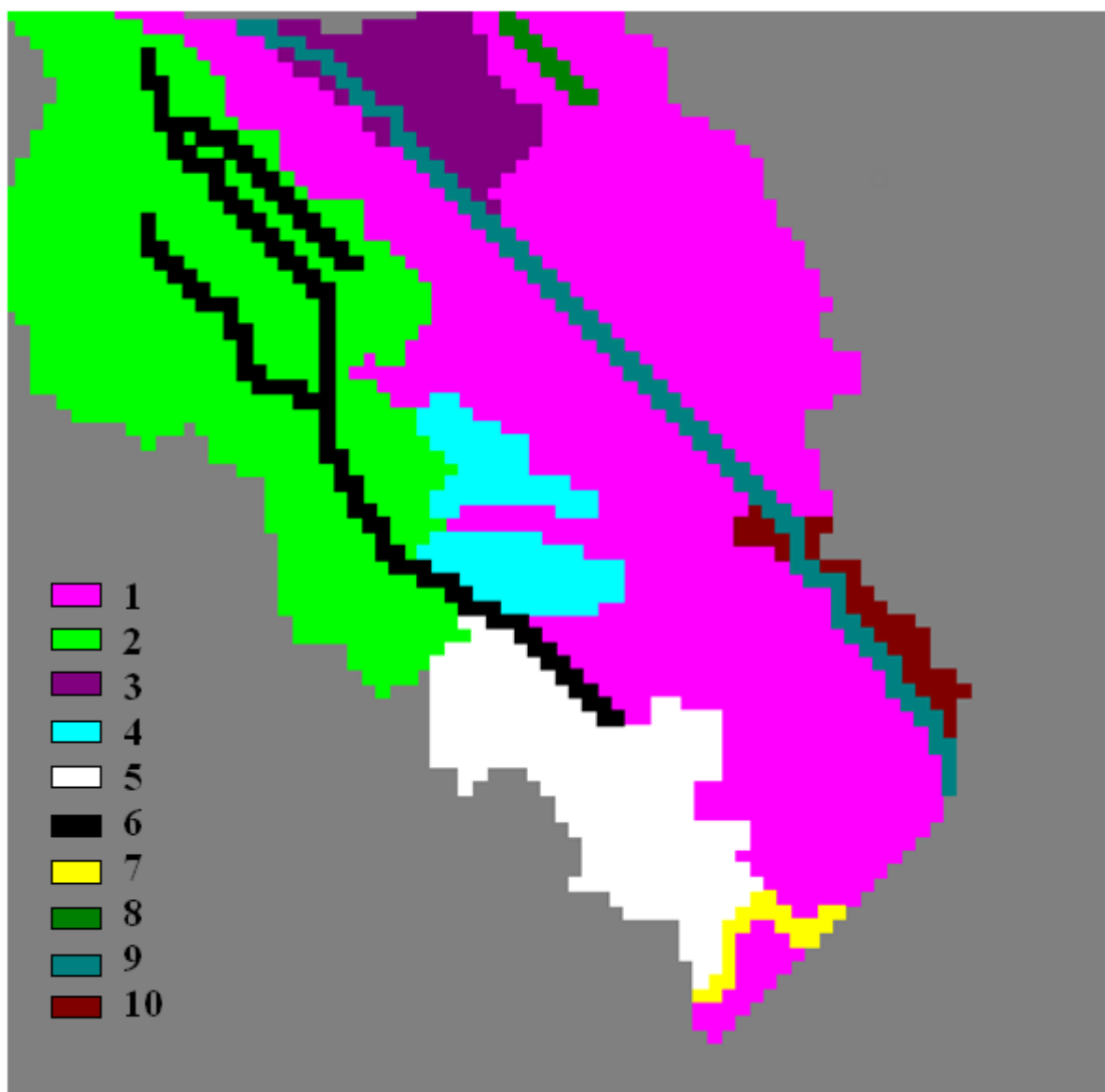


Figure 48. *A geological scenario: continuation of Mwanza fault. Hydraulic conductivities for each zone are from calibration (table 9)*

The resulting groundwater heads are mildly different as shown in the same sections in figure 49. The high peak in section C-C' is reduced, though still exists. In sections A-A' & B-B' the

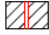
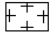
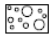


groundwater tends to flow more horizontally. However, the resulting groundwater flow to the hot spots found by particle backtracking remains as before.

In sections A-A' and B-B', there is now a conduit fault in the discharge area, through which the groundwater flow now may rise dramatically. This is very interesting regarding the hot spots.

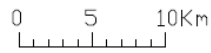
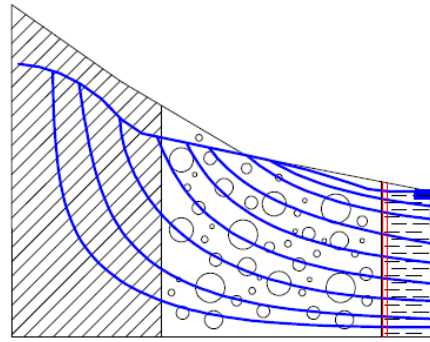
Of course like in the original scenario, the effect of layers with higher K being on the top of layer with lower K should be also considered.

vertical exaggeration: 50

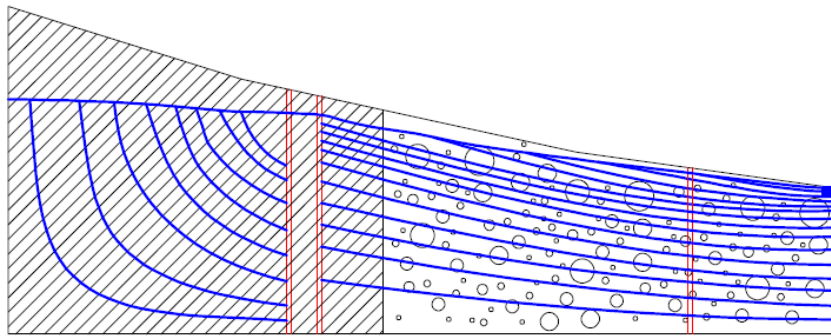
LEGEND

	Fault
	Precambrian bedrock
	Alluvial sediments
	Marsh
	Karroo

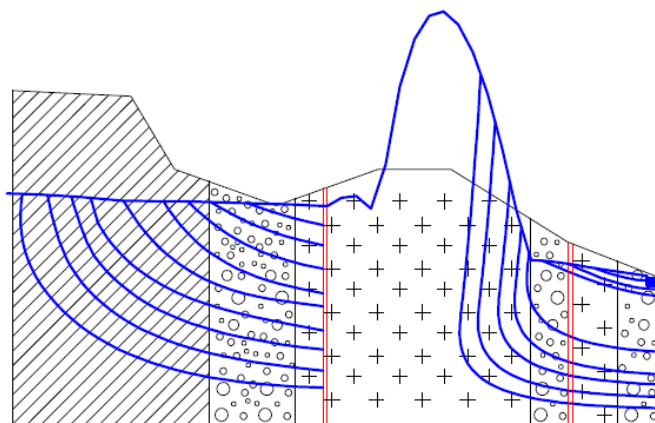
0 5 10Km

section A-A'



section B-B'



section C-C'

Figure 49. Sections with their groundwater level and flow lines calculated by the model for the possible geological scenario

DISCUSSION

In the process of building the model and preparing its inputs the intention was to avoid complex algorithms (especially in the calculations for areal recharge to the groundwater) considering both the availability and quality of data and our current knowledge of the area.

The model calibration in the steady state flow simulation gives both optimum and reasonable parameter values for hydraulic conductivities. However, the sensitivity analysis results display evidences of overparameterization. The calculated hydraulic heads for boreholes have a quite nice correlation to the observations made considering the uncertainty in the data. However, because all observations are used in the calibration, one would expect this correlation.

The uncertainty in data carry weight especially since it is only the seasonal fluctuations that are estimated in the available literature and the amount of declines/rises in the groundwater table during the period 1973-2008 is not known at the time of this study.

The interpolated groundwater table based on the observations from boreholes displays a very low level near Nchalo. Such low head is not obtained from the model and is doubted to exist since it is based on one borehole with an outstanding observed head of 16.77 m.a.s.l.

The groundwater fluctuation found in transient flow simulation is within the range estimated by Chilton & Smith-Carington (1984) and Mandeville & Batchelor (1990) and seems to increase in the southern parts of the area due to more variation in the recharge calculated in Ngabu, but it has not been in the intentions of the author to include the results of the transient flow simulation in the analysis of the flow system; for although a regular sensitivity analysis has not been performed on the values decided for the specific yield S_y , during the simulation it was observed that the maximum fluctuations vary significantly with the changes in S_y and/or its distribution.

The faults have been modelled separately as chains of cells (since in MODFLOW the groundwater flows from sides of the cell) in the model which can be criticized for their simplicity. The gravitational groundwater flow is yet clearly affected by the major faults, especially in the discharge area where the flow lines may rise up through the possible

continuation of Mwanza fault under the alluvium. Although due to simplicity, the results from the model do not exhibit these upward flow lines at the moment.

The model can be improved by:

- a) Obtaining geophysical data and therefore rebuild the model in multi-layer format where the sub-surface geology and faults are better represented and the bottom of the aquifer is known.
- b) Collecting soil samples from alluvial sediments and developing a good quality map of distribution of clays, sands and gravels.
- c) Recording data in time series from borehole in order to calibrate the specific yield.
- d) Performing pumping tests in the area.

CONCLUSION

The performance of the model seems satisfactory in producing groundwater head distribution based on the current data; both in steady state and transient flow simulation. Moreover, based on the results the gravitational groundwater flow is clearly affected by the major faults Panga, Telegraph, Nkombedzi and Mwanza.

The groundwater seems to go under confined and artesian conditions in the Precambrian basement, which is not confirmed by any borehole observation (since there is not any borehole in that area) but corresponds to the existence of Hot springs that are found along the Mwanza Fault.

The initial suspicion of Mwanza fault being the source of the high salinities aligned with it, is not confirmed directly by the model. However, studying the flow line in cross sections under the possible geological scenario in which the Mwanza fault may continue along the Shire River suggests that in the discharge area close to the river there may be upward groundwater flow through the Mwanza fault. It is quite possible that these flows carry dissolved salt from the Red beds in Karroo or from Lupata Series and are responsible for the salinity in the hot spots.

Seeing the available data and the simplicity of the model, the author wishes to improve the model, especially regarding its subsurface geology, before making any solid conclusion.

ACKNOWLEDGEMENT

The author would like to thank her supervisors Per Aagaard and Chong-Yu Xu for providing excellent guidance. The author also would like to thank Charifa Al Echcheikh El Alaoui for contributing to the study by providing digital maps of the area; Per Alve Glad, Cosmo Ngongondo and Maurice Monjerezi for the data and maps; Martin Morawietz for help with the software PMWIN; and last but not least the NUFU project for the opportunity to work on the groundwater system in the Chikwawa district, southern Malawi.

REFERENCE

- Castaing, C. 1990. *Structural study of the Lengwe and Mwabvi basins*. Bureau de Recherches Géologiques et Minières Service Géologique National
- Chapola, L.S. and Kaphwiyo, C.E. 1992. The Malawi Rift - Geology, Tectonics and Seismicity. *Tectonophysics* 209, 159-164.
- Chiang, W.-H. and Kinzelbach, W. 2001. *Groundwater Modeling with PMWIN: a simulation system for modeling groundwater flow and pollution*: Springer-Verlag Berlin Heidelberg.
- Chilton, P.J. and Smith-Carington, A.K. 1984. Characteristics of the weathered basement aquifer in Malawi in relation to rural water supplies. In Symposium, H. (ed). *Challenges in African Hydrology and Water Resources*. IAHS publication -- no. 144: International Association of Hydrological Sciences.
- Cooper, W.G.G. and Bloomfield, K. 1961. Geology of the Tambani-Salambidwe area. *Geol Surv Malawi Bull* 13.
- D.A. Morris, A.I.J. 1967. *Summary of hydrologic and physical properties of rock and soil materials, as analyzed by the Hydrologic Laboratory of the U.S. Geological Survey 1948-1960*.
- Dill, H.G. and Ludwig, R.R. 2008. Geomorphological-sedimentological studies of landform types and modern placer deposits in the savanna (Southern Malawi). *Ore Geology Reviews* 33, 411-434.
- Encyclopædia-Britannica. 2011. *Shire River*. *Encyclopædia-Britannica Web*.
- Glad, P.A. 2010. *Meteorological and hydrological conditions leading to severe regional drought in Malawi*, Department of Geoscience, Faculty of Mathematics and Natural Sciences, University of Oslo, Oslo.
- Habgood, F. 1963. *The geology of the country west of the Shire river between Chikwawa and Chiromo*, Zomba: Ministry of Forestry and Natural Resources, Geological Survey Department.
- Healy, R.W. 2010. *Estimating Groundwater Recharge*: Cambridge University Press.
- Huschke, R.E. 1952. *Glossary of Meteorology*. Second printing-1970, Boston: American Meteorological Society.
- Maida, J.H.A. 1985. Some physical and chemical properties of selected Malawi soils. *Luso* 6, 1-10.

- Malawi-Meteorological-Services. *Climate of Malawi* 2006 [Accessed: 20/05/2011. Available at <http://www.metmalawi.com/climate/climate.php>.
- Mandeville, A.N. and Batchelor, C.H. 1990. *Estimation of actual evapotranspiration in Malawi*. Institute of Hydrology Growmarsh Gifford Wallingford Oxfordshire, 110.
- Mkandawire, P.P. 2002. Groundwater resources of Malawi. *Managing shared aquifers in Africa*: United Nations Educational, Scientific and Cultural Organization.
- Monjerezi, M., Vogt, R.D., Aagaard, P. and Saka, J.D.K. 2011. Hydro-geochemical processes in an area with saline groundwater in lower Shire River valley, Malawi: An integrated application of hierarchical cluster and principal component analyses. *Applied Geochemistry* In Press, Accepted Manuscript.
- Mougenot, D., Recq, M., Virlogeux, P. and Lepvrier, C. 1986. Seaward extension of the East African Rift. *Nature* 321, 599-603.
- Nestebý, H. 1989. *avsetning og diagenetisk utvikling av Karroo (pre-trias) and red sandstone (jura-kritt) sedimenter Tukuyu-Rukiere omridet fra Tanzania*, University of Oslo.
- Palamuleni, L.G.C. 2010. *Land cover change and hydrological regimes in the Shire River Catchment, Malawi*, Department of Geography, Environmental Management and Energy Studies, University of Johannesburg, Johannesburg.
- Ring, U. and Betzler, C. 1995. Geology of the Malawi Rift: kinematic and tectonosedimentary background to the Chiwondo beds, northern Malawi. *Journal of Human Evolution* 28, 21.
- Ring, U., Betzler, C. and Delvaux, D. 1992. Normal vs. strike-slip faulting during rift development in East Africa; the Malawi Rift. *The Geological Society of America* 20, 1015-1018.
- Staines, M. 2002. *Water/Wastewater Problems and Solutions in Rural Malawi*, University of Strathclyde, Glasgow.
- Thornwaite, C. 1948. An approach toward a rational classification of climate. *Geographical review* 38, 55-94.
- TÓTH, J. 2009. *Gravitational Systems of Groundwater Flow, Theory, Evaluation, Utilization*: Cambridge University Press.
- UN-Water. *Statistics: Graphs and Maps* 2011 [Accessed: 19/05/2011. Available at http://www.unwater.org/statistics_res.html.

- Xu, C.Y. and Chen, D. 2005. Comparison of seven models for estimation of evapotranspiration and groundwater recharge using lysimeter measurement data in Germany. *Hydrological Processes* 19, 3717-3734.
- Xu, C.Y. and Singh, V.P. 2002. Cross Comparison of Empirical Equations for Calculating Potential Evapotranspiration with Data from Switzerland. *Water Resources Management* 16, 197-219.

Appendix A: Precipitation data

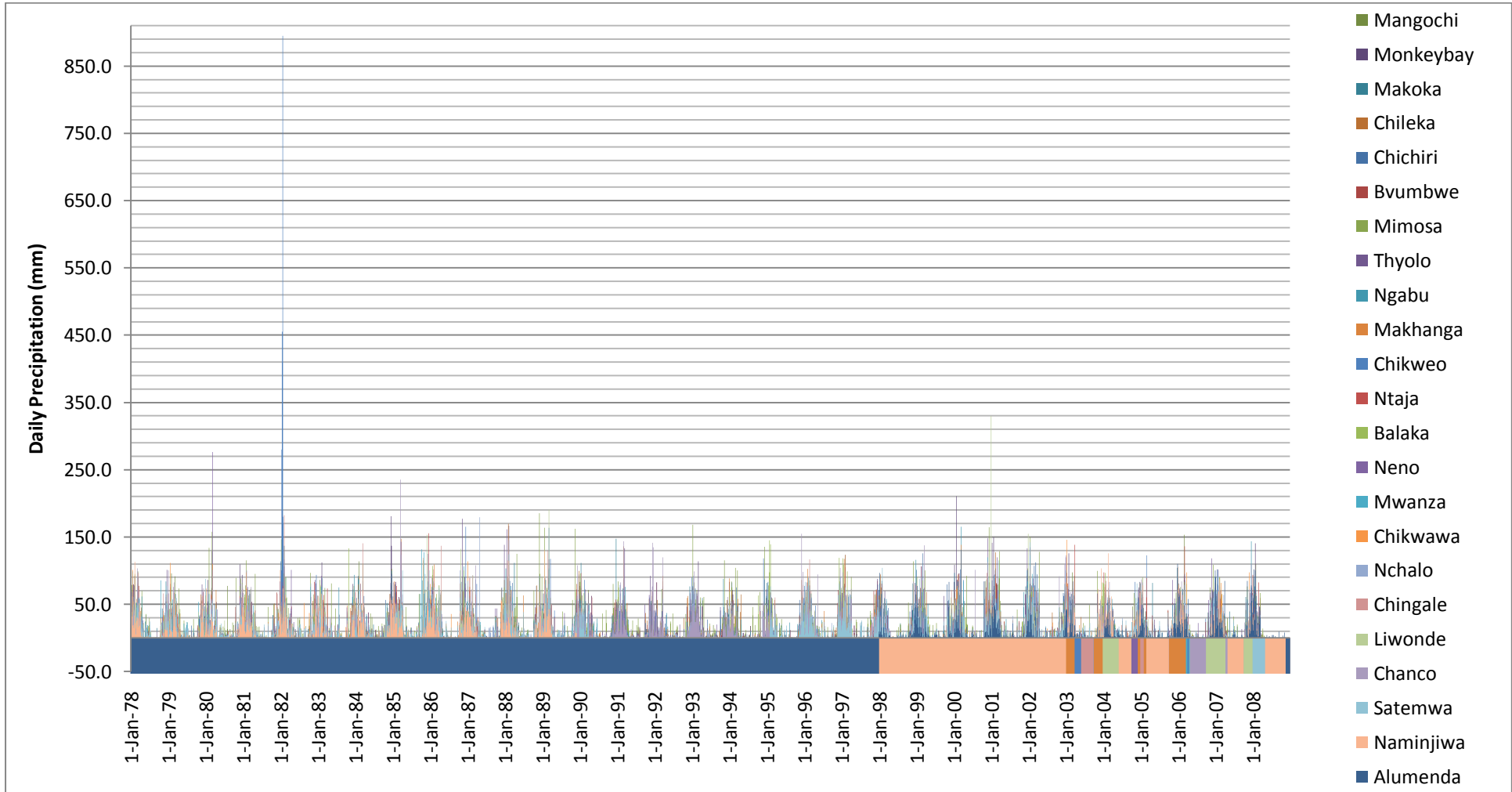


Figure 50. Precipitation data(negative values for missing periods)

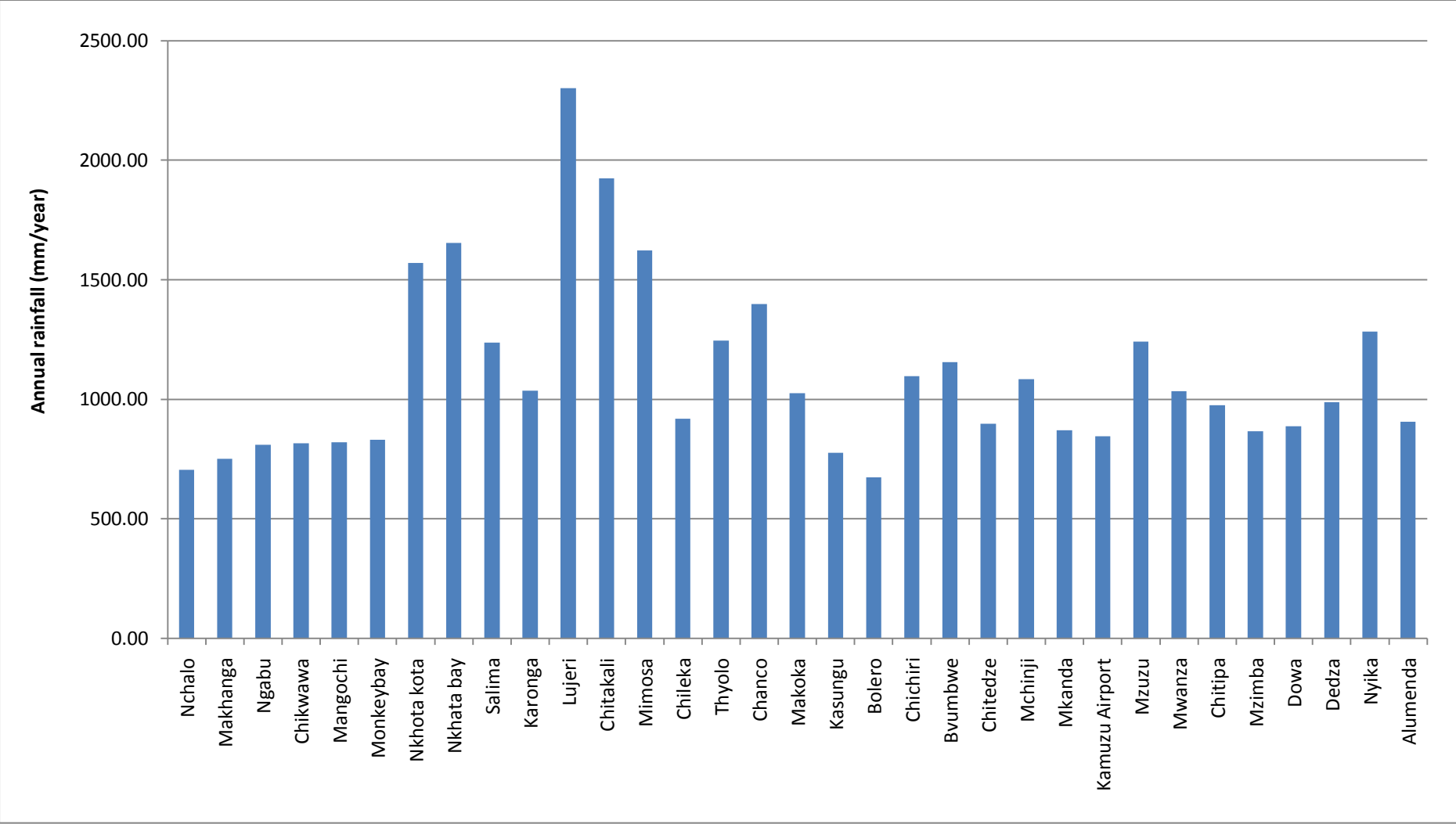


Figure 51. Annual precipitation for the stations

Appendix B: Temperature record

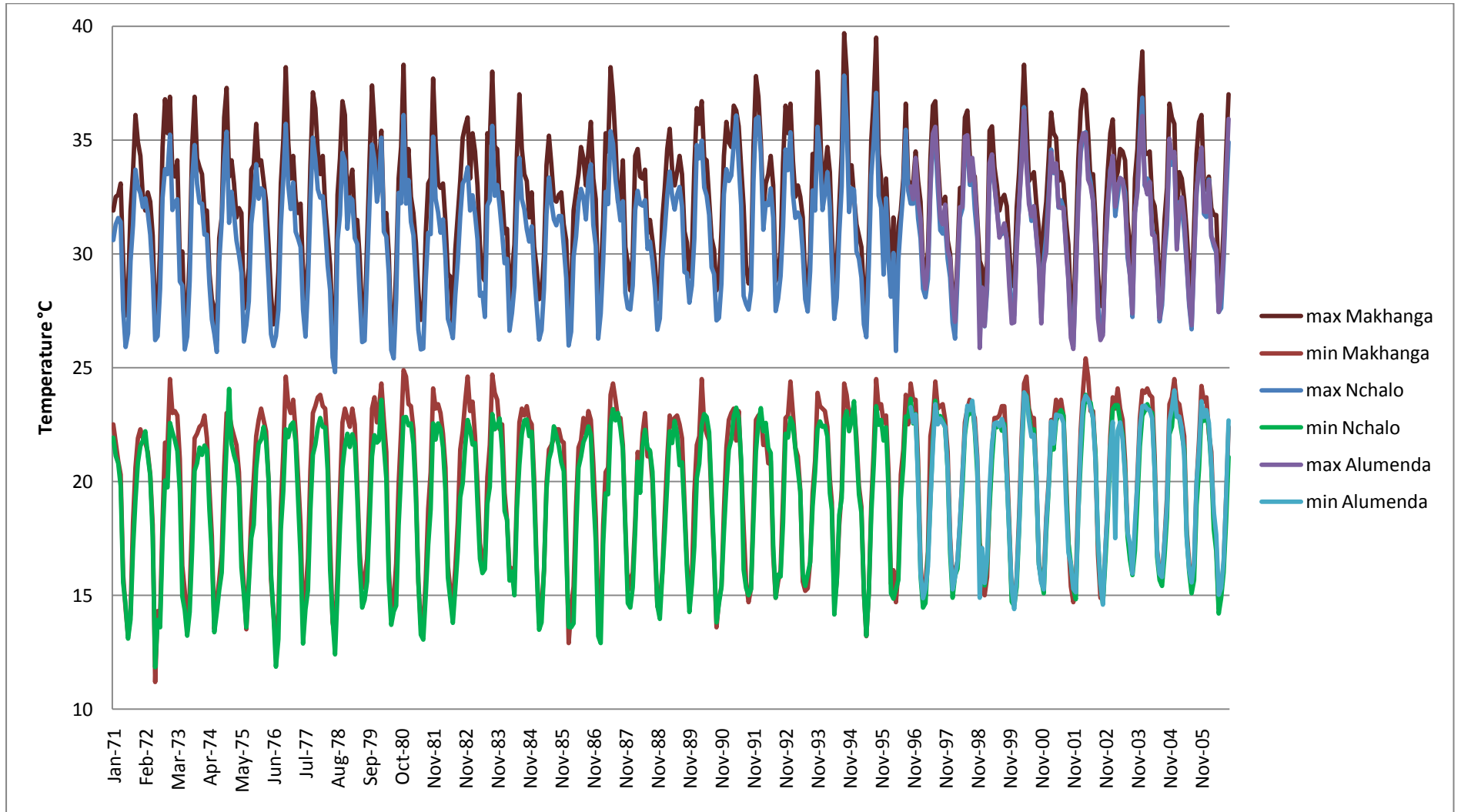


Figure 52. Maximum and minimum monthly temperature record for Alumenda, Makhanga and Nchalo

Appendix C: Boreholes data for the model

No.	x	y	observed head (m.a.s.l)
1	660600	8229400	190.4907
2	662700	8226200	176.7753
3	664400	8225900	170.6796
4	664700	8226000	161.5361
5	667500	8223100	160.0121
6	669000	8201200	149.3447
7	670000	8223500	158.4882
8	670600	8217600	143.249
9	671300	8220500	147.8207
10	672900	8220100	131.0576
11	673200	8217400	132.5815
12	673300	8220200	129.5336
13	673900	8219900	135.6294
14	675000	8216500	131.0576
15	675700	8221500	129.5337
16	675800	8218000	129.5337
17	675800	8203400	143.249
18	676400	8202900	134.1055
19	676500	8216900	126.4858
20	676700	8203300	144.7729
21	676700	8219500	134.1055
22	677500	8204500	140.2012
23	677500	8207300	140.2012
24	677800	8208400	138.6772
25	677900	8205500	138.6772
26	678300	8208200	124.9619
27	679200	8207100	121.9141
28	679400	8205500	129.5337
29	679900	8214000	146.2969
30	680200	8213800	117.3423
31	680200	8207600	115.8183
32	680200	8204300	124.9619

33	680500	8206000	111.2466
34	680600	8205900	126.4858
35	681200	8205800	121.9141
36	681600	8205900	118.8662
37	681600	8208000	112.7705
38	681800	8208800	112.7705
39	682000	8206400	85.3398
40	682100	8206600	121.9141
41	682100	8212800	106.6748
42	682500	8207300	108.1987
43	682800	8212400	106.6748
44	683400	8214500	117.3423
45	683500	8211300	105.1509
46	683700	8207600	108.1987
47	683900	8228500	131.0576
48	684000	8209100	103.6269
49	684200	8211200	102.103
50	684300	8206100	103.6269
51	684400	8226100	137.1533
52	685300	8225900	121.9141
53	685900	8208900	102.103
54	686000	8225300	111.2466
55	686100	8213900	99.0552
56	686300	8223100	121.9141
57	686300	8213500	99.0552
58	686400	8223100	114.2944
59	686700	8212600	97.5312
60	687000	8186000	167.6318
61	687200	8211200	97.5312
62	687500	8220900	91.4355
63	687700	8225100	96.0073
64	688200	8213800	86.8638
65	688500	8210000	94.4834
66	688700	8210600	92.9595
67	689200	8182500	164.584
68	689300	8210600	92.9595
69	689400	8209200	88.3877

70	689400	8186000	166.1079
71	689500	8210400	89.9116
72	689600	8211000	86.8638
73	689700	8211000	71.6245
74	689700	8190500	128.0098
75	689700	8186000	158.4883
76	690400	8213000	85.3398
77	690600	8208700	76.1963
78	690600	8191200	120.3901
79	690700	8224700	84.7303
80	690700	8158500	inactive
81	690800	8208400	79.2441
82	690800	8192000	112.7705
83	691100	8206300	76.1963
84	691200	8216300	54.8613
85	691300	8193500	114.2944
86	691300	8192700	111.2466
87	691500	8229200	73.1484
88	691800	8222000	70.1006
89	691800	8226500	68.5767
90	691800	8183400	131.0576
91	691800	8180400	152.3926
92	692000	8228700	79.2441
93	692200	8214700	79.2441
94	692200	8211200	85.3398
95	692300	8200800	76.1963
96	692400	8185400	134.1055
97	692500	8197300	79.2441
98	692800	8196700	79.2441
99	693000	8226800	80.7681
100	693200	8208200	76.1963
101	693300	8215900	76.1963
102	693300	8196200	62.481
103	693300	8193800	67.0527
104	693500	8210800	79.2441
105	693500	8196600	85.3398
106	693500	8185100	123.438

107	693900	8206900	67.0527
108	694000	8196200	68.5767
109	694100	8216300	70.1006
110	694300	8222200	76.1963
111	694300	8197100	68.5767
112	694400	8185000	126.4858
113	694600	8174200	182.8711
114	694700	8197200	82.292
115	694700	8192700	86.8638
116	694800	8280000	inactive
117	695000	8214900	74.6724
118	695100	8208000	77.7202
119	695200	8207600	73.1484
120	695300	8208800	74.6724
121	695400	8192900	64.0049
122	695400	8177500	148.4304
123	695700	8184700	106.6748
124	695800	8199800	67.0527
125	696000	8229200	inactive
126	696000	8197900	67.0527
127	696100	8201400	64.0049
128	696200	8198700	74.6724
129	696300	8201400	65.5288
130	696300	8196600	79.2441
131	696500	8204700	62.481
132	696500	8173300	149.3447
133	696600	8177700	124.9619
134	696600	8174400	138.6772
135	696800	8226700	inactive
136	696800	8199200	65.5288
137	696800	8184900	96.0073
138	696900	8206900	68.5767
139	697000	8208000	67.0527
140	697000	8193300	60.957
141	697000	8191000	65.5288
142	697200	8214200	70.1006
143	697300	8200200	62.481

144	697300	8191800	59.4331
145	697500	8205800	68.5767
146	697600	8197200	62.481
147	697900	8190200	70.1006
148	697900	8188300	79.2441
149	697900	8189600	54.8613
150	698000	8200400	67.0527
151	698000	8185600	88.3877
152	698300	8192000	51.8135
153	698400	8179100	118.8662
154	698400	8175600	132.5815
155	698500	8206600	67.0527
156	698500	8188800	45.7178
157	698500	8181500	100.5791
158	698600	8186900	86.8638
159	698700	8212900	71.6245
160	698800	8208100	70.1006
161	698900	8225500	inactive
162	698900	8185500	85.3398
163	698900	8193200	53.3374
164	698900	8188800	77.7202
165	699000	8187300	79.2441
166	699000	8184400	86.8638
167	699200	8194500	54.8613
168	699300	8201800	64.0049
169	699300	8201800	60.957
170	699500	8196800	83.8159
171	699500	8196800	62.481
172	699500	8196800	56.3852
173	699500	8194500	54.8613
174	699500	8201000	60.957
175	699600	8211000	70.1006
176	699600	8185600	85.3398
177	699800	8222600	inactive
178	699800	8181600	93.569
179	699900	8206800	68.5767
180	700000	8195900	41.146

181	700100	8183800	80.7681
182	700200	8178900	102.103
183	700300	8205100	65.5288
184	700300	8178600	106.6748
185	700400	8170700	152.3926
186	700500	8185900	82.292
187	700500	8183000	80.7681
188	700700	8197500	16.7632
189	700800	8199600	59.4331
190	700900	8178300	111.2466
191	700900	8179500	100.5791
192	700900	8182400	83.8159
193	701200	8214800	69.491
194	701200	8213500	68.5767
195	701200	8210700	67.0527
196	701200	8221400	inactive
197	701200	8181000	79.2441
198	701300	8207200	62.481
199	701300	8172300	132.5815
200	701500	8201800	62.481
201	701500	8199500	53.3374
202	701600	8180700	88.3877
203	701700	8174700	121.9141
204	701900	8179600	96.0073
205	701900	8170700	137.1533
206	702000	8179300	96.0073
207	702100	8177800	99.0552
208	702200	8185400	51.8135
209	702200	8179700	88.3877
210	702500	8178900	91.4355
211	702500	8187400	54.8613
212	702600	8212500	68.5767
213	702700	8178100	120.3901
214	702800	8170900	135.6294
215	702900	8166400	156.9643
216	702900	8166200	164.584
217	703100	8174600	114.2944

218	703200	8179900	94.4834
219	703400	8217600	inactive
220	703400	8176700	99.0552
221	703700	8178700	91.4355
222	703700	8169200	134.1055
223	703900	8175600	100.5791
224	704000	8186600	56.3852
225	704200	8178100	88.3877
226	704200	8172500	115.8183
227	704900	8206900	59.4331
228	704900	8181500	73.1484
229	704900	8169200	131.0576
230	705000	8184900	50.2895
231	705100	8183200	62.481
232	705100	8169300	126.4858
233	705100	8169300	126.4858
234	705200	8169300	120.3901
235	705300	8168300	131.0576
236	705400	8184100	67.0527
237	705400	8172500	112.7705
238	705400	8171500	114.2944
239	705500	8184500	62.481
240	705700	8187200	50.2895
241	705900	8167400	131.0576
242	706000	8217800	inactive
243	706000	8198400	inactive
244	706100	8177200	83.8159
245	706100	8165800	132.5815
246	706200	8204100	60.957
247	706200	8280900	inactive
248	706500	8174400	88.3877
249	706500	8166700	129.5337
250	707000	8179700	71.6245
251	707200	8186200	53.3374
252	707200	8171400	103.6269
253	707400	8170500	112.7705
254	707400	8168600	115.8183

255	707700	8167100	118.8662
256	707800	8181100	68.5767
257	707900	8173900	89.9116
258	707999	8182200	64.0049
259	708100	8165000	128.0098
260	708400	8179000	64.0049
261	708400	8176500	74.6724
262	708900	8214500	inactive
263	708900	8172500	88.3877
264	709200	8164100	inactive
265	709500	8213200	inactive
266	709500	8171000	97.5312
267	709700	8168500	99.0552
268	710300	8169800	100.5791
269	710600	8182200	56.3852
270	710700	8174300	73.1484
271	710800	8167600	96.0073
272	711500	8172700	82.292
273	711500	8168200	94.4834
274	711900	8281000	inactive
275	712000	8209700	inactive
276	712400	8178100	56.3852
277	712400	8170400	79.2441
278	712700	8171500	71.6245
279	712900	8169600	80.7681
280	712900	8167900	inactive
281	713100	8210900	inactive
282	714200	8208500	inactive
283	714500	8209100	inactive
284	714900	8209000	inactive
285	716600	8205900	inactive
286	717500	8204400	inactive
287	718800	8202800	inactive
288	720200	8184600	inactive
289	721700	8193700	inactive
290	723600	8193200	inactive
291	727300	8185600	inactive

292	727700	8188400	inactive
293	728500	8186900	inactive
294	728600	8187100	inactive
295	729600	8184600	inactive
296	729800	8185500	inactive
297	729900	8176800	inactive
298	730500	8174800	inactive
299	731100	8177500	inactive
300	731700	8183600	inactive
301	731900	8179100	inactive
302	732400	8183600	inactive
303	732500	8182400	inactive
304	733400	8176900	inactive
305	733800	8180900	inactive